Spring 2009

Synoptic controls on ozone over the northeastern US and continental export

Jennifer D. Hegarty

University of New Hampshire, Durham

Follow this and additional works at: https://scholars.unh.edu/dissertation

SYNOPTIC CONTROLS ON OZONE OVER THE NORTHEASTERN U.S. AND

CONTINENTAL EXPORT

BY

JENNIFER D. HEGARTY

BS, University of Massachusetts Lowell, 1987

MS, The Pennsylvania State University, 1991

DISSERTATION

Submitted to the University of New Hampshire

in Partial Fulfillment of

the Requirements for the Degree of

Doctor of Philosophy

in

Earth and Environmental Sciences

May, 2009

UMI Number: 3363720

INFORMATION TO USERS

The quality of this reproduction is dependent upon the quality of the copy submitted. Broken or indistinct print, colored or poor quality illustrations and photographs, print bleed-through, substandard margins, and improper alignment can adversely affect reproduction.
In the unlikely event that the author did not send a complete manuscript and there are missing pages, these will be noted. Also, if unauthorized copyright material had to be removed, a note will indicate the deletion.
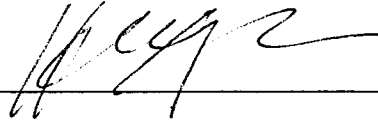
UMI®
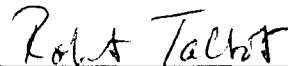
This dissertation has been examined and approved.

_____
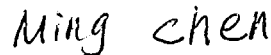
Dissertation Director, Huiting Mao,
Research Associate Professor of Earth,
Oceans and Space

_____
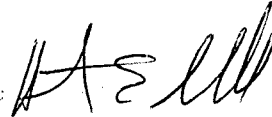
Robert W. Talbot, Research Professor of
Earth Sciences and Earth, Oceans and Space

_____
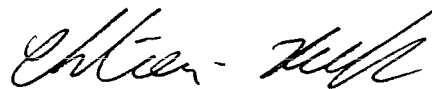
Ming Chen, Associate Scientist, Earth and
Sun Systems Laboratory, National Center
for Atmospheric Research

_____
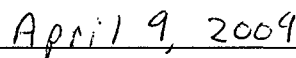
Hilary E. "Ned" Snell, Vice President,
Remote Sensing Division, Atmospheric and
Environmental Research, Inc.

_____

Christian Hogrefe, Adjunct Research
Associate, Atmospheric Sciences Research
Center, State University of New York at
Albany

_____

April 9, 2009

Date

ACKNOWLEDGEMENTS

I would like to thank my dissertation committee: Dr. Huiting Mao, Dr. Robert W. Talbot, Dr. Ming Chen, Dr. Christian Hogrefe and Dr. Ned Snell for their valuable guidance and support.

TABLE OF CONTENTS

LIST OF FIGURES

ABSTRACT

SYNOPTIC CONTROLS ON OZONE LEVELS OVER THE NORTHEASTERN U.S. AND CONTINENTAL EXPORT

by

Jennifer D. Hegarty

University of New Hampshire, May 2009

This dissertation focused on the impact of circulation, a key climate variable, on air quality from regional to global scale. The relationships between circulation and tropospheric ozone (O_3) levels were investigated for the surface over the northeastern U.S. as well as for the spring-, winter- and summertime North American export and trans-Atlantic Transport. The latter studies utilized the Tropospheric Emission Spectrometer (TES) retrievals of O_3 and carbon monoxide (CO) to explore the three-dimensional structure of continental outflow and to identify anthropogenic influence on the free troposphere over the remote oceanic region. The key findings are summarized as follows. First, the most common among the top five circulation patterns across the northeastern U.S. for summers 2000–2004, identified with a correlation-based synoptic categorization technique, was associated with stagnant warm conditions that were intimately associated with occurrence of high O_3. O_3 varied on an interannual timescale from a mean daily maximum value of 64 ppbv in 2002 to 52 ppbv in 2004. The sea level pressure (SLP) system intensity and frequency of each map type accounted for 46% of the interannual variability. The remainder was possibly due to non-linear relationships between climate and biogenic emissions and decreasing power plant emissions over the analysis period.

Second, during spring continental export was evident from enhanced O_3 (>55 ppbv) and CO (>115 ppbv) at the 681 hPa retrieval level suggesting anthropogenic influence. The export was found to be facilitated by both the primary and secondary branches of the warm conveyor belt (WCB) of cyclones which lofted pollutants from the continental boundary layer to the free troposphere enabling fast long distance transport with subsequent global impact. Ample evidence suggested stratospheric intrusions associated with cyclonic circulations particularly to the north of 45° N. Third, during winter the O_3 levels at 681 hPa were uniformly low (~45 ppbv) and the continental export was only evident in enhanced CO. Export to the free troposphere was mainly via the WCB and shallow convection behind cold fronts resulting from cold air flowing over warmer ocean waters. In summer O_3 levels were highly variable and the main export band was shifted northward around the Bermuda High, except during the passage of weak cyclones and cold fronts when export was shifted further south.

CHAPTER I

OVERVIEW

Air pollutants such as ozone (O_3) and its precursors play important roles in regulating climate and air quality. Ozone influences the Earth's radiative balance as a greenhouse gas and indirectly through its central role in atmospheric chemistry. Ozone affects air quality both as an atmospheric cleansing agent oxidizing other compounds and as a harmful air pollutant having serious adverse effects on both human and plant health (http://www.epa.gov/air/ozonepollution/health.html). There is compelling evidence that background surface O_3 levels in the northern hemisphere have almost doubled since observations were first taken in the 19th century, with the most rapid increase occurring since 1950 [*Vingarzin*, 2004; *Staehlin*, 2004]. Background surface O_3 levels in the northern hemisphere are expected to continue rising through the 21st century due to anthropogenic emissions [*Vingarzan*, 2004; *IPCC*, 2001].

Regional O_3 levels are the result of *in situ* chemistry, transport, and deposition, which are largely dependent on regional weather patterns. For example, daily maximum O_3 levels in the urban and industrial northeastern U.S. generally peak in summer due to O_3 production under warm stagnant weather conditions as well as regional transport [*Vukovich and Sherwell*, 2003]. Regional weather is controlled by synoptic circulation patterns. These synoptic circulation patterns also affect the long-range transport of

pollutants through interactions between sources in the planetary boundary layer and fast-moving free tropospheric winds.

Synoptic circulation patterns have been categorized to show relationships between regional air quality events and circulation in the northeastern U.S. [*Heidorn and Yap*, 1986; *Comrie and Yarnal*, 1992; *Hogrefe et al.*, 2004]. However, the link between the interannual variability of circulation patterns and interannual variability of summertime O_3 levels in the northeastern U.S. has not been firmly established as only the frequency variability of circulation patterns has been considered. This dissertation addresses the relationship between interannual variability of O_3 and circulation in the northeastern US by including an examination of circulation intensity and storm track along with frequency.

Intensive field campaigns such as the summer 2004 intensive study conducted by the International Consortium for Atmospheric Research on Transport and Transformation (ICARTT) [*Mao et al.*, 2006; *Singh et al.*, 2006] have been dedicated to understanding the export and long-range transport of pollutants from North America. While these studies have indicated that under certain circulation patterns pollutants from North America may be quickly transported in the free troposphere across the Atlantic Ocean to Europe, the lack of continuous, long-term measurements of pollutants at different levels in the free troposphere has presented challenges to confirming the speculated transport mechanisms. An ongoing area of research addressing these challenges is the retrieval of atmospheric pollutant concentrations from satellite measurements of the outgoing electromagnetic radiation from the earth-atmosphere system. In this dissertation satellite observations of O_3 and carbon monoxide (CO), referred to as retrievals, from a new

instrument called the Tropospheric Emission Spectrometer (TES), which is onboard the EOS-Aura satellite and provides global coverage every other day at a number of different altitudes in the troposphere, were used to examine export from North America and its relationships to the speculated transport mechanisms.

In summary, the dissertation focused on the following main objectives:

Objective I: Develop techniques to investigate the spatial and interannual relationships between summertime surface O_3 and synoptic-scale atmospheric circulation patterns in the northeastern U.S. using primarily surface measurements of O_3 and its precursors.

Objective II: Examine export of O_3 and its precursors from North America using techniques developed in *Objective I* together with satellite observations from Aura and trajectory models.

The main body of this dissertation is divided into 3 chapters. Chapter II presents the application of map typing technique in the investigation of relationships between summertime synoptic circulation and surface O_3 in the northeastern U.S. Chapter III is a study of the influence of circulation patterns on North American continental export during the spring using TES measurements. Chapter IV presents an analysis of TES observations in the winter and summer to explore the seasonal variability of North American continental export.

CHAPTER II

SYNOPTIC CONTROLS ON SUMMERTIME SURFACE OZONE IN THE
NORTHEASTERN U.S.

Introduction

Tropospheric ozone (O_3) is produced by complex photochemical reactions involving nitrogen oxides (NO_x which includes NO and NO_2) and hydrocarbons emitted from both anthropogenic and natural sources. The formation of O_3 is influenced strongly by climatological factors including air temperature, moisture, and solar radiation [*Seinfeld*, 1989; *Comrie and Yarnal*, 1992; *Vukovich*, 1995; *Vukovich and Sherwell*, 2003]. Atmospheric circulations exert important influence on the distribution of O_3 and its precursors on various scales, and can be especially important in modulating local meteorological controls on photochemical production and build-up of regional O_3 levels [e.g., *Li et al.*, 2002; *Vukovich and Sherwell*, 2003; *Cooper et al.*, 2002; *Mao and Talbot*, 2004; and *Huntreiser et al.*, 2005].

The influence of transport on the surface-level O_3 has been investigated through numerous air mass trajectory studies, particularly in the northeastern U.S. where intensive measurement campaigns and continuous monitoring programs have helped to identify principal source regions [*Taubman et al.*, 2006; *Cooper et al.*, 2001; *Schichtel and Husar*, 2000; *Moody et al.*, 1998; *Mao and Talbot*, 2004]. However, trajectory analysis alone does not adequately reveal the climatological conditions leading to regional O_3 episodes.

A comprehensive examination of circulation patterns is required to connect them with important transport trajectory pathways and ascertain critical meteorological conditions responsible for regional and local build-up of O_3.

Patterns in atmospheric circulations have been categorized to determine their relationship with surface O_3 levels. For example, *Heidorn and Yap* [1986] an*d Comrie and Yarnal* [1992] used manual classifications to establish that summertime high/low O_3 days in Southern Ontario, Canada and Pittsburgh, Pennsylvania (PA) were associated with the back/front of a surface high pressure system. *Comrie* [1992a] developed a circulation pattern sequencing technique that showed a 2-3 day succession in certain circulation types can be crucial to the formation of high O_3 levels. *Hogrefe et al.* [2004], using the correlation-based synoptic classification technique of *Lund* [1963], identified three key sea level pressure (SLP) types over the Northeast that led to high O_3 during summers 1996-2001: the Bermuda High, a high centered over the Midwest with a trough along the East Coast, and a high centered directly over New England. The distribution of surface O_3 was strongly influenced by these circulation patterns, with the most widespread daily maximum O_3 associated with the Bermuda High.

Previous studies have focused mainly on the impact of different circulation patterns and their sequencing on the spatial distribution of surface O_3 for a specific episode day(s). *Comrie and Yarnal* [1992] investigated the relationship between the frequency of surface circulation types and interannual variability of surface O_3 in Pittsburgh, PA. In another study *Comrie* [1994] attributed high levels of O_3 in rural Pennsylvania during summer 1988 to unusually hot and dry conditions associated with a more northerly storm track compared to summers 1989 and 1990. However, neither

study established a significant link between interannual variability in circulation patterns and surface O_3 levels.

The intensity (i.e., central pressure value of a high/low pressure system) of a given circulation pattern and its subsequent impact on regional levels of surface O_3 is at present unexplored. The effective intensity of a circulation pattern for a given region is a function of its actual intensity, size, and relative position of its major features. For example, a Bermuda High pattern with a strong anticyclone that extends well into the central United States would have a greater effective intensity in the Northeast than one with a smaller, weaker anticyclone or an anticyclone of equal strength and size but centered further east. The Bermuda High pattern with the greater effective intensity would displace the convective warm conveyor belt region of the next approaching Canadian low further west, resulting in fewer clouds, suppressed boundary layer venting and consequently poorer air quality in the Northeast. In contrast, a strong Canadian high pressure system that extends well into the United States would likely produce greater transport of cooler and presumably less polluted air (i.e., aged air) to the northeastern U.S. than one with a weaker high or one of equal strength positioned more northward.

This study was an in-depth investigation of both the spatial and interannual relationships between surface O_3 and synoptic-scale atmospheric circulation patterns in the northeastern U.S. for summers 2000-2004. Our goals were: 1) to identify the predominant summertime circulation patterns over the Northeast, 2) to establish relationships between identified circulation patterns and surface O_3 levels, 3) to determine the impact of the interannual variability in circulation patterns and their intensity on surface level O_3, and 4) to examine the influence of storm tracks and the

number of tropical cyclones transecting the eastern U.S.

Methods and Data

Classification of Synoptic-Scale Circulations

Synoptic-scale circulation patterns over a specified region can be classified using either eigenvector-based [*Lorenz*, 1956; *Richman*, 1981; *Yarnal*, 1993] or correlation-based analyses [*Lund*, 1963; *Kirchhofer*, 1973]. The synoptic data are typically segregated based on circulation commonalities and their frequency of occurrence in daily SLP or geopotential height (GPH) maps. While the eigenvector-based method is concise, the resultant component maps are not readily interpretable as real weather maps [*Yarnal*, 1993; *Yarnal et al.*, 2001].

The classification of synoptic-scale circulations during our study period was conducted using the correlation-based technique [*Lund*, 1963; *Kirchhofer*, 1973]. The patterns at the surface were classified for each day during 01 June – 30 September 2000 – 2004. The data used here included the 1200 UT SLP fields with a resolution of $1° \times 1°$ from the National Centers for Environmental Prediction (NCEP) Global Final Analysis (FNL) (http://dss.ucar.edu/datasets/ds083.2). The map-typing domain was centered over New York and Pennsylvania and covered the area from 36°- 48°N in latitude and 88°-64°W in longitude (Figure 2.1).

The map typing algorithm consisted of four steps. First, the correlation coefficient, r_{xy}, was calculated for each pair of grids using Equation 2.1;

$$r_{xy} = \frac{\sum_{i=1}^{n}[(x_i - \bar{x})(y_i - \bar{y})]}{[\sum_{i=1}^{n}(x_i - \bar{x})^2 \sum_{i=1}^{n}(y_i - \bar{y})^2]^{1/2}} \qquad (2.1)$$

7

where, x and y represented the SLP or GPH values at two different times at the same grid location i. The number of grid points per field was represented by n. Second, the grid that correlates with the largest number of grids at $r_{xy}>0.7$ was identified as Map Type I, and this grid and all the correlated grids were removed from the matrix. Reiterations of these two steps identified 5 map types (I – V) before at least 5% of the total number of maps could no longer be formed. The analysis was repeated one final time to provide for re-assignment of a grid to a map type which may have been subsequently identified.

The correlation criteria $r_{xy}>0.7$ was determined through repeated trials which showed that for $r_{xy}<0.7$, maps with significantly different circulation patterns could be assigned to the same category. For $r_{xy}>0.7$ more than 10 map types were needed to classify a significant percentage (>60%) of the circulations. This finding was consistent with previous work [*Lund*, 1963; *Hogrefe*, 2004; *Hogrefe*, personal communication, 2006].

Storm Track Data

We further investigated links between circulation pattern intensity and interannual climate variability by examining interannual variability in storm tracks. The storm parameters were calculated from the NCAR/NCEP 2.5° × 2.5° Reanalysis (NNRA, http://www.cdc.noaa.gov/cdc/reanalysis) interpolated to an equal area 250 km × 250 km grid with an algorithm based on the one described by *Serreze* [1995]. The relevant outputs consisted of the positions of all cyclones occurring over the Northern Hemisphere for the years 1958 – 2005. Using this data we calculated frequency and intensity statistics for each grid point to determine the major storm tracks for summers 2002 and 2004. We also examined tropical cyclone tracks available from the National Hurricane

8

Center (NHC, http://www.nhc.noaa.gov/tracks) to determine their influence on the circulation pattern analysis. We determined the total number of tropical cyclones tracking through an expanded version of our map typing study domain and defined tropical storm days as the number of days in which a tropical system or its extra-tropical counterpart were located within this expanded study domain at 1200 UT. The expanded study domain consisted of the original map typing study domain of Figure 2.1 expanded by 5° latitude and longitude on each border.

Ozone, Carbon Monoxide, and PM$_{2.5}$ Data

We used hourly averaged O$_3$ data over the time period of 1 June – 30 September 2000 – 2004 obtained from the Air Quality System (AQS) database (http://www.epa.gov/ttn/airs/airsaqs/) which is maintained by the Environmental Protection Agency (EPA). The O$_3$ data was derived from measurements at 474 monitoring sites scattered throughout the northeastern U.S. (Figure 2.1). In addition we included O$_3$ data from the 5 AIRMAP monitoring sites in New Hampshire (NH) and Maine (ME): Thompson Farm, Mount Washington Observatory, Appledore Island (ME), Pack Monadnock, and Castle Springs, which dated from April 2001 (www.airmap.unh.edu). The AIRMAP stations have site elevations ranging from sea level to 2 km, with locations designated by red circles in Figure 2.1.

Carbon monoxide (CO) and particulate matter with an aerodynamic diameter <2.5 μm (PM$_{2.5}$) are indicative of combustion emissions. In the northeastern U.S. high concentrations of these species are associated with anthropogenic activities [*Mao and Talbot*, 2004], and they can serve as tracers for precursor species involved in

9
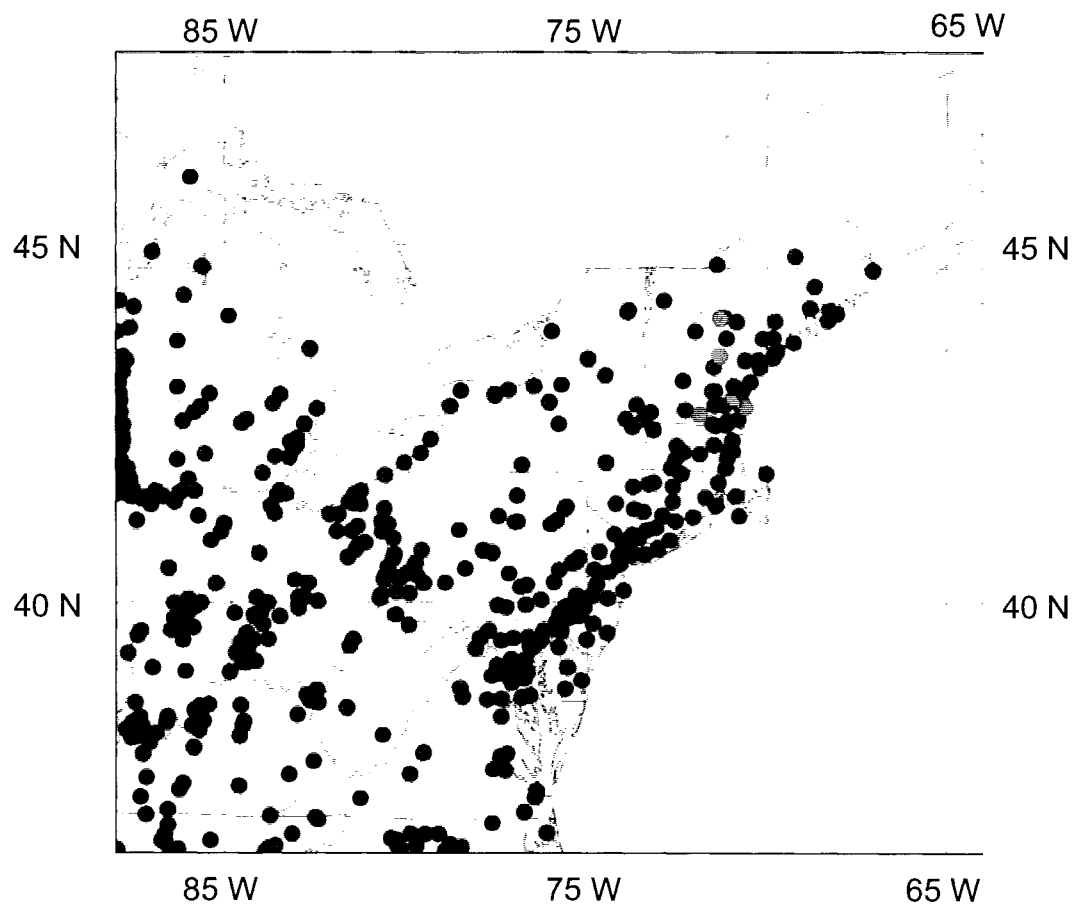
Figure 2.1. Map typing domain. Blue dots indicate locations of the monitoring sites from the AQS observing network and red dots indicate locations of AIRMAP stations.

photochemical O_3 production. Daily mean mixing ratios of CO were derived from hourly-averaged observations from 172 AQS sites and 1-minute average data from 5 AIRMAP sites. Daily mean concentrations of $PM_{2.5}$ were obtained from hourly-averaged observations at 133 AQS sites.

Predominant Map Types and Associated Surface O_3 Levels

Five map types corresponding to the characteristic summertime circulation patterns over the Northeast are depicted in Figure 2.2 along with coincident distributions of O_3, CO, and $PM_{2.5}$. The O_3 maps represent the mean daily maximum values. The $PM_{2.5}$ maps represent the mean daily mean values. For CO we show the difference, ΔCO, between the daily mean for each map type and the seasonal daily mean to enhance small variations across the domain.

During the study period 65% of the days had a surface circulation pattern classifiable as one of the 5 predominant map types. Map Type I occurred most frequently, with 21% of the summertime days classified as this type. The Map Type II circulation pattern occurred on 14% of the days, Map Type III 11%, Map Type V 10%, and Map Type IV only 9%. The weather conditions corresponding to each map type are summarized in Table 2.1. Briefly, Map Type I was typically associated with the most widespread warm, humid, stagnant conditions throughout the Northeast. Map Type II generally featured mixed conditions where primarily warm and humid air extended from the southwest corner of the domain northward into Western Michigan (MI). Cooler and drier air covered the region from the Upper Peninsula of MI to Southern New Jersey (NJ). Map Type III featured widespread cool conditions and northerly flow on the east
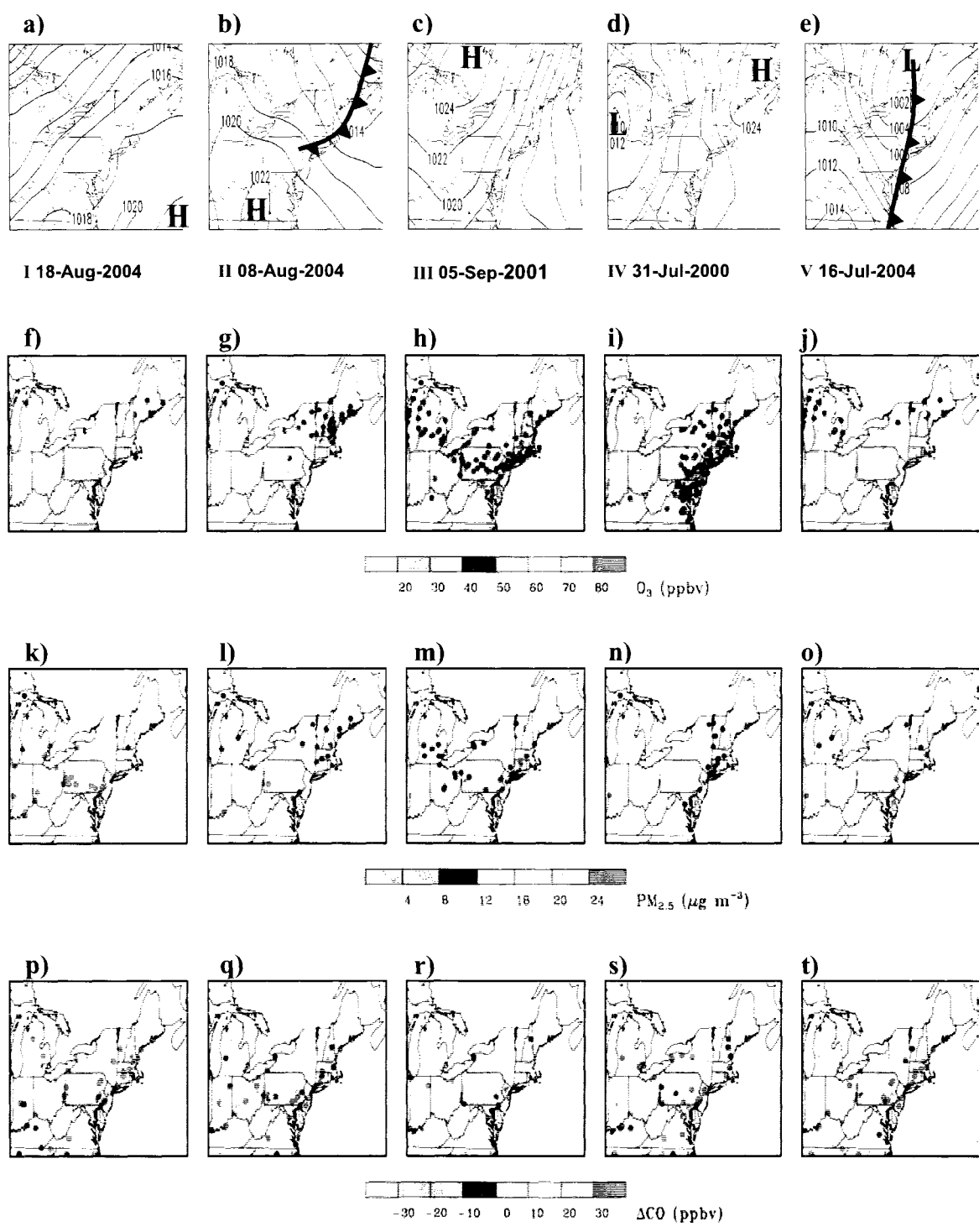
Figure 2.2. The representative SLP (hPa) map for Map Types I – V with the date listed below each plot (a-e), and for each map type the mean daily maximum O_3 (ppbv) (f – j), the mean daily $PM_{2.5}$ ($\mu g\ m^{-3}$) (k - o) , and the mean daily ΔCO (ppbv) (p - t). The ΔCO is defined as the difference between the mean daily CO mixing ratio for each map type and the mean daily CO mixing ratio for all days.

Table 2.1. Map type frequencies and meteorological characteristics.

Map Type	Frequency (%)	Characteristics
I	21	• Bermuda High • Slow south-southwesterly flow at the surface (<5 m s^{-1}) veering to southwesterly and westerly flow (5-10 m s^{-1}) at the top of the (daytime or 850 hPa) boundary layer across the Northeast • Warm and humid, sporadic clouds and isolated convection
II	14	• High pressure centered over Southern Ohio Valley and a trough off the coast • Northwesterly flow over Southwestern Pennsylvania to the Virginia coastline up to Northern Maine. Slow southerly to southwesterly surface flow (<2 m s^{-1})west of the Appalachians extending into the Ohio Valley • Northwesterly flow of 5-10 m s^{-1} at top of boundary layer (or 850 hPa) over entire Northeast • Dry and clear in northwesterly flow • Humid with sporadic thunderstorms in southerly flow west of the high
III	11	• Large high pressure system centered north of the Upper Peninsula of Michigan • Northerly and northeasterly subsiding flows of 5 – 15 m s^{-1} throughout boundary layer. • Clear, cool and dry
IV	9	• High pressure centered east of Maine; Low pressure center or trough near Western Michigan • Southerly and southeasterly surface flows at 3- 6 m s^{-1} • Southwesterly flow of 5 – 10 m s^{-1} at top of boundary layer (850 hPa) • Marine air near the coast • Widespread clouds and/or precipitation inland
V	10	• A sharp trough extending from a low over Quebec through Eastern New York and down the East Coast, likely in association with a cold front • Southwesterly flow east of the trough; Northwesterly flow west of the trough at 5 -15 m s^{-1} throughout boundary layer. • Warm and humid east of the trough; Cool and, dry to the west of the trough

side of the high pressure center migrating southeast from Central Canada. Cooler conditions were also prevalent with Map Type IV and were accompanied by cloud cover associated with an area of low pressure in extreme western portion of the domain. Conditions associated with Map Type V were mixed, with warm humid air in the southwesterly flow to the east of the cold front along the East Coast and cooler drier conditions in the northwesterly flow to the west of the front.

The highest O_3 mixing ratios were associated with Map Type I (Table 2.2), where the domain-averaged daily maximum mixing ratio was 64 ppbv with the highest values (>70 ppbv) occurring over the East Coast Megalopolis extending from Washington, D.C. to Boston, Massachusetts (MA) (Figure 2.2f). Under Map Type I conditions, the Northeast was largely under the influence of the Bermuda High as shown in Figure 2.2a. Previous studies suggest that the occurrence of pollution episodes with high O_3 levels in the eastern U.S. is often linked to such dynamical systems [e.g., *Seaman and Michelson*, 2000; *Gaza*, 1998].

Table 2.2. Domain–averaged O_3 mixing ratios (ppbv) for the five map types.
[a]Departure from the 5-year mean significant at the p = 0.05 level.
[b]Departure from the 5-year mean significant at the p = 0.10 level.

Map Type	All Summers	2000	2001	2002	2003	2004
I	64.1	59.8	66.2	72.8[a]	62.6	56.2[b]
II	60.7	54.5	60.8	73.8[a]	60.8	53.4
III	50.3	47.3	49.3	55.6[b]	52.5	44.7[a]
IV	51.3	51.3	53.4[a]	51.7	50.4	50.9
V	60.1	54.6[b]	59.1	66.2[b]	63.6	54.9[b]
Unclassified	54.3	51.9	58.8	59.7	52.8	50.2
All	57.0	53.5	59.2	64.2[a]	56.5	51.7[b]

While the back edge of the Bermuda High is often an area of convection and inflow into the warm conveyor belt region of an approaching cyclone, a considerable

region between the center of the high and the back edge often extends across the Northeast. In this region light south-southwesterly surface flow provides a continuous supply of warm air, while cloud formation, precipitation and venting of pollutants from the boundary layer are suppressed due to synoptic-scale subsidence associated with the high. In addition, more westerly and somewhat faster flow near the top of the boundary layer can transport O_3 and precursors from the industrial and urban centers in the Midwest eastward where they can be mixed down to the surface and contribute to the build-up of high levels of O_3 along the East Coast.

To further illustrate the poor air quality conditions that can develop in response to suppressed boundary layer ventilation in Map Type I, we examined the distribution of mean daily $PM_{2.5}$ and ΔCO (Figures 2.2k and 2.2p). These species have long enough lifetimes to build up under multi-day high pressure conditions. $PM_{2.5}$ concentrations >18 $\mu g\ m^{-3}$ and ΔCO values >20 ppbv were found in the same regions with high O_3. This is strong evidence for a regional build-up of pollutants from air mass stagnation and unfavorable ventilation conditions.

A good example of a Map Type I pollution scenario was the significant pollution event on 9-17 August 2002 (Figure 2.3). Ozone mixing ratios built up to daily one-hour maximums exceeding 100 ppbv over a wide area extending from southern Maine (ME) to eastern Ohio (OH). Even at the relatively rural location of Thompson Farm (TF) near Durham, NH daily maximum O_3 exceeded 100 ppbv and peaked at 143 ppbv on August 14th (Figure 2.3a). Throughout the episode, the daily maximum temperature near the surface at TF rose from 27°C on 9 August to 36°C on 14 August, and the JNO_2 measurements suggested mostly clear sky conditions (Figures 2.3b-2.3c). The circulation

for August 9th was classified as Map Type III, and was followed by 7 days of Map Type I

flow. The persistent pattern finally dissipated on August 17th with the passage of a weak

cold front and onset of Map Type V conditions (Figures 2.3c-2.3e).
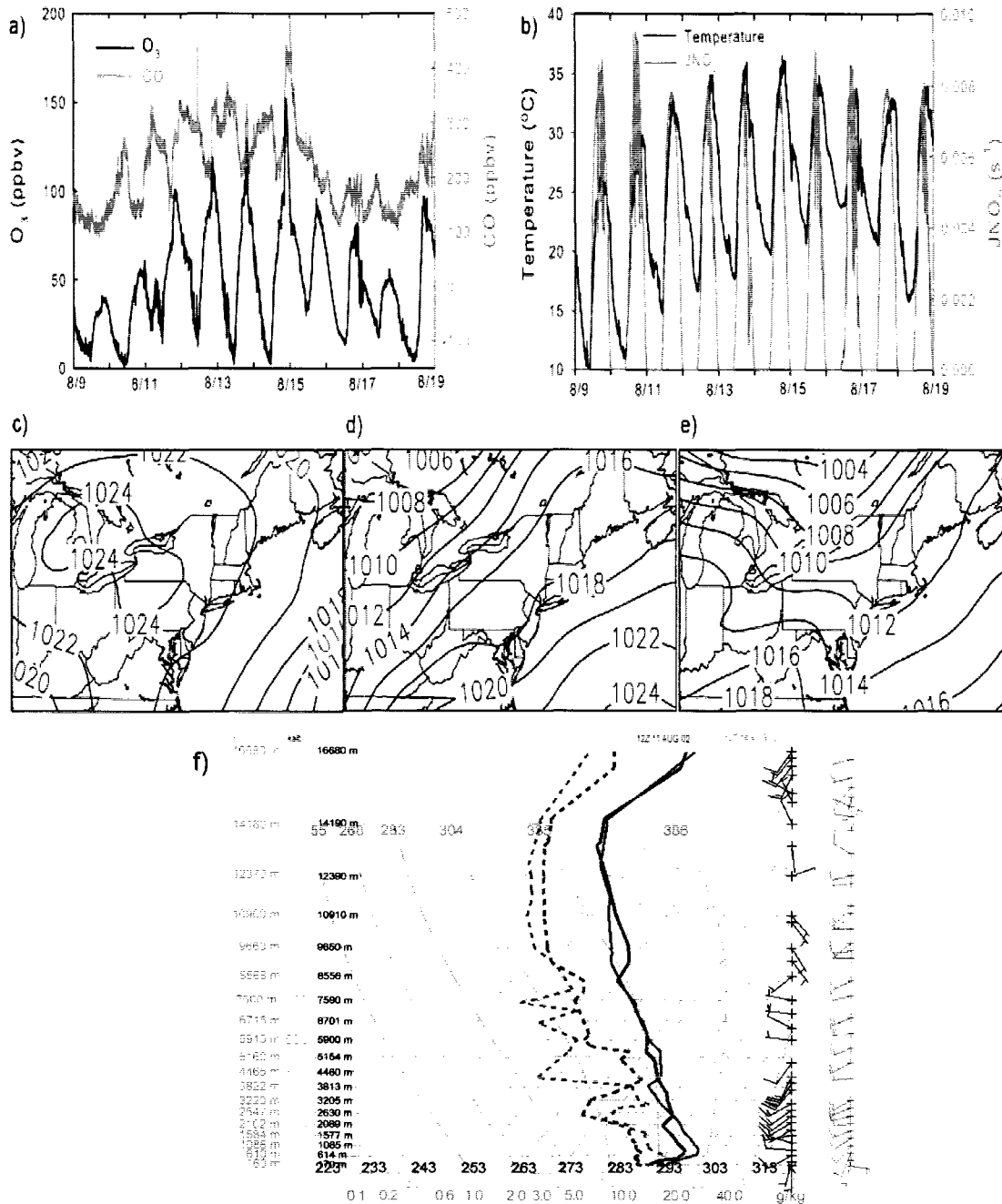
Figure 2.3. The August 2002 Northeast pollution event; Thompson Farm time series of a) O_3 (ppbv) and CO (ppbv), and b) temperature (°C) and NO_2 photolysis rate (JNO_2, s^{-1}); 1200 UTC sea level pressure analysis for c) 9 August, d) 14 August, and e) 18 August; f) Skew-T Log-P sounding plot at Albany, NY for 1200 UTC 11 August (temperature solid black, dewpoint dashed black) and 14 August (temperature solid red, dewpoint dashed red), wind barbs (knots), pressure (hPa).

17

During the period of 10-14 August the GOES satellite images [http://vortex.plymouth.edu/sat-u.html] showed a repeating diurnal cycle of mostly clear skies throughout the Northeast in the morning, followed by late afternoon thunderstorms over the northwestern portion of the domain. Generally storms only propagated as far eastward as OH before dissipating in the evening hours with cloud fragments drifting into Pennsylvania (PA) and upstate New York (NY). Soundings at Albany, NY, Pittsburgh, PA, and Wilmington, OH (http://vortex.plymouth.edu/get_raob-u.html) indicated a distinct synoptic-scale subsidence inversion with its base located between 2600 - 4000 m on the 10th, 11th, and 14th (Figure 2.3f). During the evening of the 13th it was much less pronounced, possibly due to dissipating cloud fragments from daytime thunderstorms in the OH area. The daily maximum hourly O_3 level west of the OH-PA border was 90 - 120 ppbv on 10 -11 August but decreased to 50 - 80 ppbv by 14 August. In contrast the daily maximum hourly O_3 level east of the PA-OH border started out lower at 70-80 ppbv on 10 August and steadily rose to extreme levels on 14 August. On 14 August most of the stations along the East Coast from Washington D.C. to southern ME and westward to central PA reported daily hourly maximum O_3 mixing ratios exceeding 120 ppbv. Over the period of 15-17 August afternoon thunderstorms became more widespread in the western portion of the domain and propagated eastward as the Bermuda High retreated from the East Coast. Ozone levels that were still high (50 - 80 ppbv inland and 80 - 110 ppbv along the East Coast) began to decrease during this period as the effective intensity of this pattern weakened.

Surface O_3 mixing ratios associated with Map Type II were also fairly high. Domain-averaged O_3 was 61 ppbv (Table 2.2), attributable to the stagnant and warm

conditions to the west and south of a high pressure system located south of the OH Valley. Under these conditions, New England, NY, Northern PA, and NJ exhibited O_3 mixing ratios <60 ppbv. This resulted from northwesterly flow between the high pressure ridge and the trough off the New England coast that brought in cooler, drier and aged Canadian air. Evidence for aged air masses under this meteorological situation is provided by $PM_{2.5}$ concentrations ≤ 12 μg m^{-3} and negative ΔCO values outside of major urban areas in New England and New York (Figure 2.21).

The lowest O_3 mixing ratios over the Northeast occurred during time periods influenced by Map Types III and IV, corresponding to which domain-averaged O_3 was 50 and 51 ppbv respectively. Under Map Type III the high pressure system centered over the Upper Peninsula of Michigan supplied most of the Northeast with relatively aged Canadian air bearing the least anthropogenic influence as indicated by the lowest $PM_{2.5}$ and ΔCO levels (Figures 2.2m and 2.2r). For Map Type IV the easterly and southeasterly winds over much of the Northeast transported relatively aged marine air onshore which led to decreased O_3 levels along the East Coast. The persistence of reduced O_3 levels over the continent likely resulted from increased cloud cover associated with an area of low pressure in the northwestern portion of the domain.

Map Type V represents a transitional weather pattern from warm humid conditions to a cool drier environment in the Northeast initiated by passage of a cold front trailing from a surface low in Canada. To the east of the front in New England, Eastern NY, NJ, and Eastern PA, southwesterly flow carrying pollutants from upwind industrial and urban centers likely increased O_3 levels in this area. West of the front, northwesterly flow from Canada funneled aged air into the region with lowered levels of

O_3. The overall domain-averaged O_3 mixing ratio was 60 ppbv, ranking these pollution conditions in the middle of the five map types.

The map typing analysis suggested close ties between varying synoptic-scale circulations and the spatial distribution and relative abundance of surface O_3. However, to better elucidate the contribution of circulation dynamics to the relative amounts of surface O_3, links between interannual variability of synoptic circulations and surface O_3 need to be established quantitatively.

Interannual Variability in Map Type Frequency and Its Impact on O_3

The interannual variability in summertime surface O_3 levels during the 5-year study period is documented in Table 2.2. Domain-averaged O_3 reached a maximum of 64 ppbv in 2002, and decreased to a minimum of 52 ppbv in 2004. Likewise, O_3 was low at 54 ppbv in 2000, while in 2001 and 2003 it was intermediate. Student's t-tests indicated that the departure of the domain-averaged O_3 mixing ratio in 2002 from the 5-year mean was statistically significant at the $p = 0.05$ level. In 2004 it was statistically significant at the $p = 0.10$ level, while during other years the departures were not significant.

Interannual variability was also observed in the frequency of surface circulation patterns (Figure 2.4). The summer of 2002 had the highest percentage of Map Type I occurrences (25%) and O_3 levels. However, 2002 also exhibited the highest percentage of Map Type III occurrences (15%) which were associated with low O_3 (Figure 2.2h). In contrast, 2004 had about the same number of Map Type I occurrences as did the moderate years 2000, 2001, and 2003 and actually had fewer Map Type III occurrences (9%) than 2002. We also examined the average persistence of each map type during the

five years and found that there were no distinct differences between the persistence

values from year to year that could explain the differences in O_3 levels. Clearly, summer

O_3 concentrations are dependent on a complex interplay between ozone precursors,

photochemistry, and meteorology that is not easy to predict.
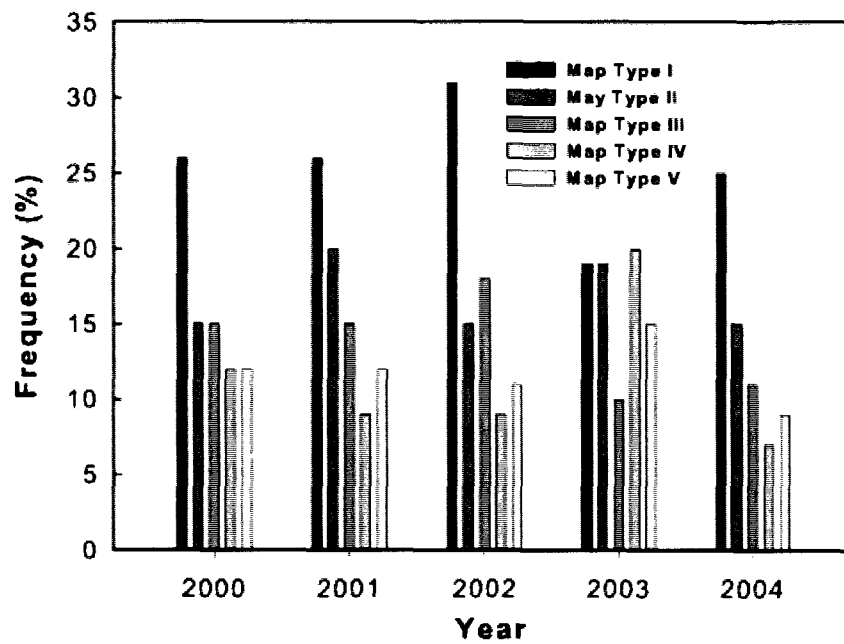
Figure 2.4. The frequency distribution of Map Types I-V for the five summers (2000-2004).

To quantify interannual variability captured by the surface circulation patterns, we multiplied the mean O_3 mixing ratios for each map type times the frequency of occurrence of each map type per year;

$$\overline{\overline{O_{3m}}} = \sum_{k=1}^{5} \overline{O_{3k}} F_{km} \qquad (2.2)$$

where, $\overline{\overline{O_{3m}}}$ is the mean O_3 mixing ratio per summer season m for the entire domain, $\overline{O_{3k}}$ is the mean O_3 mixing ratio per Map Type k and F_{km} is the frequency of occurrence of Map Type k for summer season m. The quantity $\overline{\overline{O_{3m}}}$ is analogous to the climatological component of the matrix operation developed by *Comrie* [1992b] to separate interannual variability of an environmental variable into its climatological (*e.g.* circulation types, temperature, humidity, and radiation) and environmental components (*e.g.* climate-induced changes in biogenic emissions and policy-mandated reductions in power plant NO_x emissions). The possible impact of the power plant NO_x reductions on O_3 levels is discussed in the section called "Improved Parameterization of O_3" which appears later in this chapter.

Using Equation 2.2, the reconstructed interannual variability was nearly flat with a maximum-minimum difference of ~1 ppbv and a peak value of 59 ppbv (Figure 2.5). The actual interannual variability for all days showed a peak-to-peak difference of 12 ppbv with a maximum of 64 ppbv in 2002 and minimum of 52 ppbv in 2004 (Figure 2.5). Based on the frequency of Map Type occurrences alone, the reconstruction captured <10% of the observed variability.
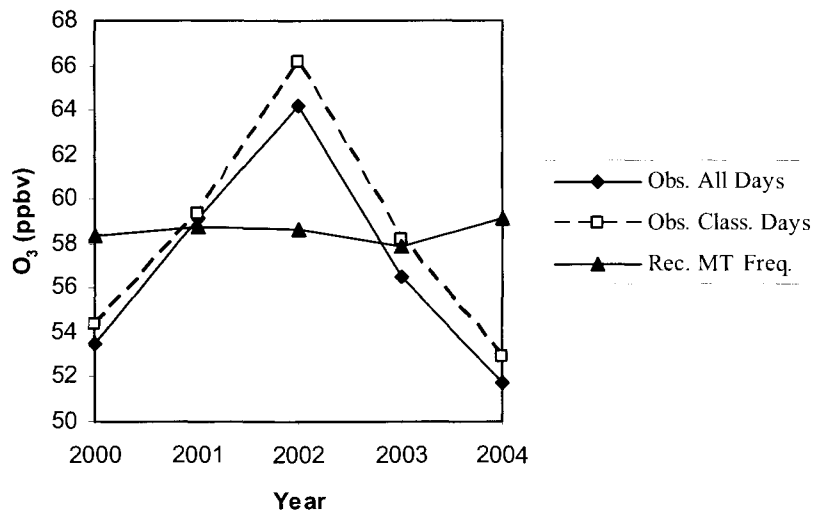
Figure 2.5. The domain-averaged interannual O_3 trend for the study domain for the observations on all 610 days (Obs. All Days in solid diamonds), the observations on the 396 days that had classified circulations (Obs. Class. Days in open squares), and the reconstruction from the map type frequencies according to Equation 2.2 (Rec. MT Freq. in solid triangles).

The reason for the poor performance of the summer O_3 reconstructions based on map type frequency may be twofold. First, there were a large number of unclassified days with high or low O_3 which were not included in our analysis. However, except for an average bias of 1.2 ppbv, the interannual variability of the mean summertime O_3 for the subset of days with classifiable circulations compared well with the interannual variability for all days (Figure 2.5). This result indicates that the classified days were representative of the actual interannual variability. Second, there was interannual variability of mean circulation features within each of the circulation types (hereinafter referred to as within-type) which contributed to varying O_3 levels in each map type with uncharacterized importance.

Linkage of Interannual Variability in Circulation Intensity with O_3

On a seasonal time scale the within-type circulation variations could be depicted as differences in the mean position, size or central pressure of the dominant circulation feature (i.e., a high or low center). This was demonstrated by the mean SLP analysis for each map type as depicted in Figure 2.6. Small shifts in position and size are possible in the map typing classification scheme since the correlation criteria was not 1.0. In addition, differences in central pressures of circulations are not accounted for since all the grid point values are normalized by the domain mean values $\bar{x}$ and $\bar{y}$ in Equation 2.1. Within-type circulation variations produced deviations from the mean map type meteorological and air quality conditions, thus producing an effective circulation intensity. There was apparent interannual variability in effective circulation intensity during five-year study period, most notably between the years 2002 and 2004.
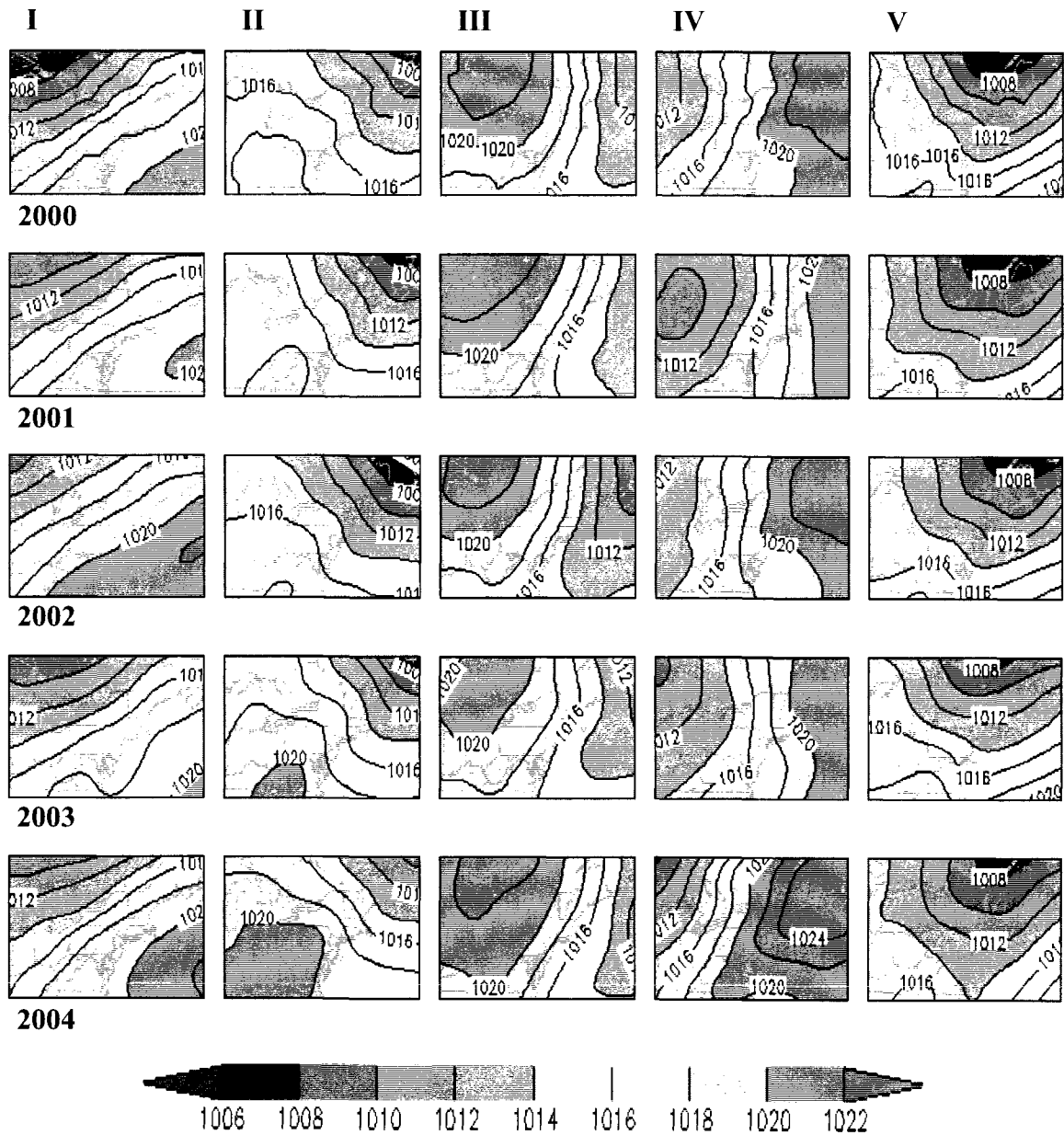
Figure 2.6. The Mean SLP (hPa) for each map type and summer. The year (2000-2004) of each summer appears below each row on the left and the map type (I-V) is indicated at the top of each column. The SLP contour interval is 4 hPa.

For Map Type I the 1020 hPa contour was much further on-shore in 2002 than in any other year suggesting a more intense Bermuda High pattern which produced warmer, more stagnant and less cloudy conditions over the Northeast. In contrast, the high pressure system of Map Type II was weakest in 2002 with a central pressure just over 1018 hPa in the extreme southeast corner of the domain. It was strongest in 2004 with a central pressure near 1022 hPa. These characteristics resulted in weakened transport of cooler, aged Canadian air into the northeastern half of the study domain during 2002 compared to 2004.

The large Canadian high pressure represented by Map Type III was by far the strongest in 2004, with an average central pressure near 1023 hPa and a closed 1016 hPa isobar extending to the east coast of New England and as far south as the Gulf of Mexico (expanded domain plot not shown). It also appeared strong for 2000 and 2001 but was weakened considerably in 2002 and 2003. This indicates that cooler, drier and relatively aged air was situated over much of the Northeast in 2004, 2000, and 2001, in contrast to 2003 and especially 2002.

For Map Type IV, the most striking difference was the strength of the offshore high in 2004. This system had a closed 1024 hPa isobar extending into southwestern New England and a 1020 hPa isobar protruding into the southern Appalachian Mountains. For this map type, 2004 featured cooler conditions and a greater influence of maritime air over the Northeast than during any of the other years. Examination of Map Type V showed only minor differences in the strength of the trough along the East Coast. However, the trough was somewhat deeper in 2004 as evidenced by the location of the

1014 hPa isobar which extended to just off the coast of the Carolinas, a meteorological situation that facilitates stronger and more penetrating cold fronts.

We used an analysis of summertime storm tracks to further illustrate and understand interannual variability in the effective intensity of map type patterns. To do this, changes in storm track dynamics were assessed for the highly divergent years of 2002 and 2004. The track of cyclones, which facilitates Canada-U.S. transboundary transport as well as the North American outflow, affects the characteristics of the synoptic pressure systems over the eastern U.S. Hence changes in position and frequency of these systems can impact the conditions that are relevant to regional in situ O_3 chemistry, its influx to the Northeast, and subsequent export to the North Atlantic.

Our examination of the storm tracks over the eastern portion of North America using NNRA cyclone frequency data revealed marked differences between the summers of 2002 and 2004 (Figure 2.7). In 2002 the Northern Canadian storm track merged with a narrow track emanating east of the Rocky Mountains and continued eastward in a narrow band before finally merging with the East Coast track east of Labrador. It was apparent that most of the continental cyclones tracked well north of our study area and cyclones along the East Coast were infrequent and usually originated well offshore. Based on the NHC storm tracks, there were only 5 different tropical systems during 2002 that tracked through our domain resulting in 9 tropical storm days.

In contrast, during 2004 there was a weak storm track in Northern Canada that merged with the Rocky Mountain track to form a broad storm track over Southern Canada and the Northeast. Again, many of the cyclones tracked well north of the study domain, but about a third of them tracked right along or just south of the U.S.-Canadian

border. There was also a very active cyclone track that extended from the Gulf of Mexico, across the Southeastern U.S. and northeastward toward Newfoundland where it merged with the Southern Canadian track. Many East Coast cyclones in 2004 were tropical in nature, with 8 different systems transecting our domain resulting in 24 tropical storm days. The tropical storm tracks for other study years were similar to those of 2002, highlighting the seemingly large and unusual influence of tropical systems on Northeast circulation dynamics during 2004.

The different storm tracks impacted interannual variability of the occurrence of map types and subsequently that of surface O_3 in two ways. First, the more southerly Canadian storm track and more vigorous East Coast storm track in 2004 created circulation patterns that were not common to the other study years. Consequently, summer 2004 had the lowest percentage of classified days with 55%. Second, the combination of the more southerly Canadian and stronger East Coast storm tracks caused cooler conditions with greater transport of aged air from Canada to the Northeast. This meteorological situation acted to reduce the frequency and effective intensity of stagnant high pressure systems over the eastern U.S. and minimize conditions favorable for in situ photochemical production of O_3. For example, the median mixing ratio of CO at TF was 181 ppbv in summer 2002 and 159 ppbv in 2004, along with temperatures in the northeastern U.S. during 2002 and 2004 that were +1.5°C warmer and -1.1°C cooler respectively compared to the 30-year average (1971 - 2000) (http://www.nrcc.cornell.edu/climate/Climate_summary.html).
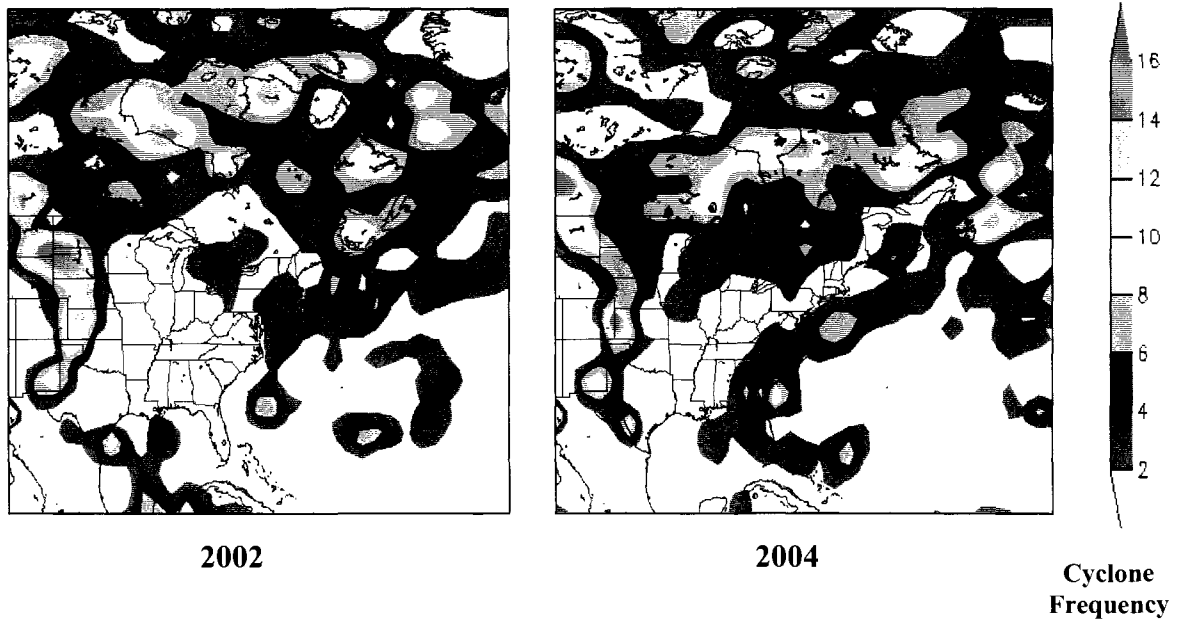
Figure 2.7. The frequency of cyclone centers passing through each grid point of the 250 km x 250 km equal area grid for the years 2002 and 2004.

Improved Parameterization of O_3

We identified potential links to the observed interannual variability of O_3 using indices that quantified the variability of effective intensity of circulation patterns. The indices included average transport gradients, positions of key isobars, the magnitude of corresponding upper level circulation features, and domain-averaged SLP. Domain-averaged SLP was the most universal metric that could be applied readily to all map types.

The physical connection of the domain-averaged pressure to the effective map type intensity should be similar for Map Types I – IV which are dominated by high pressure systems. In the case of Map Type V, a more intense East Coast trough would be reflected in a lower domain-averaged pressure. To examine this, domain-averaged pressure for each map type and year were calculated and the value termed the effective circulation intensity index (CII). Further, the quantities ΔO_3, the difference between the domain-averaged daily-maximum O_3 for a given summer and the corresponding 5-year summer average were determined.

We found moderate to strong linear correlations between ΔO_3 and CII for all map types except Map Type V (Table 2.3), and these results appear to be physically consistent with the circulation dynamics. The weaker correlation coefficient for Map Type V can probably be explained by the dual role of the East Coast trough which tends to increase O_3 levels on its eastern side but decrease O_3 to the west. Based on the linear correlations, we modified Equation 2.2 by adding the ΔO_3 term to the reconstructed mean value for each map type.

$$\overline{\overline{O}}_{3m} = \sum_{k=1}^{5} \left(\overline{O}_{3k} + \Delta O_{3km} \right) F_{km} \qquad (2.3)$$

The ΔO_3 value for each year was calculated from a linear fit of ΔO_3 to CII for each map type as shown in Figure 2.8 for Map Type III.

Table 2.3 Linear correlation coefficients for ΔO_3 versus the circulation intensity index for each map type and for all types together.

Map Type	Correlation Coefficient (r)
I	0.55
II	-0.72
III	-0.94
IV	-0.46
V	0.23
All Types	-0.17

These modifications produced an interannual variability curve that was in reasonable agreement with the observed one (Figure 2.9). It produced a peak value of 63 ppbv in 2002 compared to the observed value of 64 ppbv for all days and 66 ppbv for classified days only. There was a decrease in 2004 to the lowest value of 57 ppbv, which was somewhat higher than the observed 52 ppbv for all days and 53 ppbv for the classified subset. Overall, the curve covered a range of 5.7 ppbv that represented ~46 % of the observations for all days and 44 % for classified days. Although not considered in this study, some of the observed O_3 variability was undoubtedly attributable to environmental factors such as the sensitivity of biogenic emissions to temperature and perhaps more importantly to a significant reduction in anthropogenic O_3 precursors during the study period.
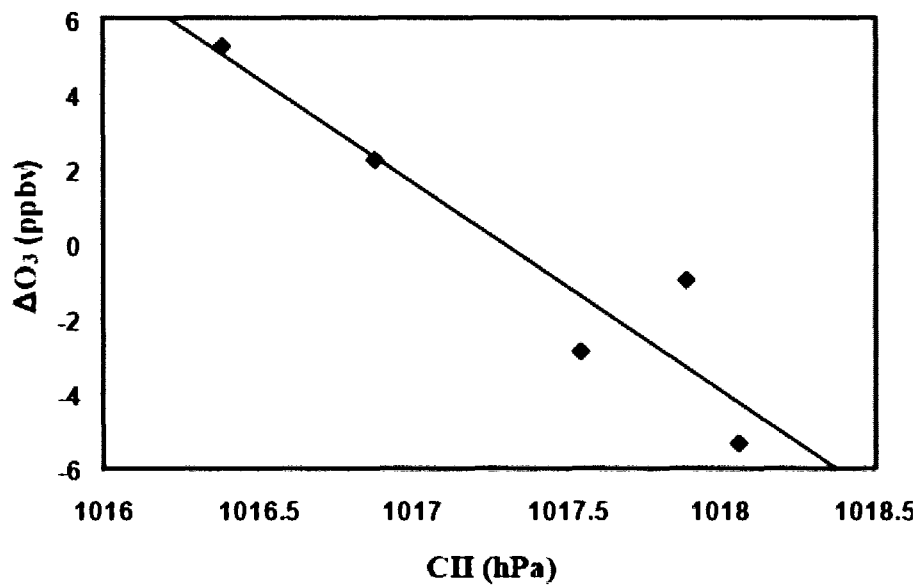
Figure 2.8. Scatter plot of ΔO_3 (ppbv) versus the circulation intensity index (CII, hPa) for Map Type III. The CII is the mean sea level pressure for the map type for a summer. The best fit line and correlation coefficient (r) appear on the plot.
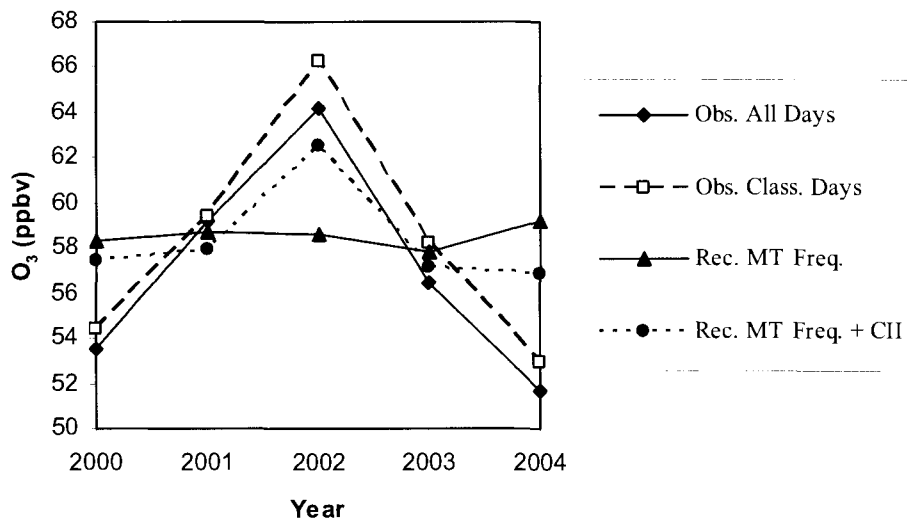
Figure 2.9. The domain-averaged interannual O$_3$ trend for the study domain for the observations on all 610 days (Obs. All Days in solid diamonds), the observations on the 396 days that had classified circulations (Obs. Class. Days in open squares), the reconstruction from the map type frequencies according to Equation 2.2 (Rec. MT Freq. in solid triangle) and the reconstruction from map type frequencies and the circulation intensity index (CII) term according to Equation 2.3 (Rec. MT Freq. + CII in solid dots).

34

In compliance with several statutes passed in the 1990s power plants in the eastern U.S. reduced summertime emissions of NO_x by approximately 50% between 1999 and 2003 [*Frost et al.*, 2006]. Since 2003 the EPA estimates even greater NO_x reductions [*EPA*, 2005]. These reductions could contribute to the dramatic drop in O_3 levels from 2002 to 2004. However, the changes in overall NO_x emissions are not clear because the NO_x emissions from mobile sources have reportedly increased at the rate of 1.9% yr^{-1} during the past 15 years [*Parrish*, 2006]. Moreover, many of the largest reductions in power plant emissions have come in typically NO_x-rich regions which would make them less effective in reducing O_3 levels. In fact, a case study by *Frost et. al.* [2006] which incorporated the reduced power plant emissions into the Weather Research and Forecasting model with online Chemistry (WRF-Chem) actually showed an increase of 2 ppbv in O_3 levels over much of western PA, OH, and MD. Thus it is difficult to directly estimate what impacts these reductions power plant NO_x had on the O_3 interannual variability reported for our study domain.

In an independent study the EPA used a statistical model to account for the impact of weather (e.g. temperature, humidity, winds) on average daily maximum 8-hour O_3 levels over the eastern U.S. for the May – September O_3 seasons of 2002 and 2004 [*EPA*, 2005]. The study indicated that O_3 levels were 17% lower in 2004 than in 2002, and that 41% of the total reduction in those two years respectively was due to weather, i.e. it was much cooler and wetter in 2004 than in 2002. This result agrees reasonably well with our reconstructed O_3 trend based on circulation dynamics which captured 46 % of the actual trend. The modest differences between the two results were likely due to a combination of factors including the choice of study domain, the use of average daily

maximum 1-hour versus 8-hour O_3 level, and different statistical uncertainties in each of the techniques. Nonetheless, our results suggest that the intensity of dominant pressure systems during summertime is an important factor in understanding regional O_3 on seasonal and interannual time scales in the Northeast.

Conclusion

The five most common synoptic surface circulation patterns, referred to as map types, over the northeastern U.S. for summers 2000 - 2004 were identified objectively using a correlation-based classification technique. The highest O_3 levels over the entire Northeast were associated with Map Type I, the most common pattern that featured the Bermuda High. Elevated O_3 levels also existed on the western side of the high pressure system south of the Ohio Valley in Map type II. It also occurred east of an advancing cold front or the western side of a retreating anticyclone in Map Type V.

Low O_3 levels were associated with Map Types III and IV which depicted an anticyclone centered over the Upper Great Lakes and Southern Canada, and a coastal anticyclone/Midwest cyclone or trough combination respectively. The anticyclone of Map Type III appeared to suppress O_3 levels by providing air with low levels of O_3 precursors from Canada to the Northeast, while the onshore winds and cloud cover associated with Map Type IV likely acted to further inhibit O_3 production over land.

There was notable interannual variability in O_3 levels throughout the study period. The domain-averaged seasonal mean daily maximum O_3 level rose to a peak of 64 ppbv in 2002, which represented a statistically significant departure from the 5-year mean at the p = 0.05 level. Ozone declined to its lowest value of 52 ppbv in 2004 (p = 0.10 level).

An improved reconstruction of O_3 interannual variability was developed by incorporating a ΔO_3 term based on the circulation intensity index for each map type. This reproduced 46% the observed O_3 interannual variability, compared to <10% using only a frequency of occurrence term. The rest of the variability was probably due to circulations not adequately addressed by our classification procedure and to environmental factors including recent reductions in power plant emissions of NO_x over the Eastern U.S. and the impact of temperature on biogenic precursor emissions. Finally, by analyzing NCAR/NCEP Reanalysis storm tracks we demonstrated a link between interannual variability of climate and the intensity of map type patterns.

There are three potential improvements which may help yield a more accurate reproduction of the interannual variability of O_3. First, increasing the number of map types by tightening the correlation criteria might strengthen the relationships between circulation and O_3 level. However, the drawback to this approach is that an increase in the number of circulation types would require much longer study periods to establish meaningful per-type mean O_3 levels. This longer time period might incorporate even more changes in emission levels than occurred during the current study period which could potentially obscure the circulation-O_3 relationships. Second, interannual circulation variability may be better characterized by multiple indices rather than a single circulation intensity index. Third, the actual relationship between summertime O_3 level and circulation might be better characterized with a non-linear function. Future research should focus on developing more sophisticated parameterization of the relationship between the interannual variability of circulation and surface O_3.

37

CHAPTER III

SYNOPTIC INFLUENCES ON SPRINGTIME TROPOSPHERIC O_3 AND CO OVER
THE NORTH AMERICAN EXPORT REGION OBSERVED BY TES

<u>Introduction</u>

The tropospheric ozone (O_3) column abundance sheds insight on the influence of
anthropogenic activities on the global atmospheric composition. For decades the
tropospheric O_3 column was estimated based on the satellite measurements of the total
column and the stratospheric profile due to lack of tropospheric vertical profiles
[*Fishman et al.,* 1990, 2005; *Creilson et al.,* 2003; *Stohl et al.,* 2003a]. These estimates
were highly uncertain, and it was difficult to obtain an understanding of vertical transport
of surface pollutants and stratospheric intrusions.

The launch of EOS-AURA on July 15, 2004 with the Tropospheric Emission
Spectrometer (TES) onboard, enabled for the first time quantification of the tropospheric
column and profile of O_3. TES is a Fourier transform infrared spectrometer designed to
measure global distributions of tropospheric O_3 and its precursors such as carbon
monoxide (CO) [*Beer et al.,* 2001]. These measurements may prove to be crucial for
the study of many global air quality problems, including the estimation of
intercontinental transport (ICT) of pollutants exported from North America.

North American outflow can travel from within the continental boundary layer to the Atlantic Ocean by low-level westerly winds, and portions of these plumes may be incorporated into the marine free troposphere because of the difference in continental and marine boundary layer structure [*Angevine et al.*, 2004; *Rodrigues et al.*, 2004]. This scenario enables O_3 to be slowly transported across the Atlantic Ocean (~10 days transport times in summer months) at low levels (2-4 km) but cut-off from the destructive (halogen) chemistry of the MBL [*Owen et al.*, 2006]. Pollutants may also be transported from the continental boundary layer in a warm conveyor belt (WCB) of a synoptic-scale mid-latitude cyclone into streams of fast moving middle and upper tropospheric westerly winds [*Eckhardt et al.*, 2004; *Crielson et al.*, 2003; *Stohl et al.*, 2003a]. Some WCBs originating over North America can transport O_3 and precursors to the free troposphere over Europe within 4-5 days [*Stohl et al.*, 1999, 2003a] where descending motions carry them back toward the surface causing ground-level O_3 mixing ratios to rise, but so far this has only been observed at high elevation sites in the Alps [*Huntreiser et al.*, 2005]. However, the same cyclones responsible for lofting O_3-forming anthropogenic pollutants from the continental boundary layer to the free troposphere may also mix down O_3 of stratospheric origin, which inevitably complicates the quantification of the tropospheric O_3 budgets [*Cooper et al.*, 2001, 2002a; *Moody et al*, 1996; *Merrill et al.*, 1996; *Oltmans et al.*, 1996; *Polvani and Esler*, 2007]. Thus information on the 3-dimensional distribution of O_3 and its precursors as well as the air mass transport history are required to ascertain the contributions of the various sources to observed O_3 levels.

A number of field missions (e.g., NARE, NEAQS2002, and INTEXA/ICARTT2004) have been dedicated to understanding the composition of North

American outflow [e.g., *Parrish et al.,* 1993, 1998; *Banic et al.,* 1996; *Berkowitz et al.,* 1996; *Cooper et al.,* 2001, 2002a, 2005; *Fehsenfeld et al.,* 2006; *Singh et al.,* 2006; *Mao et al.,* 2006]. In many of these studies critical vertical information was obtained via highly coordinated measurement programs involving ozonesonde networks, ships and aircraft. However, these observations were only feasible for short intensive study periods over limited areas and were sparse in overall density. Therefore long-term continuous measurements over extensive areas are highly desirable to fill this critical data gap.

A few modeling studies have complimented the field campaigns by examining 3-dimensional distributions of O_3 over the North Atlantic and Europe as a result of North American outflow for extended periods [*Kasibhathatla et al.,* 1996; *Jacob et al.,* 1993; *Li et al.,* 2005; *Auvray and Bey,* 2005]. However, uncertainties in emissions profiles, the lack of observations for the initialization of chemical fields, and the inherent uncertainties in the modeling of atmospheric circulations and chemical processes present significant challenges in interpretation of the results [*Auvray et al.,* 2007].

The ultimate application of TES measurements is to help address some of these challenges by providing a continuous independent 3-dimensional observational data base for comparison with other observations and model simulations, and to improve model performance through data assimilation techniques. However, they must first be thoroughly examined and evaluated for accuracy and information content. Such efforts are currently ongoing and have included the statistical validation of TES O_3 profiles against global sets of ozonesondes [*Worden et al.,* 2007, *Nassar et al.,* 2008] and comparisons with aircraft and ground-based measurements over the highly polluted regions such as Mexico City [*Shim et al.,* 2007]. *Zhang et al.,* [2006] have examined

North American export and found a positive correlation between lower-middle tropospheric TES O_3 and CO downwind of the U.S. for July 2005. However, a yet unexplored critical issue to the study of North American export is what these measurements suggest corresponding to the highly variable circulation patterns that affect the continental east coast and in particular the northeastern U.S. and adjacent Atlantic Ocean. In this study we aimed to identify and examine any discernable associations between the variability in O_3 and CO captured in TES observations and springtime synoptic-scale atmospheric circulations which regulate transport and dispersion of pollutants in the North American export region.

Tropospheric O_3 levels in many locations in the Northern Hemisphere show a distinct seasonal variation with levels peaking in spring and remaining high during the summer months [*Monks,* 2000]. However, the frequency of mid-latitude cyclones and anticyclones decreases in summertime and circulation over the eastern U.S. and western North Atlantic tends to be dominated by the large persistent subtropical Bermuda/Azores High [*Ziska and Smith,* 1980; *Bell and Bosart,* 1980; *Serreze et al.,* 1997; *Key and Chan,* 1999; *Owen et al.,* 2006]. Therefore, in this study we focused on the spring, i.e., March, April, and May (MAM), and classified the TES retrievals for the 2005 and 2006 seasons by circulation type over a domain covering the eastern U.S., southeastern Canada and the adjacent western North Atlantic Ocean.

Data and Methods

TES Data

Aura is in near polar, sun-synchronous orbit around the Earth with an ascending equatorial crossing at approximately 13:45 local time [*Schoeberl et al.,* 2006] (http://aura.gsfc.nasa.gov). Onboard Aura, TES scans the atmosphere in the infrared to measure O_3 and O_3 precursors such as CO. TES produces a 16-orbit Global Survey every other day while the alternate days are reserved for special observations over selected parts of the globe. For this study we used the TES Level 2 V002 Global Survey data [*Osterman et al.,* 2007a] during MAM of 2005 and 2006. The nadir on-the-ground footprint is approximately 5.3 km × 8.4 km [*Bowman et al.,* 2002; *Beer et al.,* 2001; *Beer et al.,* 2006]. The along-orbit spacing between footprints for the Global Survey runs was approximately 544 km before May 25, 2005 but improved to approximately 182 km after the limb scans were eliminated and replaced by an additional nadir scan [*Osterman et al.,* 2007b]. Each orbit was approximately 22° longitude apart. TES vertical coverage extends from 0 – ~33 km and in cloud-free conditions the vertical resolution is approximately 6 km with sensitivity to both lower and upper troposphere as well as the stratosphere [*Bowman et al.,* 2002; *Worden et al.,* 2004].

Atmospheric parameters are retrieved from the measured TES radiances using algorithms described by *Rodgers* [2000], *Worden et al.* [2004] and *Bowman et al.* [2002, 2006]. The retrieved vertical profiles can be related to the true profiles and a priori constraint profiles with the relationship:

$$\hat{x} = x_c + A(x - x_c) \qquad (3.1)$$

The vectors $\hat{x}$, x and x_c represent the retrieved, true and a prior constraint profiles respectively. Since the measured TES radiances are affected by a significant vertical extent of the atmosphere, the true state at any given atmospheric level can influence the retrieved state values at many adjacent levels. The averaging kernel matrix A defines the contribution of the each element of the true state vector to the retrieval at a particular pressure (or altitude) level. For example, the averaging kernel for a retrieved profile near 31° N and 74° W on April 6, 2006 indicated that the 681 hPa O_3 estimate was affected by the true state O_3 profile not only at 681 hPa but from all levels between approximately 900 and 450 hPa (Figure 3.1). This vertical smoothing effect which varies from profile to profile based on the meteorological parameters such as temperature humidity and cloud cover as well as the vertical distribution of O_3 or CO must be factored into any interpretation of the TES measurements.
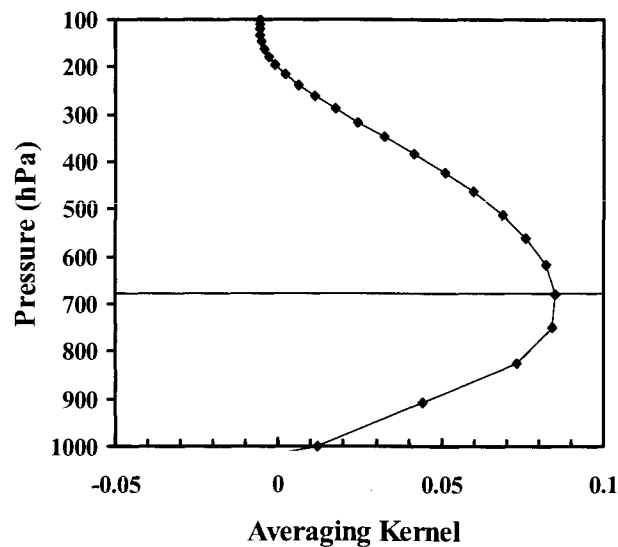
Figure 3.1. TES averaging kernel for 681 hPa O_3 for profile near 31° N and 74° W on April 6, 2006. A horizontal line marks the 681 hPa level.

43

A weakness of TES is its general inability to accurately measure boundary layer parameters for typical atmospheric conditions, except in regions where surface temperatures are over 300 K and the temperature contrast between the surface and the air is larger than 10 K [*Worden, J., et al.,* 2007]. However, retrievals of the lower free troposphere may show evidence of pollutants recently lofted from the boundary layer. In the context of the vertically smooth averaging kernels of the TES measurements we consider the lower free troposphere to range from approximately 850 – 550 hPa. For that purpose we chose to examine the O_3 and corresponding CO distributions at the 681 hPa retrieval level for which TES should have good sensitivity. We also examined the distributions at the 316 hPa level to contrast the upper and lower tropospheric distributions and to gain insight into different mechanisms controlling the lower free tropospheric O_3 in the export region of North America.

The TES retrieval products contain diagnostic information and flags for screening out failed profiles or those with reduced sensitivity [*Osterman et al., 2006b; Kulawik et al., 2006*]. We used the general retrieval quality flag which removes the most suspect profiles. In addition, we screened for clouds since they can impact the retrievals. For instance, *Kulawik et al.* [2006] estimated that the TES sensitivity to O_3 below a cloud with an optical depth of 1.0 will drop to approximately 30% of the clear sky sensitivity. The TES retrievals included information on cloud optical depth and cloud top pressure. The choice of a cloud optical depth threshold is complicated by the fact that the sensitivity below the cloud is influenced not only by the cloud optical depth, but also the temperature, surface conditions, and O_3 concentration. However, simulations of O_3 retrievals seemed to indicate that errors in retrieved total column and tropospheric

column in the presence of low clouds increased at optical depths of 0.75 and above (see Figure 7, *Kulawik et al.*, 2006). Therefore we screened out any retrieval with an average cloud optical depth in the $1000 - 1250$ cm^{-1} O$_3$ retrieval band greater than this value. For consistency we used the same optical depth threshold for the CO retrievals but also included the average cloud optical depth in the 2000-2200 cm^{-1} CO band. To avoid screening observations above the clouds we only applied the cloud screening for 681 hPa retrievals with cloud top pressure <700 hPa and for 316 hPa retrievals with cloud top pressure <350 hPa. We also screened for overall measurement sensitivity at the given retrieval level using the averaging kernel matrix, which is provided as a post-processing diagnostic, by eliminating those profiles for which the diagonal value at the level we were examining (681 or 316 hPa) was less than 0.01.

TES retrievals use the optimal estimation approach described by *Rodgers* [2000]. The retrievals require an a priori constraint to insure mathematical uniqueness. For O$_3$ and CO the constraint consists of a prior profiles and covariance matrices from a climatology developed using the MOZART model [*Brasseur et al.*, 1998]. The climatological a priori is made up of MOZART profiles averaged monthly over 10° x 60° latitude-longitude boxes [*Bowman et al.*, 2006]. The geographically variable a priori adds artificial structure, which can potentially obscure some of the real geographical variability of a trace gas. This artifact can be removed by reprocessing the TES O$_3$ and CO profiles with a universal a priori using a procedure developed by *Zhang et al.* [2006]. We generated a universal a priori by averaging all original a prior profiles in the 60° N - 60°S band and reprocessed the TES O$_3$ and CO data following *Zhang et al.* [2006]. Hereafter in this study all of the TES data presented will refer to the reprocessed data.

45

Meteorological Analyses

We used Global Final Analysis (FNL) data from the National Centers for Environmental Prediction (NCEP) to identify the predominant atmospheric circulation patterns over eastern North America and the North Atlantic Ocean during the time period 2000 – 2006. FNL products are available for 4 time intervals each day (00, 06, 12, and 18 UTC) on a 1° × 1° horizontal grid at the surface and 26 pressure levels vertically ranging from 1000 to 10 hPa [http://dss.ucar.edu/datasets/ds083.2].

In addition, we used HYSPLIT [*Draxler and Rolph*, 2003, http://www.arl.noaa.gov/ready/hysplit4.html] backward trajectories to aid us in determining the likely source regions for any O_3 and CO enhancements observed in the TES data downstream of North America. The HYSPLIT model was used in single trajectory and ensemble mode with both Global Data Assimilation System (GDAS) [*Derber et al.*, 1991; http://www.arl.noaa.gov/ss/transport/gdas1.html] and Eta Data Assimilation System (EDAS) [http://www.arl.noaa.gov/ss/transport/edas40.html] inputs. The GDAS data were on a 1° x 1° global grid and with vertical coverage from the surface to 20 hPa. The EDAS data were on a horizontal grid with 40 km spacing centered over the continental U.S. and extending northward into Canada to approximately 60° N, southward into Mexico to approximately 15° N, westward into the Pacific Ocean to approximately 140° W and eastward into the Atlantic Ocean to approximately 60° W [http://www.arl.noaa.gov/data/archives/edas40/EDAS40.gif]. The EDAS data extended vertically from the surface to 50 hPa. In the ensemble mode HYSPLIT generates a set of 27 trajectories by shifting the meteorological input fields by one grid point each in the east, west and vertical directions. By doing so the ensemble gives the probable range of

possible trajectories from a given location. This is helpful for circulation patterns with a high degree of spatial variability in which a small error in the selection of the starting point or in the meteorological input fields can result in large differences in trajectory pathways.

We also investigated the link between observed tropospheric O_3 enhancements and stratospheric intrusions using isentropic potential vorticity from the NCAR/NCEP 2.5° × 2.5° Reanalysis [NNRA, http://www.cdc.noaa.gov/cdc/reanalysis]. The NNRA isentropic potential vorticity analyses were available 4 times per day (00, 06, 12, and 18 UTC) at 11 isentropic levels for 270, 280, 290, 300, 315, 330, 350, 400, 450, 550, and – 650 K. We interpolated these data to constant pressure levels to facilitate use with NCEP FNL analyses and TES retrievals which were also on pressure levels.

Circulation Classification

Synoptic-scale circulation patterns over the North Atlantic were classified by applying the correlation-based map typing algorithm of *Lund* (1963) to the NCEP FNL SLP fields following the procedure described in Chapter II. However, for the case of springtime we used a critical correlation coefficient $r_{xy}=0.6$. Typically either the SLP or upper-level geopotential height (GPH) fields are chosen to represent the circulation patterns in the map typing algorithm. We found that, in comparison to SLP, the classification of the upper-level GPH was much less accurate with many patterns being incorrectly classified based on our subjective judgment of a representative sample. This is because the upper-level GPH fields tended to have smoother and less distinct features than SLP. Therefore we settled on using the SLP fields which are usually correlated with the upper–level patterns and yet exhibit distinct synoptic features such as cyclones,

anticyclones and frontal troughs.

The map typing domain extended from 35° N to 50° N latitude and from 80° W to 50° W longitude (Figure 3.2a). It covered much of the northeastern coast of the United States including the Washington D.C. to Boston megalopolis and extended eastward about a third of the way across the North Atlantic Ocean. The dimensions of the map typing domain were chosen to be just large enough to identify the unique synoptic features of each circulation pattern along the mid-latitudes of the North American east coast, which we hypothesized to be important controls on pollutant export, but small enough to insure accuracy in the synoptic classification. Synoptic patterns over larger domains are more difficult to classify because of the additional spatial variability inherently present over a greater area. To examine the larger-scale impact of the circulation patterns on the tropospheric distributions of O_3 and CO exported from North America the map typing domain was embedded into a larger study domain which extended from 25° N to 60° N and from 90° W to 40° W (Figure 3.2a).
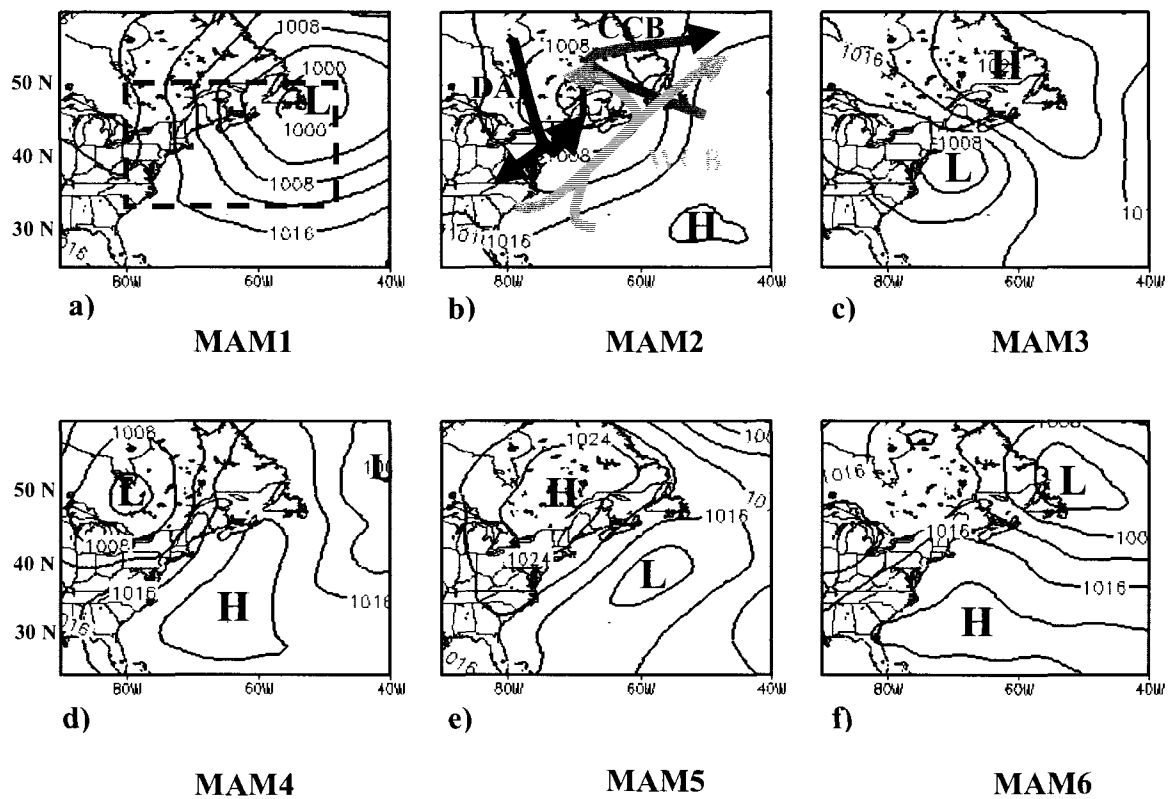
Figure 3.2. Composite sea level pressure (hPa) analyses from 2005-2006 for map types MAM1 – MAM6 (a-f). The boundaries of the map typing domain are show as dashed lines on a) and schematic representations of the warm conveyor belt (red curve), dry airstream (blue curve) and cold conveyor belt (green curve) are shown on b).

Synoptic Circulation Classification

We classified days based on six map types (denoted as MAM1-MAM6) identified for the spring seasons of 2005-2006 when TES V002 data was available. The map type frequencies and the important meteorological features associated with each map type are summarized in Table 3.1. Here we present a brief discussion as to how the patterns might relate to the major hypothesized transport pathways. In the next section we discuss in detail the impact of these circulation patterns on the tropospheric O_3 distributions observed by TES.

Map type MAM1 was the most frequent pattern, occurring on 24% of the days in springs 2005 – 2006 (Table 3.1). It featured a large, intense, and closed low centered east of Newfoundland, Canada (Figure 3.2a), which was typically the result of a rapidly deepening cyclone migrating northeastward along the U.S. east coast. Often these systems become so large and vertically deep that they disrupt the normal west to east progression of storm systems and they become quasi-stationary. Analysis of the sequencing of map types indicated that MAM1 persisted for 2-4 days in a row with a maximum duration of up to 10 days, particularly early in the season. The persistent pattern could thus produce a well-mixed troposphere by continuous vertical mixing around the center of the low. Another characteristic of MAM1 was that the surface low was typically associated with a closed upper-level circulation that extended above the 300 hPa pressure level and with 400 hPa potential vorticity (PV) > 1.4 potential vorticity units (PVU) on its western side (Figure 3.3a). The tropopause is typically defined as falling between 1 (*Shapiro,* 1987) and 2 PVU (*Appenzeller et al.,* 1996; *Lamarque et al.,* 1996; *Parrish et al.,* 2000). Therefore PV values over the range of 1 - 2 PVU extending

down into the troposphere are typically regions of stratospheric intrusions. This indicates that in MAM1 stratospheric influence reached at least as low as the 400 hPa level over south of Newfoundland, which may explain the higher levels of the 681 hPa O_3 in that area as discussed in the next section.

Table 3.1. Map types and meteorological characteristics.

Map Type	2005-2006 Frequency (%)	Characteristics
MAM1	24	• Large semi-stationary low pressure center northeast of Canadian Maritimes • Persistent subsiding northwest flow over northeast U.S. • Rising motion due to weak cyclonic disturbances to the south and WCB well offshore
MAM2	19	• Cyclone tracking into northern New England and Canadian Maritimes • Some weak secondary coastal development, • Rising motion along east coast and offshore in WCB
MAM3	15	• Developing coastal cyclone possibly associated with mature cyclone inland, • East-northeast flow along coast with • Rising motion over the ocean and northern coastal areas in WCB • Some cyclones persistent particularly in late spring
MAM4	5	• Anticyclone offshore • Subsiding flow over ocean near coast • Strong descent in DA of cyclone well out-to-sea
MAM5	11	• Cyclone offshore with WCB rising motion to the south and east and DA descent between cyclone and coast • Anticyclone in southeastern Canada with weak subsidence right along east coast
MAM6	7	• Large subtropical anticyclone off east coast • Weak subsidence along U.S. coast and immediately offshore in light southwesterly and westerly • Cyclone center near Labrador with DA descent in northwest flow over Canadian Maritime provinces extending out to sea
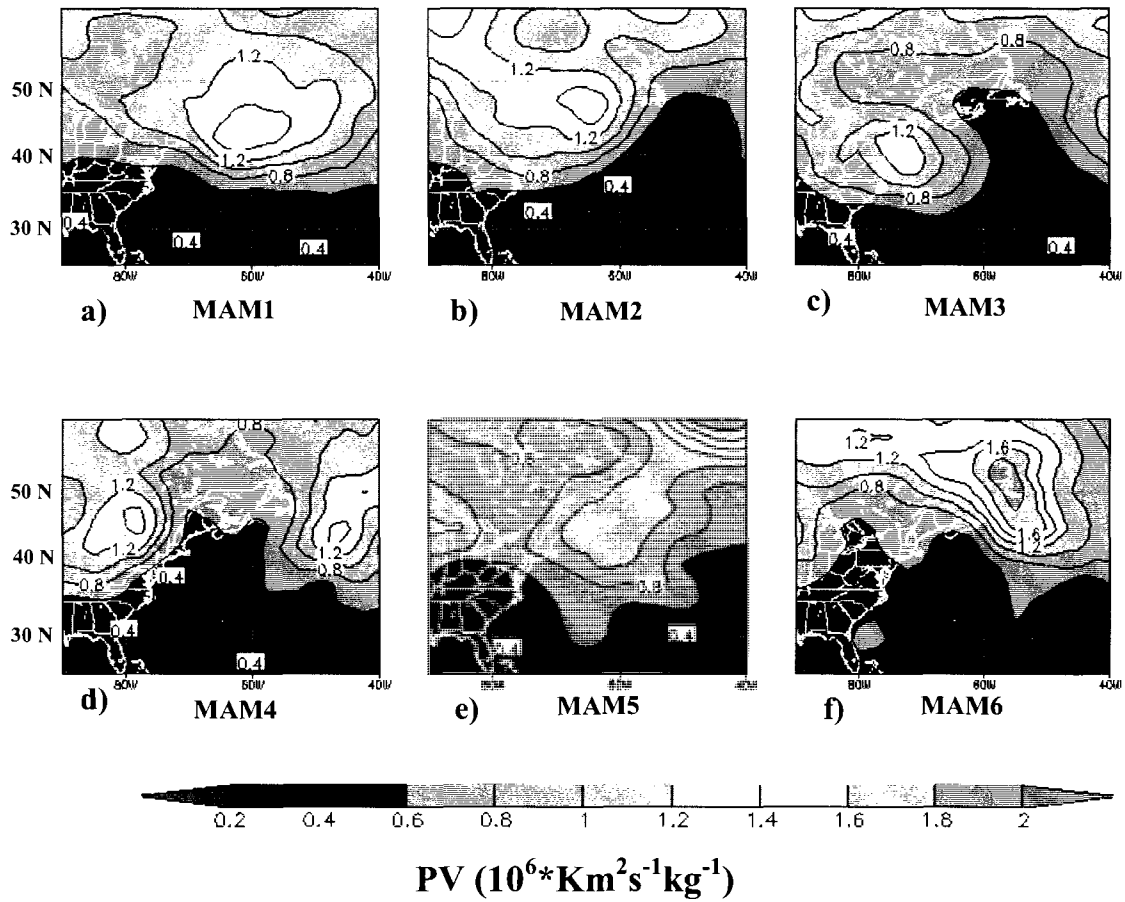
Figure 3.3. Mean 400 hPa potential vorticity (PV) for MAM1-MAM6 interpolated from the isentropic surfaces of the NCAR/NCEP Reanalysis (a-f). 1 PVU is $10^6 * Km^2 s^{-1} kg^{-1}$

Map types MAM2 and MAM3 depict smaller and generally more mobile cyclones near the east coast (Figures 3.2b-3.2c). These systems occurred on a total of 50% of the spring days in 2005 - 2006 and typically featured distinct ascending and descending air streams (Table 3.1). The WCB, one of the main ascending streams, is located to the east of the cold front and generally originates in the lower troposphere [*Carlson*, 1980; *Eckhardt et al.*, 2004]. In the northern hemisphere the WCB is located on the eastern side of an upper level trough and ascends into the mid- and upper troposphere on a general southwest to northeast trajectory (Figure 3.2b). The WCB may be intercepted by the fast moving upper level winds that transport pollutants rapidly downstream of the cyclone. This process has been documented through aircraft measurements [*Cooper et al.*, 2001, 2002a; *Parrish et al.*, 2000; *Stohl and Trickl*, 1999; *Stohl et al.*, 2003b; *Trickl et al*, 2003]. This transport pathway is also described by *Owen et al.* [2006] with regards to transport to the Azores.

Note that a part of the WCB, termed the secondary WCB, may branch off to the west and turn cyclonically around the center of the low. Steered by the northwesterly winds on the western side of the low the air mass can experience isentropic descent into the mid and lower troposphere (Figure 3.2b). This pathway, described as a secondary WCB, could also be an important mechanism for transporting pollutants from the urban areas of the U.S. east coast to the lower free troposphere of the western North Atlantic. The other major ascending air stream is the cold conveyor belt (CCB) (Figure 3.2b) (*Carlson*, 1980). For east coast cyclones this airstream typically originates from the lower troposphere over the ocean where it intercepts primarily aged air, but it can entrain pollution as it heads west across eastern North America. However, it occurs

characteristically within very cloudy regions not conducive to photochemical production of O_3 (*Cooper et al.*, 2001, 2002a).

The main descending airstream of the cyclone is usually referred to as the dry airstream (DA) (Figure 3.2b) because it transports drier air from the upper troposphere and lower stratosphere to the mid-troposphere with some strong systems allowing for direct transport to the lower troposphere [*Carlson*, 1980, *Cooper et al.*, 2002a]. Along with low humidity the air transported in the DA is also normally O_3-rich and therefore influences the O_3 distributions of the lower troposphere [*Merrill et al.*, 1996; *Moody et al.*, 1996; *Oltmans et al.*, 1996; *Cooper et al.*, 2001, 2002a].

The differences in the map types MAM2 and MAM3 were mainly due to the position and history of the cyclones. The cyclones depicted in MAM2 were generally mature systems that had tracked from the central U.S. to the Canadian Maritimes over several days. The WCB of these systems possibly encountered many high emission regions of eastern North America. The MAM3 map type depicted cyclones that developed along the U.S. east coast with areas of easterly flow in northeastern states. In late spring the MAM3 pattern tended toward episodes of persistence as small cyclones developed along the coast to the east of an inland upper-level cut-off low, and then stalled along the coast or rotated back around the inland system. For example in both May 2005 and 2006 there were episodes of MAM3 which persisted for 6 days or more.

Map types MAM4-MAM6 featured anticyclones along the U.S. east coast with cyclones well-inland or out-to-sea, and thus for these map types WCB lofting of continental boundary layer air was less influential than for map types MAM2 and MAM3. However, the DAs to the rear of the ocean cyclones of MAM4 and MAM5 seemed to

influence areas of the western North Atlantic Ocean as will be discussed in Section 4. Map type MAM6 occurring on only 7% of the days, featured a broader subtropical anticyclone centered off the east coast extending well out-to-sea and westward into the southeastern U.S. with a cyclone well to the northeast near Labrador. Such a circulation pattern typically produces a large area of weak subsidence extending from the east coast to the central North Atlantic Ocean restricting synoptic-scale lofting of boundary layer pollutants to the free troposphere. Furthermore, the northerly location of the cyclone and its orientation shown in Figure 3.2f suggests that the influence of the DA might also be weak throughout most of our study domain; leading to generally smooth pollutant distributions.

Association between O$_3$ Distributions and Circulation Types

Composites of the 681 hPa and 316 hPa O$_3$ and CO for the entire season and individual map types were created by interpolating measurements from the orbital overpasses to a 1° x 1° grid using a Gaussian weighting scheme similar to that described in *Luo et al.* [2002]. If no observations existed within 350 km of a grid point, typically because of quality or cloud screening, this point was masked out of the analysis.

First, we created full seasonal composites for the 681 hPa O$_3$ and CO which included all the observations regardless of map type (Figure 3.4). The mean 681 hPa O$_3$ seasonal composite indicated elevated levels (55 - 65 ppbv) over the western Atlantic Ocean south of 45° N, ~1000 km downwind of the U.S. (Figure 3.4a). There was a corresponding feature in the mean CO composite with mixing ratios of 115 - 125 ppbv forming a belt emanating from the U.S. east coast that dissipated and narrowed before

turning northeastward following the prevailing lower tropospheric wind flow (Figure 3.4b). In the area of highest CO extending from the U.S. coast, between $75°W - 55°W$ and $30°N - 45°N$ (denoted hereafter as Region 1), we found a slight positive correlation of 0.22 between O_3 and CO with a slope of 0.13 mol mol^{-1} (Figure 3.5a and Table 3.2). However, further to the north and east in a region bounded by $45°N - 55°N$ and $65°W - 45°W$ (referred to hereafter as Region 2), where O_3 gradually dropped off to 50 - 55 ppbv, there was virtually no O_3-CO correlation (Figure 3.5b, Table 3.2).

The correlation of observed O_3 and CO is a useful diagnostic indicator of the photochemical processing of an air mass, and the O_3-CO slope value can be used to estimate the influence of exported anthropogenic pollutants and the efficiency of photochemical O_3 production [*Parrish et al.*, 1993, 1998; *Mao et al.*, 2004]. A large number of measurements at surface sites in eastern North America have indicated that typical summertime O_3-CO slopes range from $0.2 - 0.35$ mol mol^{-1} [*Parrish et al.*, 1993, 1998; *Chin et al.*, 1994; *Mao et al.*, 2004]. Aircraft measurements during the NARE93 and ICARTT 2004 summer campaigns indicated similar slopes, which took place in the lower free troposphere just east of the North American coastline [*Daum et al.*, 1996; *Zhang et al.*, 2006].
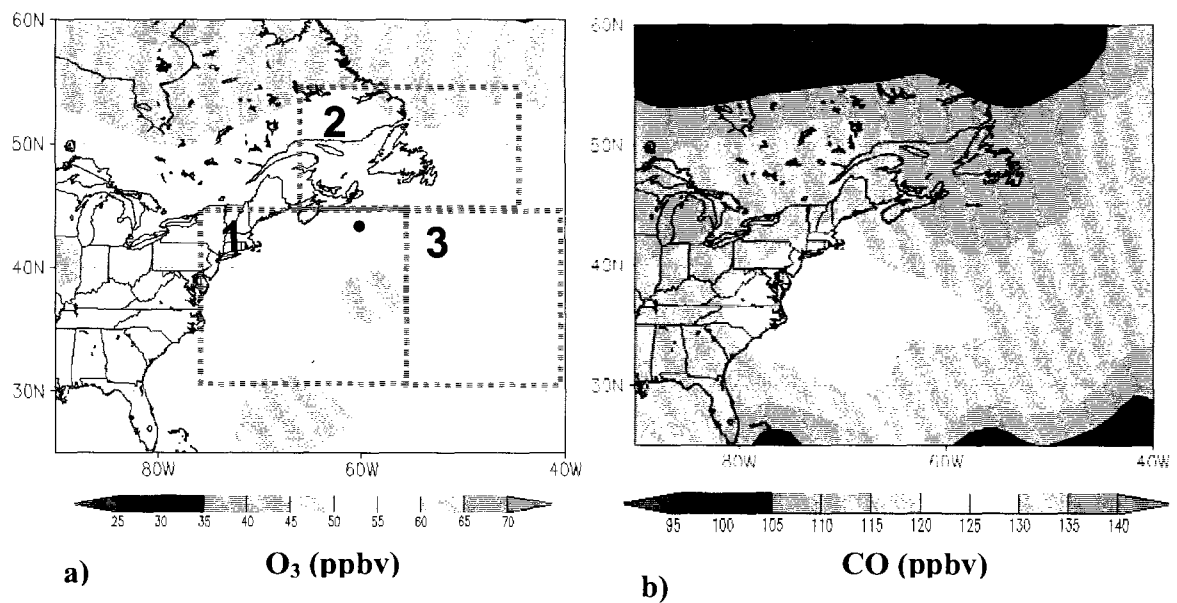
Figure 3.4. Spring seasonal composites for 2005-2006 of a) TES 681hPa O₃ (ppbv) and b) TES 681 hPa CO (ppbv). In a) the borders of Regions 1, 2, and 3 are shown as dashed lines and the location of Sable Island, NS is shown as a black dot.
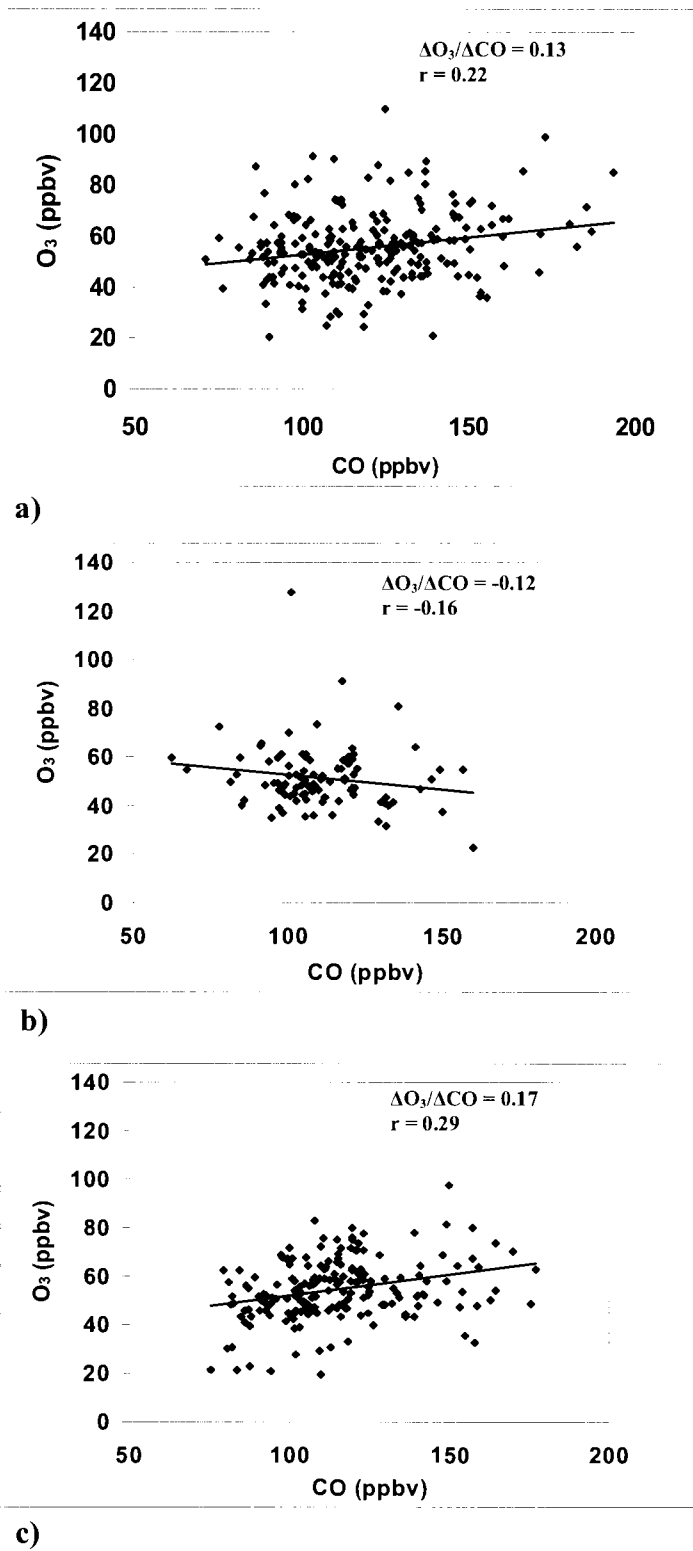
Figure 3.5. Scatter plots of TES 681 hPa O₃ versus CO retrievals during MAM 2005 -2006 for a) Region 1, b) Region 2 and c) Region 3.

Table 3.2. O_3-CO slope, correlation coefficient (r), and sample size N for circulation types in Region 1 30 – 45° N, 75-55° W, Region 2 45- 55° N, 65-45° W, and Region 3 30-45° N, 55-40° W.

	Region 1	Region 2	Region 3
All	0.13 (0.22)	-0.11 (-0.16)	0.17 (0.29)
	N=226	N=93	N=184
MAM1	0.12 (0.26)	-0.24 (-0.32)	0.20 (0.34)
	N=58	N=22	N=65
MAM2	0.19 (0.27)	-0.11 (-0.30)	0.27 (0.34)
	N=41	N=19	N=34
MAM3	0.20 (0.32)	0.38 (0.62)	0.29 (0.40)
	N=31	N=13	N=23

Fewer studies have been conducted for springtime, but analysis of spring measurements over 4 years in the 1990s at Sable Island, Nova Scotia indicated that the O_3-CO slope increases dramatically from near zero in March to approximately 0.35 mol mol^{-1} in May [*Parrish et al.*, 1998]. We acknowledge that care must be taken in comparing the O_3-CO slopes to earlier studies due to changing emissions of NO_x and CO in North America over time which may have impacted typical O_3-CO slopes [*Parrish et al.*, 2006; *Kim et al.*, 2006]. Nonetheless, our free tropospheric value of 0.13 mol mol^{-1} in Region 1 falls in the middle of this range and suggests that similar to summertime the pollutant plumes lofted to the free troposphere retain their near surface features. In Region 2, the lack of O_3-CO correlation indicated no significant photochemical production due to either limited sunshine or the lack of fresh exported pollutants. The fact that this area showed a relative minimum in CO (Figure 3.4b) suggests that the lack of exported pollutants was a more critical factor.

The seasonal composites of Figure 3.4 and the seasonal O_3-CO slopes showed strong evidence of continental export to the lower free troposphere. However, it should be noted that the cloud screening removed approximately 36% of the 681 hPa retrievals from the composite analyses and therefore the distributions are more representative of clear-sky or thin cloud cover conditions. *Crawford et al.* [2003] made the case using data from the TRACE-P aircraft campaign that pollutant levels should have a positive bias in cloudy areas. Therefore, the actual export signal could be even greater than that depicted in the TES composites. The export signal captured by TES comes mainly from portions of cyclonic airstreams conducive to export but with thin or broken cloud cover as is discussed in Section 5. All the TES retrievals were also grouped based on the map

type classification for the calendar day of the orbital overpass and the resulting O_3 and CO distributions are discussed in the subsections that follow.

MAM1

The 681 hPa O_3 levels for MAM1 were slightly elevated (~55 – 60 ppbv) in a region extending from the Canadian Maritimes southward over the western North Atlantic Ocean (Figure 3.6a). The circulation pattern, featuring the intense persistent low near Newfoundland, produced distinct chemical characteristics in Regions 1 and 2 reflected in the O_3-CO relationship (Figures 3.6a, 3.6g, Table 3.2).

Region 1 had a large offshore area of 681 hPa composite O_3 mixing ratios ranging from 55 to 60 ppbv corresponding to a belt of slightly elevated CO (120 - 125 ppbv) (Figures 3.6a and 3.6g). The presence of both elevated O_3 and CO levels in Region 1 produced a positive O_3-CO slope of 0.12 mol mol^{-1} (Table 3.2) indicating some anthropogenic influence. A composite of HYSPLIT 4-day back trajectories using GDAS data indicated that the majority of the air arriving in this region descended from the mid- and upper troposphere on northwesterly flow, as would be expected given the pressure pattern of MAM1 (Figures 3.2a and 3.7a). However, a few trajectories ascending from the Gulf Coast area could have injected anthropogenic pollutants into the large circulation systems (Figure 3.7a, Table 3.3), which may explain the positive O_3-CO correlation. These ascending trajectories, 30 % of which passed below 700 hPa over North America (Table 3), were associated with the mobile cyclones preceding the development of the large semi-stationary cyclone or other smaller ones that may have traveled southeastward along the southwest corner of the main circulation. A composite of HYSPLIT 4-day back trajectories for Region 2 (Figure 3.8) indicted that the air exiting Region 1 at levels

near 681 hPa could completely circulate around the cyclonic system within 3 days before re-entering Region 1 on the same northwesterly trajectory shown in Figure 3.7a. This suggests that pollutants entrained into these types of closed circulation patterns could potentially circulate around several times with gradual dilution and chemical transformation, resulting in relatively uniform moderate enhancements in O_3 and CO levels.

Region 2 featured O_3 mixing ratios 60-65 ppbv and relatively low CO (100-105 ppbv in the center of the region (Figure 3.6g), which yielded a negative O_3-CO correlation of r=-0.16 (Figure 3.5b, Table 3.2). This region was also associated with an extensive area of elevated O_3 (>160 ppbv) at the 316 hPa level (Figure 3.9a) and elevated PV values (>1.5 PVU) at the 400 hPa level (Figure 3.3a). These factors, combined with a lack of ascending trajectories over continental sources of pollutants (Figure 3.8), suggested that the enhanced tropospheric O_3 mixing ratios in Region 2 over the Canadian Maritimes were primarily a result of stratospheric inputs associated with the deep low pressure system. It should be cautioned that this enhancement in 681 hPa O_3 could also be partly a result of a shift toward higher altitudes (400 – 500 hPa) of the peak 681 hPa O_3 averaging kernels (not shown) in retrieval calculations. The shape of the averaging kernels can be impacted by non-related meteorological parameters such as temperature, water vapor, and clouds, and by the vertical distribution of O_3 itself. Therefore, this shift could just be a reflection of the greater concentrations at higher altitudes and may not extend all the way down to 681 hPa.
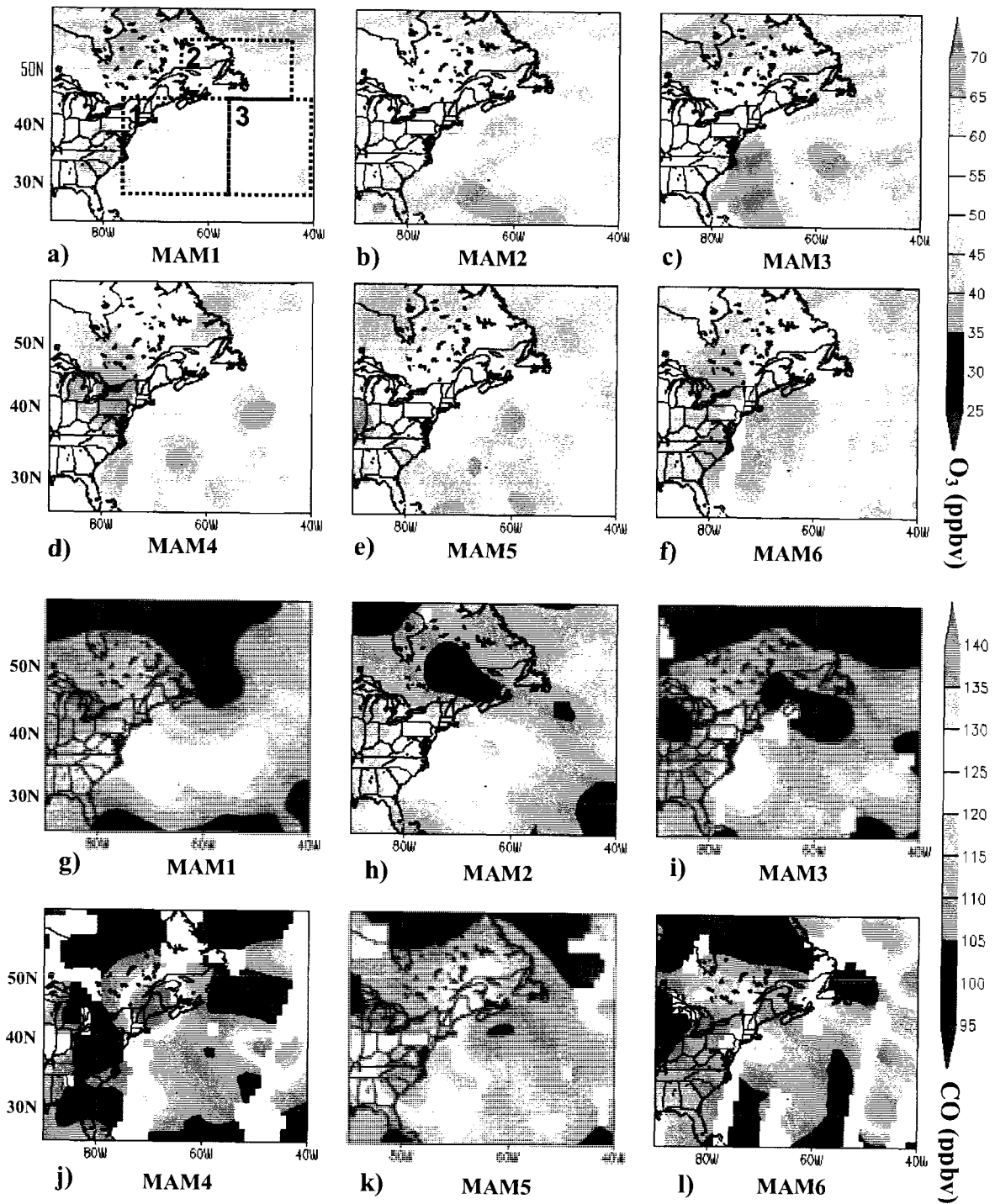
Figure 3.6. 681 hPa composites for MAM1 –MAM6 for O₃ (ppbv) (a-f) and CO (ppbv) (g-l). In a) the borders of Regions 1, 2, and 3 are shown as dashed lines.

64
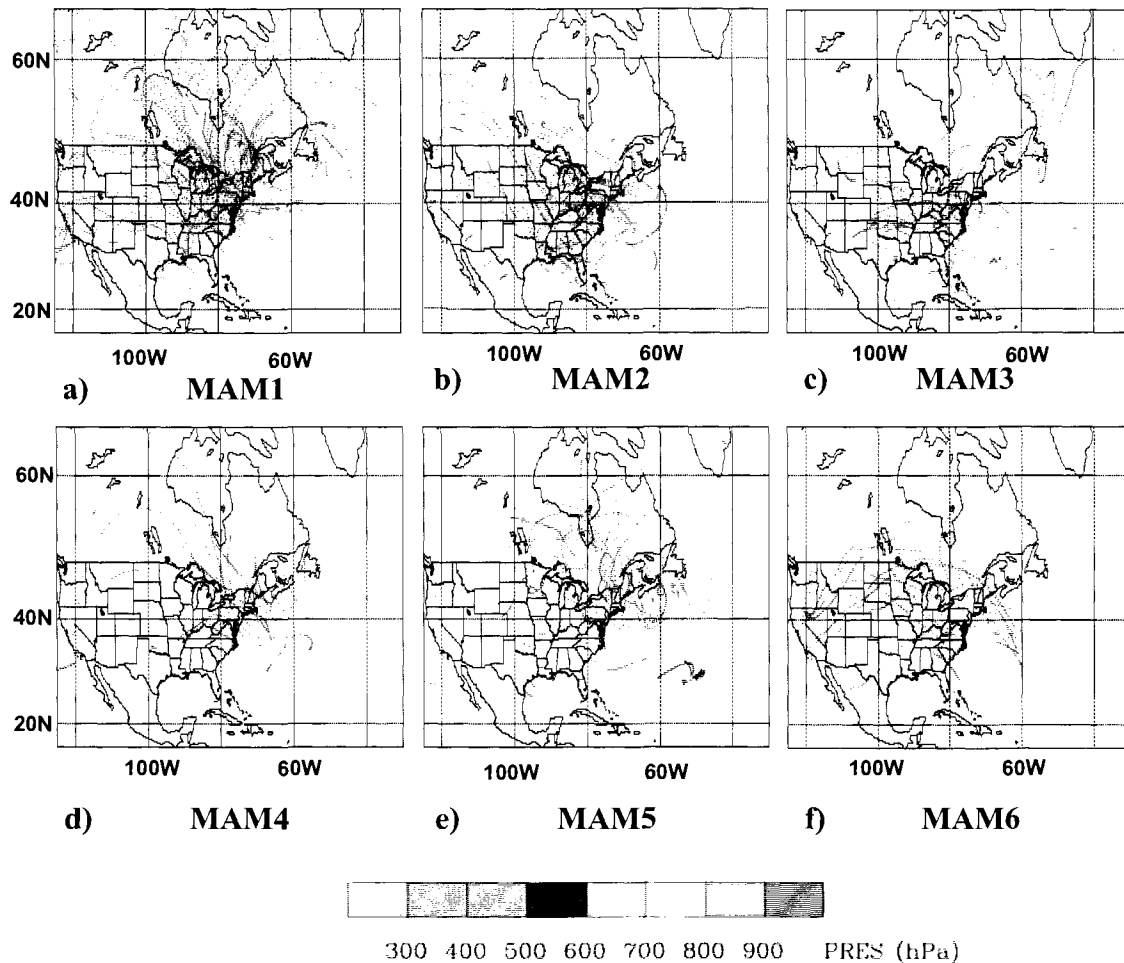
Figure 3.7. Four-day HYSPLIT back trajectories using GDAS data from locations of TES 681 hPa observations in Region 1 for map types MAM1-MAM6 (a-f). The colors indicate the pressure levels (hPa) of the trajectory parcels.

Table 3.3. The percentage of 4-day back trajectories starting from TES observation locations in Region 1 at 681 hPa that pass below pressure levels over the North America from 15-65°N and 125 – 70°W for map types MAM1 – MAM6 and for a random set of locations and times (1per day during MAM in 2006) denoted as RAN.

	(%) Below 700 hPa	(%) Below 800 hPa	(%) Below 900 hPa	N
MAM1	30	12	6	117
MAM2	44	17	6	98
MAM3	52	33	13	61
MAM4	4	0	0	23
MAM5	26	12	9	43
MAM6	25	13	5	40
RAN	43	26	11	92
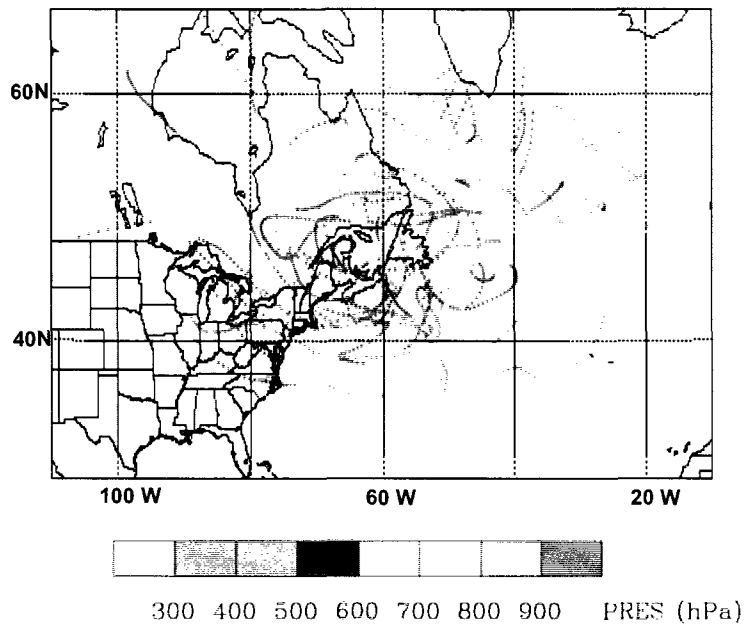
Figure 3.8. Four-day HYSPLIT back trajectories using GDAS data from locations of TES 681 hPa observations in Region 2 for map type MAM1. The colors indicate the pressure levels (hPa) of the trajectory parcels.
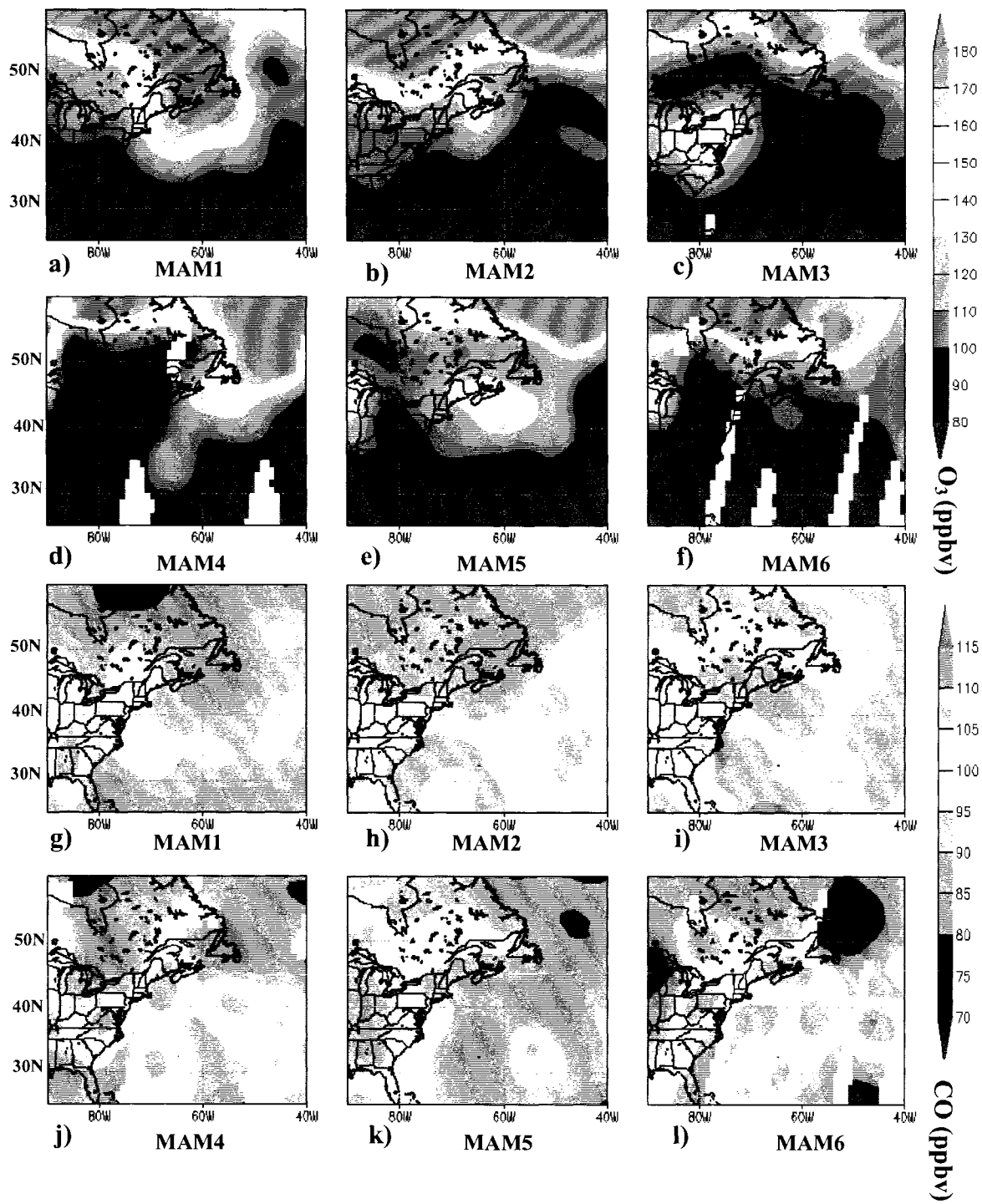
Figure 3.9. 316 hPa composites for MAM1 –MAM6 for O_3 (ppbv) (a-f) and CO (ppbv) (g-l).

MAM2 and MAM3

The smaller and more dynamic cyclonic systems located near the U.S. coast in MAM2 and MAM3 produced O_3 and CO composite distributions with greater spatial contrast compared to those in MAM1. At 681 hPa there was a general area of enhanced O_3 mixing ratios (>60 ppbv) extending from just off the U.S. coast to ~50°W south of ~45°N (Figures 3.6b and 3.6c). Enhanced O_3 roughly corresponded to enhanced CO (>120 ppbv), particularly near the U.S. coast (Figures 3.6h and 3.6i). The location of the enhanced O_3 and CO near and to the east of storm centers and downwind of the U.S. coast suggests that lofting of the pollutants from the continental boundary layer by the WCB airstreams played a major role in producing the enhanced O_3 levels for these map types.

The 4-day back trajectory composites for MAM2 and MAM3 showed that the majority of trajectories arriving in Region 1 came from the south and west which is consistent with WCB flow (Figures 3.7b and 3.7c). Some of the trajectories showed a circulation around the back of the low center in the secondary WCB branch passing over urban areas of the northeastern U.S. Furthermore, 44 – 52 % of the trajectories passed below the 700 hPa level and 17 -33 % passed below the 800 hPa level over the continent before finally being lofted to the 681 hPa level (Table 3.3). These percentages are notably greater than for any other map types and help explain the greater O_3 and CO levels in this region due to a stronger influence of WCB lofting. The fact that the percentages of lofting trajectories for MAM2 and MAM3 are only slightly greater than for a random sampling of locations, shown in the last row of Table 3.3, may be partly explained by the fact that the locations of the good TES retrievals are biased towards

areas with less cloud cover. We caution that trajectories based on 1° x 1° meteorological data may not accurately resolve the transport from the continental boundary layer and these percentages should be used to gauge the relative likelihood of receiving boundary layer air.

There were some differences in the 681 hPa O_3 and CO distributions between MAM2 and MAM3. For example the area of high O_3 over the ocean for MAM2 was generally off of the U.S. coast at latitudes north of the Carolina states, whereas for MAM3 it extended all the way to the coast and even inland. In addition, the CO enhancement in MAM3 was less and dropped off to the east more quickly than in MAM2. These differences are due in part to the circulation patterns. The MAM2 circulation featured a low over land with basically westerly to southwesterly flow at the coast, while the high and low pair in MAM3 resulted in an easterly component to the flow along the northern parts of the coast. Thus, for MAM2 the pollutants would be transported away from the coast, while for MAM3 some of the continental outflow might be re-circulated back toward the coast.

In general, we found that the 681 hPa O_3 and CO observations for map types MAM2, and MAM3 were positively correlated at r=0.27 and r=0.32, respectively, in Region 1 with corresponding positive slopes of 0.19 and 0.20 mol mol^{-1} (Figure 3.10, Table 2). These slopes are much lower than those reported by Zhang et al. (2006), who calculated a slope of 0.81 mol mol^{-1} and a correlation of r=0.53 for lower tropospheric TES measurements near this region. However, this may be partially explained by the fact that their measurements were in July for a more compact region centered further south, while ours included a larger region centered further north and included the months of

March and April when photochemical production is reduced.
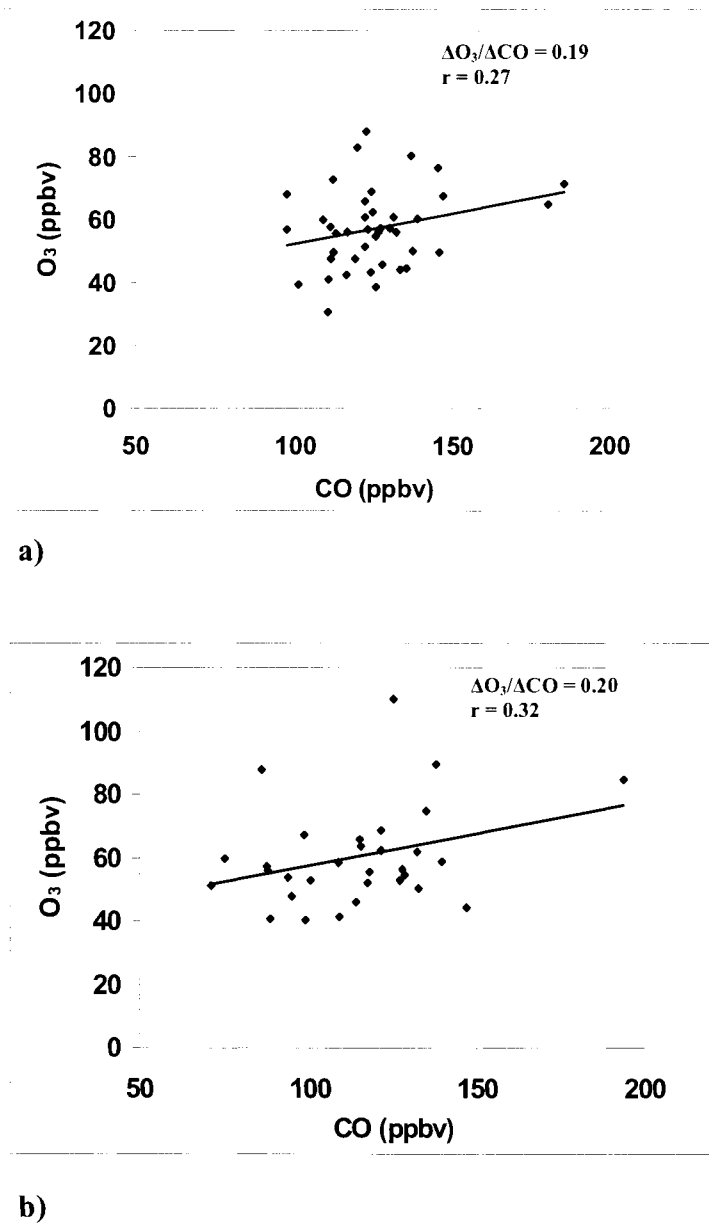
Figure 3.10. Scatter plots of TES 681 hPa O_3 versus CO retrievals in Region 1 for a) MAM2 and b) MAM3.

Since WCB lofting to the upper troposphere is an important mechanism for continental export of pollution, we examined the TES 316 hPa composites for evidence of this transport mechanism. The CO composites showed areas of enhanced CO off the southeastern U.S. coast particularly for MAM2 and MAM3. Correspondingly there were areas of enhanced CO in the lower troposphere (Figures 6g and 6h). However, while most of the GDAS 4-day back trajectories launched from the 316 hPa TES observations in this region showed general ascent from the south and west only 10 % went below 700 hPa over the continent (not shown). In fact, even when the higher resolution EDAS data was used only one of the back trajectories for the 3 days in which 316 hPa CO was greatest (>115 ppbv) briefly encountered (< 3 hours) the lower troposphere (below 700 hPa) over the continent (not shown). In actuality pollutants were possibly lofted to the upper troposphere by convection, as suggested in previous studies [*Kiley and Fuelberg et al.*, 2003; *Li et al.*, 2006; *Kim et al.*, 2008], that was associated with the cold fronts of the passing cyclones. However, convection may not always be well resolved by the EDAS (40 km grid spacing) and GDAS (1° × 1° grid spacing) meteorological data input to the trajectory models.

The 316 hPa composite CO for MAM2 did suggest continental export in the region just southeast of Newfoundland with CO >150 ppbv. An Ensemble of backward EDAS trajectories, launched from locations of TES 316 hPa observations for 2 of the 3 days coincident with the highest CO mixing ratios in this region, indicated the source was boundary layer air over the U.S. Central Plains mixing with air that had traveled near the surface from the western Gulf of Mexico and near the Los Angeles Basin (not shown). Presumably air masses with fresh emissions from the east coast ascended slowly while

moving rapidly in a general northeastward direction in the WCB and thus would not yet have reached this level within the confines of our study domain.

In addition to WCBs the DAs of the cyclones in MAM2 and MAM3 may have contributed to the O_3 enhancements at 681 hPa, primarily in the northern areas of the study domain, by transporting stratospheric air down to lower tropospheric levels. For example, enhancements in 681 hPa O_3 over Nova Scotia in MAM2 and over the Mid-Atlantic states and New England for MAM3 corresponded to slightly enhanced 316 hPa O_3, 400 hPa PV >1 PVU, and descending back trajectories (Figures 3.3b, 3.3c, 3.6b, 3.6c, 3.7b, 3.7c, 3.9b, 3.9c). All these factors together imply stratospheric or upper tropospheric influences. However, in general, the 316 hPa and 681 hPa distributions of O_3 showed little spatial correlation, which reflected the different dominant processes at the two levels. That is, contributions from continental boundary layer pollution played a significant role in the lower troposphere over western North Atlantic Ocean, especially south of 45° N, while there was greater stratospheric influence in the upper troposphere at more northern latitudes.

MAM4, MAM5 and MAM6

The map types MAM4 – MAM6 featured predominantly anticyclonic flow along the east coast which generally seemed to reduce the continental export to the free troposphere over the western North Atlantic Ocean compared to MAM2 and MAM3. For both MAM4 and MAM5 there were enhanced 681 hPa O_3 levels (>55 ppbv) over the western North Atlantic Ocean extending from the coast of Florida northeastward to east of Newfoundland and further out-to-sea (Figures 3.6d and 3.6e). However, for these two map types the areas of enhanced 681 hPa CO did not always correspond to the areas of

higher O_3 levels. Meanwhile for MAM6, both O_3 and CO at 681 hPa were generally low over most of the western North Atlantic Ocean. Overall, our interpretation of the composites for MAM4 – MAM6 was made more difficult by the low frequency of occurrence of these map types. This together with the strict quality and cloud screening left too few points of coincident O_3 and CO observations available for calculating statistically significant slope and correlation values. We therefore did not include them in Table 3.2 and focused on the flow characteristics depicted in the SLP, PV and back trajectory composites.

For MAM4 some pollutants could have been circulated around the back of the cyclone further east in the Atlantic leading to enhanced O_3 and enhanced CO to at 68 hPa near 60° N and 55° W (Figures 3.6d and 3.6j). However the general area of high 681 hPa O_3 extending from east of Newfoundland southwestward to just east of Bermuda was associated with highly variable CO levels ranging from 105 – 140 ppbv. Therefore we looked for evidence of stratospheric or upper tropospheric influence and found that the 316 hPa O_3 composite showed a lobe of high O_3 extending southwestward from the central North Atlantic near to west of Bermuda and composite back trajectories showed suggested stratospheric influence evidenced in descending flow from higher latitudes southward to the lower troposphere over the mid-latitudes of the western North Atlantic Ocean (Figure 3.7d). While the PV composite at 400 hPa did not indicate deep ozone intrusions (Figure 3.3d) that might explain the enhanced O_3 at 681 hPa it is possible that short-lived stratospheric intrusions that were not evident in the seasonal PV average of transported high O_3 air to the lower troposphere that remained there even after the intrusion dissipated. Unfortunately, further interpretation is limited by the sparse TES

data coverage and the limited frequency (< 7 % of the days) of this map type.

For MAM5 the enhanced 681 hPa O_3 and CO off the coast of the southeastern U.S. was possibly produced by WCB lofting of continental pollutants as the cyclones preceding the anticyclone tracked off the coast as suggested by a few trajectories of the composite analysis (Figures 3.2e, 3.6e, 3.6k and 3.7e). The very enhanced CO inland over the southeastern U.S. was coincidental and primarily reflected extreme measurements ranging from 144 -191 ppbv on April 20, 2006, that were possibly a result of outflow from convective storms over Texas from the previous day being incorporated into the descending flow behind a somewhat larger and more intense MAM5 cyclone. There were other areas of enhanced O_3 over the ocean that corresponded to relatively low CO (<110 ppbv), e.g., the area near 40°N and 60°W. For this region, likely in the DA of the cyclone, enhanced O_3 at 316 hPa (Figure 3.9e), PV >1 PVU at 400 hPa (Figure 3.3e), and descending back trajectories initiated from locations of 681 hPa TES locations (Figure 3.7e) all suggested stratospheric inputs as the cause. It should be noted that as with MAM1 there was a corresponding shift toward higher altitudes of the 681 hPa O_3 averaging kernels in this region. However, for MAM5 the averaging kernel peaks shifted upward to only 500 – 550 hPa and thus it seems more likely that for MAM5 the high levels of 681 hPa O_3 retrieved by TES in this region were actually due to high O_3 air making it all the way down to lower altitudes of the free troposphere.

The lowest 681 hPa O_3 levels in the western North Atlantic Ocean corresponded to circulation patterns of MAM6. For this map type composite O_3 levels in the western Atlantic were generally <55 ppbv with many areas, especially close to the U.S. east coast, being <45 ppbv (Figure 3.6f). The 681 hPa CO mixing ratios were also low in this region

with composite values generally <110 ppbv with many areas 105 ppbv (Figure 3.6l). We hypothesize that the large anticyclone centered near Bermuda and extending westward into the eastern U.S. and eastward well out to sea produced large-scale subsidence conditions which were unfavorable for lofting pollutants into the lower free troposphere. The only area of enhanced 681 hPa O_3 in the western North Atlantic Ocean was near Newfoundland and was likely associated with stratospheric intrusions. This area featured enhanced 400 hPa PV (Figure 3.3f) and a region of enhanced 316 hPa O_3 with levels exceeding 160 ppbv (Figure 3.9f).

Export Case Studies

The composite figures of O_3 and CO include instantaneous measurements from different times and locations, whereas the map types reflect the average state of circulation patterns. Naturally it is difficult to make a direct link between the two when the temporal and spatial scales of a pollution event and a weather system are not directly comparable. There are indeed many details in O_3 and CO distributions that need to be interpreted using instantaneous measurements. We thus examined individual cases to determine the likely export pathways. Two examples discussed in this section illustrate how pollutants are transported from the continent to the lower free troposphere over the western Atlantic Ocean by cyclones under specific map type conditions. Both involve transport via the WCB but depict different locations for the O_3 enhancements with respect to the position of the cyclone.

The first example was a case of MAM2 on April 2, 2006 when high O_3 and CO at 681 hPa was measured by TES in the main branch of a WCB. On March 31 a compact

surface low pressure system was located over the upper Midwest and a surface high pressure was located just off the South Carolina coast producing general southwesterly flow from the eastern Gulf of Mexico toward the northeastern states. The low pressure center tracked eastward and elongated in the north-south direction during the next two days while the high moved further off shore. By 1200 UTC the surface low center was located over eastern Quebec with a sharp trough extending southward just off the east coast (Figure 3.11a).

The TES retrieved 681 hPa O_3 exceeding 70 ppbv and 681 hPa CO exceeding 140 ppbv near the intersection of 40° N and 60° W during the afternoon ascending overpass (Figure 3.11b). From the cloud pattern the high pollutant levels appeared to be in the WCB branch of the cyclonic system. On the northwestern side of the cloud band marking the WCB the O_3 level decreased to 45 – 50 ppbv and CO to ~120 ppbv. An ensemble of backward trajectories using EDAS meteorological data (Figure 3.11c) from near the locations of elevated O_3 and CO retrievals confirmed that these parcels were part of a slowly ascending airstream passing over the southeastern U.S. boundary layer and eastern Gulf of Mexico during the previous 2-3 days where they potentially entrained anthropogenic pollutants.

The WCB is often an area of thick cloudiness obscuring satellite measurements of lower tropospheric O_3 and CO. For example, in Figure 3.11b the orbit is clearly interrupted by the cloud band and resumes on the other side. However, this case demonstrated the ability of TES to measure at least some of the impact of WCB outflow on O_3 levels over the western North Atlantic Ocean.
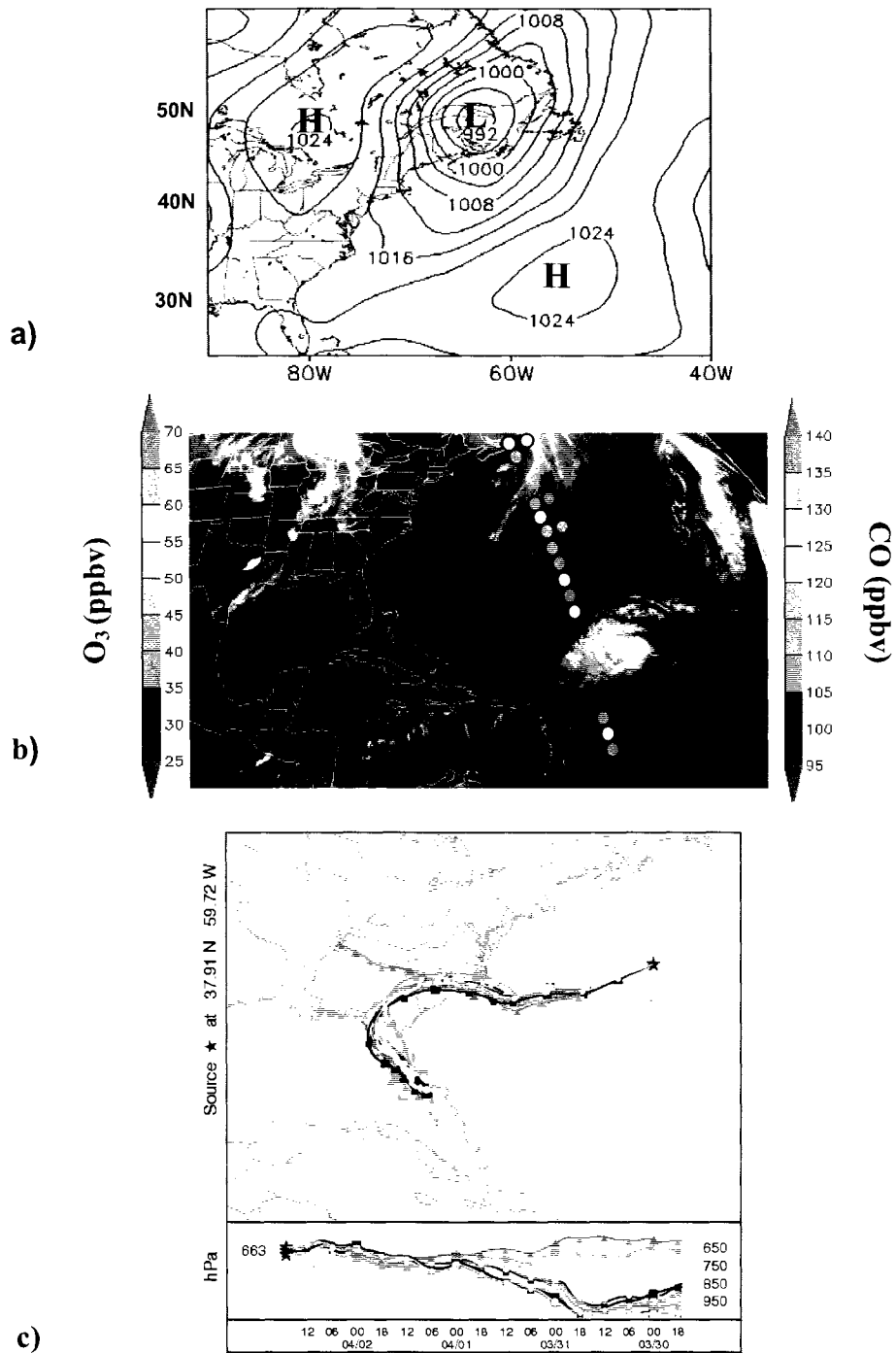
Figure 3.11. a) NCEP FNL SLP analysis for 1200 UTC April 2, 2006 b) GOES East IR image for 1715 UTC 02-April-2006 with TES 681 hPa O_3 and CO (ppbv) retrievals plotted as colored dots at approximate ground footprint locations. The CO observations are offset slightly to the right from the actual locations and the dot sizes are not representative of the footprint sizes. c) HYSPLIT ensemble back trajectories calculated using EDAS meteorological data for the corresponding time and location of the TES observations from 3500 m above mean sea level.

78

In the second example high O_3 and CO at 681 hPa occurred in mainly clear skies behind the main WCB region on April 7, 2006, a day also classified as MAM2 (Figure 3.12). A low pressure center tracking into southern Canada from the Midwest on April 3 spawned a secondary development off the New York and New Jersey coast on April 4 (Figures 3.12a and 3.12b). This new low center became the primary low as it tracked northeastward into the Canadian Maritimes on April 7 (Figure 3.12c).

At approximately 06 UTC April 7 TES measured high 681 hPa O_3 (> 70 ppbv) and CO (120 – 185 ppbv) on the descending Aura overpass which occurred just south of 40° N and near 63° W (Figure 3.12d). An ensemble of HYSPLIT backward trajectories using EDAS meteorological data showed that air parcels passed over the urban areas of the northeastern U.S. in the lower troposphere before ascending into the middle troposphere. In the meantime these air parcels moved northeastward into southeastern Canada then turned cyclonically to the west and eventually southeastward toward the ocean while descending back to the lower troposphere (Figure 3.12e). Some of the ensemble members remained in the boundary layer over the east coast urban areas before being lofted into the mid-troposphere by the developing storm system on April 4. These backward trajectories and coincident high CO and O_3 together suggest that the high mixing ratios behind or to the west of the storm center and main WCB were influenced by export of pollutants from the urban northeast corridor of the U.S.

This is an important finding because while *Owen et al,* [2006] report a case of high CO attributed to lofted continental pollutants that descended on the back side of a cyclone, generally high O_3 levels in the lower troposphere to the west of the surface low center have been linked to O_3-rich air descending from the upper troposphere or

stratosphere in the DA (*Cooper et al.,* 2001, 2002a; *Moody et al,* 1996; *Merrill et al.,* 1996; *Oltmans et al.,* 1996).   The trajectories of our case followed the same general track as the secondary WCB branch designated as W2 by Cooper et al. [2001], in which high O_3 levels were attributed to stratospheric air mixed into the polluted air of the WCB. However, since most of the back trajectories for our case remained in the lower or middle free troposphere and CO levels were high it is possible that a significant amount of the O_3 enhancement was due to anthropogenic contributions.   Thus, this case suggests that the W2 branch may also be an important pollutant export stream capable of influencing the O_3 levels over the western North Atlantic Ocean.
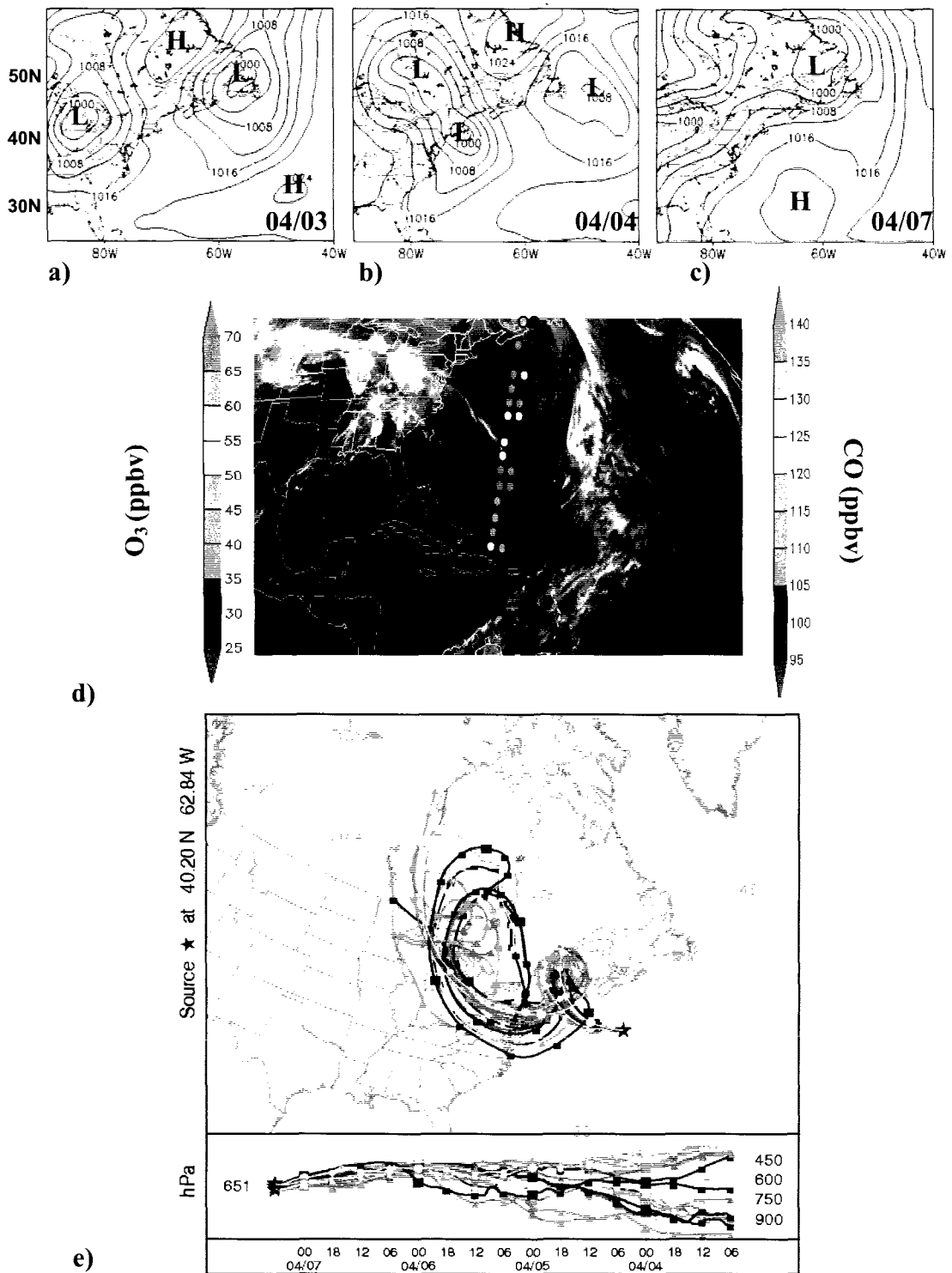
Figure 3.12. NCEP FNL SLP analyses (hPa) for 1200 UTC a) April 3, b) April 4, and c) April 7, 2006 and d) GOES East IR image for 0715 UTC 07-April-2006 with TES 681 hPa O_3 and CO (offset slightly to the right) retrievals (ppbv) plotted for one orbit as colored dots at approximate ground footprint locations. HYSPLIT ensemble back trajectories e) calculated using EDAS meteorological data for the corresponding time and location of TES observations from 3500 m above mean sea-level.

81

Evolution of Continental Outflow

Tying the O_3 and CO distributions in the central North Atlantic Ocean to the map types is challenging for a number of reasons. First, the map typing domain only extended eastward to 50° W and therefore the classification of the synoptic types did not directly consider the circulation dynamics in the center of the Atlantic Ocean. Second, the NCEP meteorological analyses used in map typing and trajectory calculations are based on fewer observations over the ocean and are therefore subject to greater errors. Third, the central North Atlantic Ocean is more distant from the sources of anthropogenic pollutants which allows for dilution and chemical transformation of exported plumes. Nevertheless, the TES composite distributions do show some interesting features which we discuss briefly in this section.

The polluted continental air in the free troposphere appeared to have been diluted as it was transported toward the central North Atlantic Ocean as the mixing ratios of CO at 681 hPa noticeably dropped off to below 120 ppbv east of 55° W (Figure 3.4b). A few studies have presented global distributions of spring CO columns from AIRS, MOPITT and SCIAMACHY satellite instruments that show a similar decrease in CO levels away from the North American coastline [*Buchwitz et al.,* 2007; *Warner et al.,* 2007; *Tangborn et al.,* 2009]. In addition *Edwards et al.* [2004] showed this trend was evident in AIRS and MOPITT 500 hPa distributions during the summer. However, unlike CO levels, the 681 hPa O_3 levels increased gradually from the U.S. east coast until approximately 60° W and then leveled off and remained at almost the same levels across the Atlantic Ocean (Figure 3.4a). In addition the seasonal mean O_3-CO slope increased to 0.17 mol mol^{-1} in Region 3 from a value of 0.13 mol mol^{-1} in Region 1 (Table 3.2), indicating more net O_3

increase and/or slower loss rate of O_3 than that of CO. This increase in slope in Region 3 was also evident in each of the most frequent map types MAM1 – MAM3 as these ranged from $0.20 – 0.29$ mol mol^{-1} (Table 3.2).

One possible explanation for the slower loss rate of O_3 compared to CO, which is consistent with the increased O_3-CO slopes, is that O_3 continued to be produced in the plume during transport [*Mao et al.*, 2006]. Summertime observations at a mountain top site in the Azores have indicated O_3-CO slopes near 1.0 attributed to air masses in North American outflow events having undergone days of photochemical processing, producing the high O_3-CO slopes [*Honrath et al.*, 2004]. Another possible explanation for the slower decrease of O_3 level compared to CO is that contributions from the upper-level air transported downward in the descending DA of cyclones further east may have enhanced the lower tropospheric O_3 keeping levels high.

In terms of the map type composite distributions, the 681 hPa CO seemed to drop off more gradually toward the east in MAM1 than for the other map types (Figure 3.6). The composite of GDAS 4-day back trajectories for Region 3 indicated that this part of the central North Atlantic Ocean was significantly influenced by the eastern edge of the WCB extending from North America as the cyclones of MAM1 swept northeastward toward Newfoundland (Figure 3.13). Interestingly, the WCB of MAM1 has a stronger influence in Region 3 than for Region 1 as discussed in Section 4 and this is due to the eastern location and large size of this low pressure system. For map types MAM2-MAM5, the trajectory composites showed a variety of pathways suggesting that pollutants exported from North America had been re-circulated and mixed with descending air from the upper troposphere and lower stratosphere diluting CO while

keeping O_3 levels enhanced (Figures 3.13b-3.13e). The area of enhanced 681 hPa CO near the southeastern corner of the domain for MAM6 which resulted from just a small number of observations exceeding 140 ppbv seemed to be an anomalous feature that could not be traced back to any continental source using 4-day back trajectory analysis. Thus the actual source was likely very distant and the feature not representative of the expected CO concentrations for this circulation pattern. Overall there still seemed to be some connection between TES distributions in the central North Atlantic Ocean and the map types, particularly when comparing the CO distribution for MAM1 with those of the other map types, though clearly it was not as strong as for the regions closer to the North American coastline.

40N

100W 60W 20W 100W 60W 20W 100W 60W 20W

a)   MAM1   b)   MAM2   c)   MAM3

40N

100W 60W 20W 100W 60W 20W 100W 60W 20W

d)   MAM4   e)   MAM5   f)   MAM6

300 400 500 600 700 800 900   PRES (hPa)
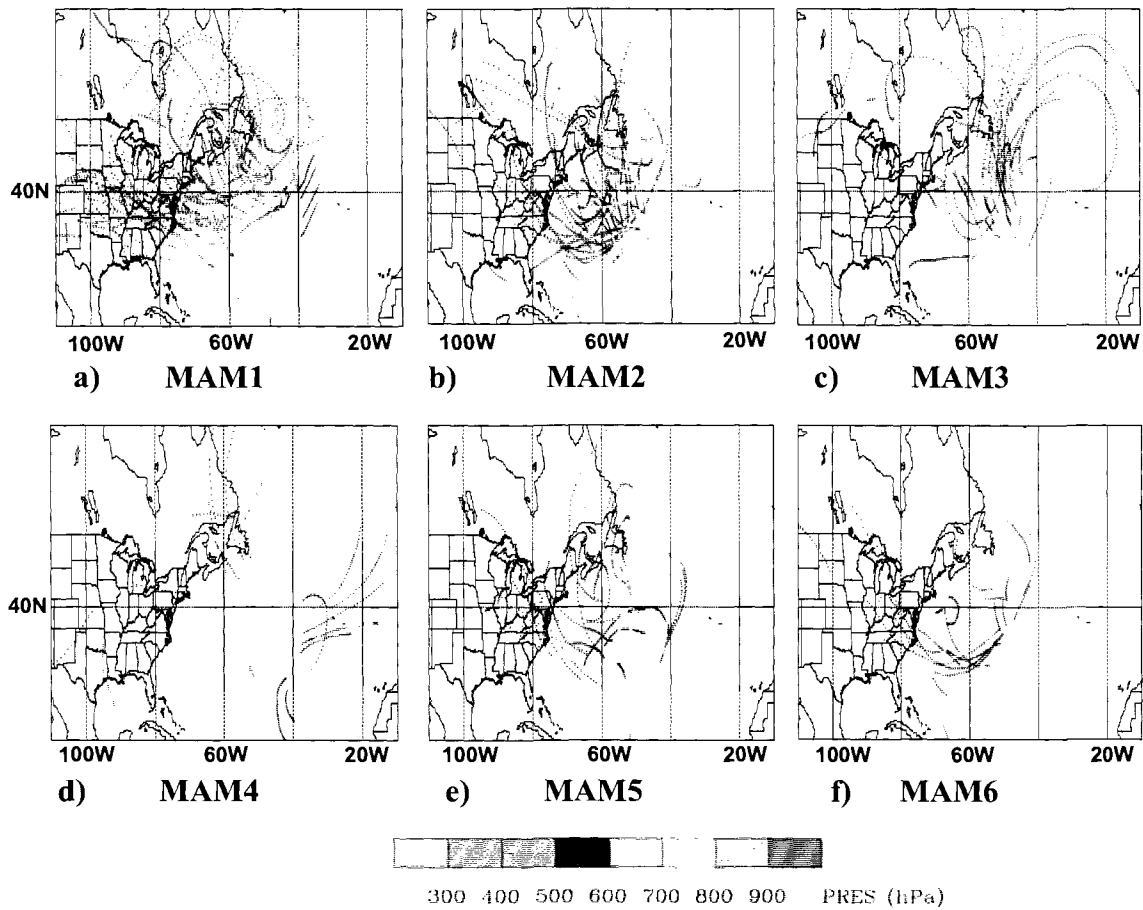
Figure 3.13. Four-day HYSPLIT back trajectories using GDAS data from locations of TES 681 hPa observations in Region 3 for map types MAM1-MAM6 (a-f). The colors indicate the pressure levels (hPa) of the trajectory parcels.

Conclusion

The springtime tropospheric O_3 and CO distributions constructed using the 2005 and 2006 TES measurements exhibited notable variability over 6 map types (MAM1 – MAM6) representing the predominant circulation patterns over eastern North America and the western North Atlantic Ocean. The highest O_3 and CO levels in the lower free troposphere of the western North Atlantic Ocean were associated with map types MAM2 – MAM3 featuring cyclones near the east coast of the U.S. We hypothesize that these elevated levels were due to lofting of anthropogenic pollutants from the continental boundary layer via the WCB of cyclones. Case studies for the cyclonic map type MAM2 demonstrated using back trajectories that retrievals of elevated 681 hPa O_3 and CO could be attributed to air parcels encountering the polluted continental boundary layer before being brought to the lower free troposphere by the WCB.

An important finding emerged from this study that boundary layer pollutants were exported to the lower free troposphere via a secondary WCB branch (W2) circling around to the back of the cyclone center, in addition to the widely studied transport route facilitated by the main branch to the east of the cold front. This result suggested an additional mechanism for O_3 enhancement in the region which had been considered to be influenced mainly by stratospheric intrusions facilitated by the DA airstream. Also, since this region is typically clearer than the main WCB branch where clouds may obscure many of the TES measurements it is potentially an important region for studying North American export from satellites.

The TES O_3 composites also revealed evidence of stratospheric intrusions associated with the cyclones depicted in the map types. Overall, these features were most

pronounced north of 45° N in the western North Atlantic Ocean. However, a complicating issue was that in these regions the averaging kernel tended to shift to higher altitudes and thus observed increases in the 681 hPa O_3 levels were partly due to the fact that the TES retrieval was weighted more toward the upper troposphere.

Composites of TES O_3 and CO retrievals showed the main export band extending from 30° N to 45° N with a seasonal O_3-CO slope of 0.13 mol mol^{-1} at 681 hPa ranging up to 0.20 mol mol^{-1} for the most favorable circulation patterns. The O_3-CO slopes derived from the TES at 681 hPa were consistent with those derived from in situ measurements at ground sites and from aircraft in the lower free troposphere downwind of urban and industrial areas of North America [*Parrish et al.*, 1993, 1998; *Daum et al.*, 1996; *Zhang et al.*, 2006]. Once over the ocean the pollutants became diluted as evident from the drop off in CO levels to the east of 55° W. However, O_3 levels continued to be elevated presumably due to photochemical production and in some cases transport of O_3 down from the upper troposphere in the DAs of cyclones further east.

There are limitations associated with using satellite retrievals to examine in detail the highly variable tropospheric O_3 distributions, namely the obscuring effects of clouds, the low vertical resolution (i.e. broad averaging kernel peaks), and lack of boundary layer sensitivity. However, the TES retrievals captured a high degree of variability with circulation patterns that was consistent with previous studies of North American export. Therefore, TES measurements incorporated into detailed observational and modeling systems should enable improvements to be made in the study of continental export.

CHAPTER IV

WINTER- AND SUMMERTIME CONTINENTAL INFLUENCES ON
TROPOSPHERIC O_3 AND CO OBSERVED BY TES OVER THE WESTERN NORTH
ATLANTIC OCEAN

Introduction

Air pollutants such as ozone (O_3) and its precursors may be lofted from the North

American boundary layer in warm conveyor belts (WCB) of synoptic-scale mid-latitude

cyclones into streams of fast moving free tropospheric westerly winds over the western

North Atlantic Ocean where in some cases they can be efficiently transported to Europe

within 4-5 days [*Eckhardt et al.,* 2004; *Crielson et al.,* 2003; *Stohl et al.,* 2003a;

Huntreiser et al., 2005]. Particularly in the summertime, pollutants may be lofted to the

top of the continental boundary layer by mesoscale convective processes (e.g., sea breeze

circulations) and slowly transported across the ocean at altitudes of 2-4 km with minimal

oxidation owing to being cut-off from the destructive (halogen) chemistry of the MBL

[*Angevine et al.,* 2004; *Rodrigues et al.,* 2004; *Owen et al.,* 2006]. However during the

cooler seasons of the year (winter, early spring, late autumn), a stratospheric intrusion

may bring O_3 and other compounds into the lower troposphere over the ocean via the dry

airstream (DA) of a synoptic-scale cyclone [*Merrill et al.,* 1996; *Moody et al.,* 1996;

Oltmans et al., 1996; *Cooper et al.,* 2001, 2002b; *Wotawa and Trainer,* 2001; *Polvani*

and Esler, 2007 *Cammas et al.,* 2008]. Thus information on the 3-dimensional

distribution of O_3 and its precursors as well as the air mass transport history which can be

derived from the circulation type are required to ascertain the contributions of the various sources to ambient levels of pollutants.

A number of field missions (e.g., NARE, NEAQS2002, and INTEXA/ICARTT2004) have been conducted to understanding the composition of North American outflow [e.g., *Parrish et al.,* 1993, 1998; *Banic et al.,* 1996; *Berkowitz et al.,* 1996; *Cooper et al.,* 2001, 2002a, 2005; *Fehsenfeld et al.,* 2006; *Singh et al.,* 2006; *Mao et al.,* 2006]. However, long-term continuous measurements over extensive areas and depicting the vertical structure of the atmospheric composition had not been available. To address this problem the EOS-AURA satellite was launched into a near sun-synchronous orbit on July 15, 2004 with a payload including the Tropospheric Emission Spectrometer (TES) [*Schoeberl et al.,* 2006]. TES is a Fourier transform infrared spectrometer designed to measure vertical profiles of tropospheric O_3 and its precursors such as carbon monoxide (CO) [*Beer et al.,* 2001]. These measurements may prove to be crucial for the study of many global air quality problems by providing a continuous record of tropospheric composition at several vertical levels over the multi-year lifetime of the instrument.

For our initial study on continental export using TES described in Chapter III we focused on the spring season since tropospheric O_3 levels generally peak in the Northern Hemisphere and synoptic-scale circulation activity remains strong [*Monks,* 2000]. In that study we found a strong relationship between TES O_3 and CO distributions and the highly variable circulation patterns over eastern North America and the western North Atlantic Ocean. In particular, we found enhanced O_3 and CO levels in regions of WCBs as well as evidence of tropospheric O_3 enhancements in the DA regions on the western

side of cyclones. These findings were consistent with previous aircraft and modeling studies and provide convincing evidence that TES measurements are capable of capturing the important variability caused by synoptic circulation systems.

In this study we extended our analysis to the winter and summer. In winter synoptic activity is strong but O_3 production is low due to the lack of solar radiation, yielding possibly overall smaller transport of O_3 compared to spring. However, during episodes of certain meteorological phenomenon such as rapidly deepening cyclonic storms known as "bombs" the trans-Atlantic transport can take as little as one day, and transport via "bombs" occurs four times more frequent in winter than in summer [*Stohl et al.*, 2003a]. Such rapid transport may be important for the budget of short-lived substances in the remote troposphere. In summer O_3 levels are high due to efficient photochemical production but synoptic cyclone activity over the mid-latitudes decreases [*Monks*, 2000; *Ziska and Smith*, 1980; *Bell and Bosart*, 1980; *Serreze et al.*, 1997; *Key and Chan*, 1999; *Owen et al.*, 2006]. Further, impact of wild fires is often observed in summer in the North American continental outflow, which can complicate the quantification of anthropogenic emissions of trace gases [*Singh et al.*, 2006, *Cammas et al.*, 2008].

In this study we aimed to: 1) characterize the seasonal distributions of TES O_3 and CO during winter and summer over eastern North America and the western North Atlantic Ocean, and 2) examine the possible association between the variability in O_3 and CO captured in the TES observations and synoptic-scale atmospheric circulations over the northeastern U.S. that regulate the transport and dispersion of pollutants from the North American continent. To accomplish these objectives we averaged the TES O_3 and

CO retrievals during the winters (DJF) of 2005 (December 2004 – February 2005) and 2006 (December 2005- February 2006) and summers (June-August, JJA) of 2005 and 2006 over a domain covering the eastern U.S., southeastern Canada and the adjacent Western Atlantic Ocean. Then we grouped the TES observations by synoptic circulation type and created composite O_3 and CO distributions, as in Chapter III, to identify the salient characteristics and their causal mechanisms.

Data

TES Data

TES produces a 16-orbit Global Survey including tropospheric profiles of O_3 and CO every other day. The nadir on-the-ground footprint is approximately 5.3 km × 8.4 km with an initial along-orbit spacing between footprints of approximately 544 km before that was improved to approximately 182 km on May 25, 2005 after the limb scans were eliminated and replaced by an additional nadir scan [*Bowman et al.*, 2002; *Beer et al.*, 2001; *Beer et al.*, 2006; *Osterman et al.*, 2007b]. Each orbit is approximately 22° longitude apart. TES vertical coverage extends from 0 – ~33 km and in cloud-free conditions the vertical resolution is approximately 6 km with sensitivity to both lower and upper troposphere as well as the stratosphere [*Bowman et al.*, 2002; *Worden et al.*, 2004]. For this study we used the TES Level 2 V002 Global Survey data [*Osterman et al.*, 2007a] during DJF and JJA of 2005 and 2006. Because TES generally cannot accurately measure boundary layer parameters due to a lack of thermal contrast with the surface and has approximately two degrees of freedom in the troposphere [*Worden, J., et*

al., 2007] we focused our attention on two levels above the boundary layer 681 hPa and

316 hPa to represent the lower and upper free troposphere respectively.

Atmospheric parameters are retrieved from the measured TES radiances using

algorithms described by *Rodgers* (2000), *Worden et al.* (2004) and *Bowman et al.* (2002,

2006a). The retrievals are mathematically constrained with a set of climatological a priori

profiles, derived from MOZART simulations (*Brasseur et al.,* 1998), representing

different geographical regions and months of the year (*Bowman et al.,* 2006a). Because

the geographically variable a priori adds artificial structure which can potentially obscure

some of the real spatial variability, (*Zhang et al.,* 2006) we removed this artifact by

reprocessing the TES O_3 and CO profiles with a universal a priori using the procedure

described in Chapter III. Hereafter in this study all of the TES data presented will refer

to the reprocessed data.

The TES retrieval products contain diagnostic information and flags for screening

out failed profiles or those with reduced sensitivity [*Bowman et al.,* 2006b; *Kulawik et al.,*

2006]. We used the general retrieval quality flag which removes the most suspect

profiles. In addition, we screened for clouds since they can impact the retrievals. Since

TES sensitivity below clouds can be severely limited [*Kulawik et al.,* 2006] we screened

for clouds as described in Chapter III. We also screened for overall measurement

sensitivity at the given retrieval level using the averaging kernel matrix, which is a post-

processing diagnostic which defines the contribution of the each element of the true state

vector to the retrieval at a particular pressure (or altitude) level. Only those profiles for

which the diagonal value at the level we were examining (681 or 316 hPa) was greater

than 0.01 were retained.

Meteorological Analyses

We used Global Final Analysis (FNL) data from the National Centers for Environmental Prediction (NCEP) to identify the predominant atmospheric circulation patterns over eastern North America and the North Atlantic Ocean during the time period 2000 – 2006. FNL products are available for 4 time intervals each day (00, 06, 12, and 18 UTC) on a $1° \times 1°$ horizontal grid at the surface and 26 pressure levels vertically ranging from 1000 to 10 hPa [http://dss.ucar.edu/datasets/ds083.2].

In addition, as in Chapter III, we used HYSPLIT [*Draxler and Rolph*, 2003, http://www.arl.noaa.gov/ready/hysplit4.html] backward trajectories, in single trajectory and ensemble mode, to aid us in determining the likely source regions for any O_3 and CO enhancements observed in the TES data downstream of North America. Rationale of the use of these two modes and details on the model input can be found in Chapter III.

Stratospheric intrusions were identified using isentropic potential vorticity from the NCAR/NCEP $2.5° \times 2.5°$ Reanalysis [NNRA, http://www.cdc.noaa.gov/cdc/reanalysis]. The NNRA isentropic potential vorticity analyses were available 4 times per day (00, 06, 12, and 18 UTC) at 11 isentropic levels for 270, 280, 290, 300, 315, 330, 350, 400, 450, 550, and 650 K. We interpolated these data to constant pressure levels to facilitate use with NCEP FNL analyses and TES retrievals which were also on pressure levels.

Synoptic Circulation Classification

Synoptic-scale circulation patterns over the North Atlantic were classified by applying the correlation-based map typing algorithm of Lund (1963) to the NCEP FNL

SLP fields. We have applied this technique successfully to synoptic classification of summer- and springtime circulation patterns over the northeastern United States and the North Atlantic respectively using the NCEP grids as described in Chapter II. In brief, the algorithm calculates a correlation coefficient between the grids representing scalar meteorological analysis fields over a given spatial domain at different times. The map types are selected using a critical correlation coefficient (*i.e.*, 0.65 for DJF and 0.70 for JJA), and then all the days in a given study period are classified as one of these types based on the degree of correlation. Typically either the SLP or upper-level geopotential height (GPH) fields are chosen to represent the circulation patterns in the map typing algorithm. We settled on using the SLP fields, which are usually related to the upper–level patterns and from which synoptic features can be easily identified, because the classification was more accurate compared to that based on the comparatively smooth and less distinct upper-level GPH fields.

During the study period of 2000 – 2006 four map types were identified for DJF (DJF1 – DJF4), and five for JJA (JJA1-JJA5) as depicted in Figures 4.1 and 4.2. The map type frequencies and the important meteorological features associated with each map type are summarized in Tables 4.1 and 4.2. Here we present a brief discussion of the patterns, their sequencing and how they might relate to the major hypothesized transport pathways.
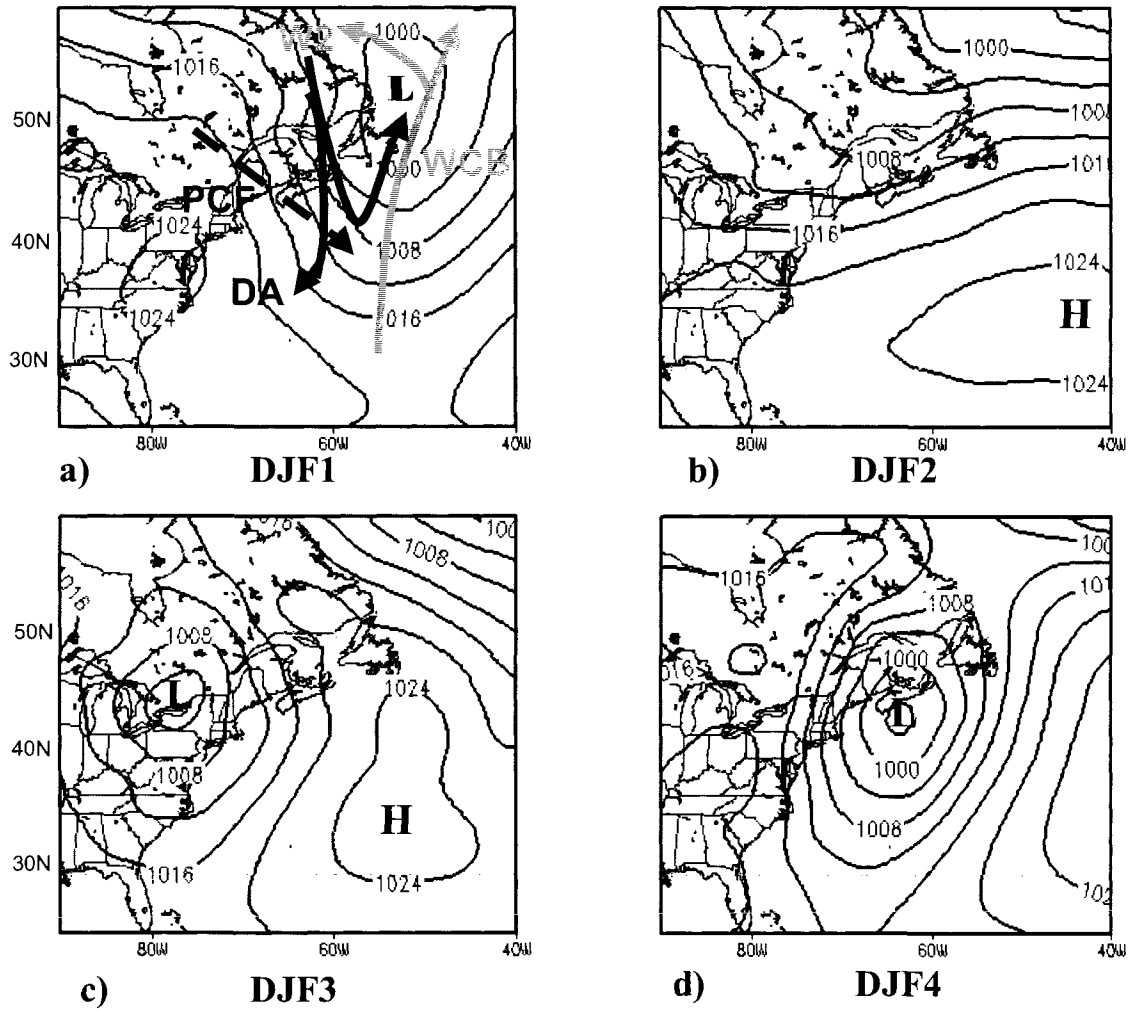
Figure 4.1. Mean sea level pressure (SLP) (hPa) analyses for DJF map types
DJF1 – DJF4 (a-d) during 2005 and 2006.
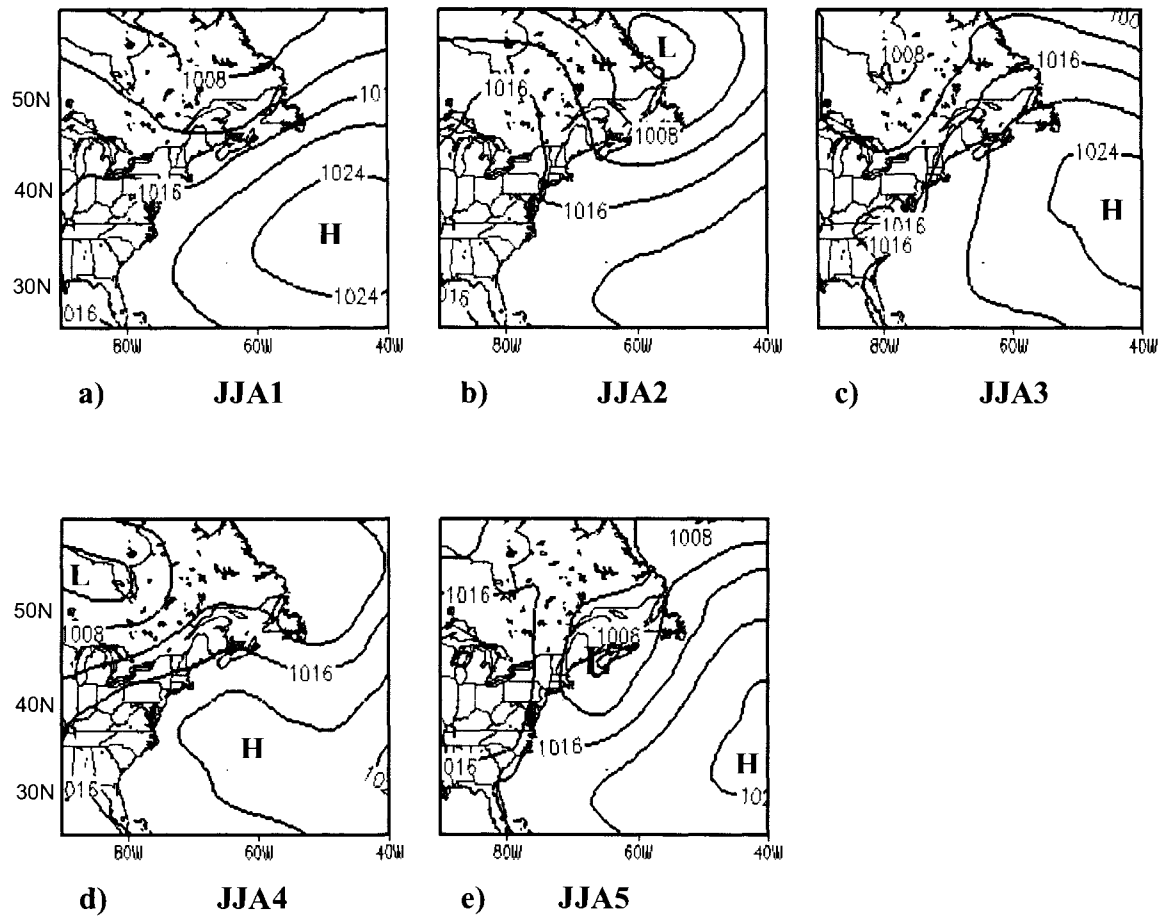
Figure 4.2. Mean sea level pressure (SLP) (hPa) analyses for JJA map types
JJA1 – JJA2 (a-d) during 2005 and 2006.

Table 4.1. DJF map types and meteorological characteristics. Frequencies are for the winters of December 2004 - February 2005 (2005), and December 2005- February

Map Type	2005-2006 Frequency (%)	Characteristics
DJF1	31	• Mature Cyclone exiting North America near Canadian Maritimes • Subsiding northwest flow around back of cyclone center covering much of northeastern U.S. and southeastern Canada
DJF2	14	• Large oceanic anticyclone • Primarily west to southwest flow over much of eastern North America • Major storm track shifted northward
DJF3	11	• Continental cyclone • Southerly flow and rising motion over much of east coast in the WCB
DJF4	7	• Coastal cyclone • Primarily developing along the coast of the southeastern U.S. and moving rapidly to the northeast • Rising motion and southerly flow over the southeastern U.S. extending out into the Atlantic in the WCB • Northerly descending flow over inland after cyclone passage DA

Table 4.2. JJA map types and meteorological characteristics.

Map Type	2005-2006 Frequency (%)	Characteristics
JJA1	28	• Subtropical anticyclone (Bermuda High) • May persist up to 8 days • Weak south and southwesterly flow and subsidence over northeastern U.S. • Isolated rising motion associated with localized convection
JJA2	17	• Low pressure trough off immediate coast • Subsiding north-northwest DA flow along coast of northeastern U.S. and southeastern Canadian coast, • Rising motion in WCB offshore • anticyclonic ridge rebuilding inland
JJA3	11	• Subtropical (Bermuda High) with approaching low or frontal trough inland • Southerly and southwesterly flow in eastern U.S. and southeastern Canada.
JJA4	5	• Low pressure trough well offshore • Subtropical anticyclone re-established inland • WCB well offshore • Weak southwesterly flow around anticyclone over eastern U.S. • Subsiding northwesterly flow in DA just east and south of Nova Scotia and Newfoundland
JJA5	5	• Coastal cyclone • WCB flow to the east of Newfoundland and • Northwesterly flow of secondary re-circulating WCB or DA over the northeastern U.S.

Wintertime Circulation

The DJF circulation was characterized by periods of frequent and intense cyclonic storm activity (DJF1, DJF3, and DJF4) separated by periods of relatively calm conditions (DJF2). In the more active mode synoptic-scale cyclones tracked eastward and northeastward from southern Canada and the U.S. (DJF3, Figure 1c) and/or developed off the U.S. east coast and continued northeastward (DJF4, Figure 1d). In almost all cases the cyclones exited North America as mature systems east of the Canadian Maritimes or the Labrador Coast as suggested in DJF1 (Figure 4.11a), which was the most frequent map type occurring 31% of the time in winter 2005-2006 (Table 4.1).

Cyclonic transport is typically presented in terms of distinct airstreams [*Carlson, 1980, Cooper et al.,* 2001, 2002a]. In the context of this study the most relevant of these would be the warm conveyor belt (WCB), the dry airstream (DA), and the post cold front (PCF) (Parrish et al., 2000), as illustrated in Figure 4.1a. The warm conveyor belt transports air masses from the boundary layer into the free troposphere along a slowly ascending north-northeastward airstream ahead of the cyclone position. In Chapter III it was shown that in addition to the main WCB branch, a secondary branch circling to the back of the cyclone center could also be an important mechanism to transport pollutants from the urban areas of the U.S. east coast to the lower free troposphere of the western North Atlantic. This secondary branch was identified in *Cooper et al.,* (2002a) and denoted as W2. We also use this convention when referring to this branch. The dry airstream transports air from the upper troposphere and lower stratosphere to the lower troposphere in a rapidly descending airstream spreading out behind the cyclone center. The PCF airstream descends from the middle troposphere of the northwest quadrant of

the cyclone to the boundary layer behind the surface cold front and under the DA [*Cooper et al.,* 2001, 2002a], which is also important for surface export from the immediate coastal region. These airstreams often have distinct chemical characteristics and influence the tropospheric distributions of O_3 and CO in the study domain [*Merrill et al.,* 1993; *Moody et al.,* 1996; *Oltmans et al.,* 1996; *Parrish et al.,* 2000; *Cooper et al.,* 2002a; *Owen et al.,* 2006; *Polvani and Esler,* 2007].

During the less active cyclone phase, the storm track shifted northward and the circulation was generally characterized by lighter west to southwest flow around a large anticyclone extending from the subtropical Atlantic Ocean northward into the midlatitudes as depicted by DJF2 (Figure 4.1b). This map type accounted for only 14 % of the classified maps in the winters of 2005 and 2006 (Table 4.1) but more than half of those days (58%) were of persistent events lasting 2-3 days in a row. During these events synoptic-scale vertical transport from continental boundary layer along the U.S. east coast was possibly restricted by the weak subsidence associated with the anticyclonic flow.

Summertime Circulation

In the summer months (JJA) the circulation was dominated by a large subtropical anticyclone off the coast, usually referred to as the Bermuda High, which extended into the eastern half of the U.S. as depicted in JJA1 (Figure 4.2a). This pattern was the most frequent occurring on 28 % of the days (Table 4.2) and could be persistent with one event in July 2006 lasting for 8 days in a row. It produced subsidence via light south-southwest lower tropospheric flow in most of eastern North America with generally warm and humid weather conditions. Under this general pattern, cyclones tracked north of the

U.S.-Canadian border, accompanied by trailing cold fronts that occasionally extended into the central U.S. producing weak cyclonic flow and causing the Bermuda High to retreat offshore (i.e. JJA3 (Figure 4.2c).

The second most frequent summertime pattern, JJA2, featured a cyclonic trough extending from the Labrador Peninsula southward just offshore of the northeastern U.S. (Figure 4.2b) and occurred on 17% of the days in summers 2005 and 2006 (Table 4.2). During June this pattern often resulted from a well-organized cyclone that tracked northeastward from the U.S. to the Labrador coastline. These types of systems produced well-defined cyclonic airstreams which exerted influence over the entire eastern U.S. In contrast, later in the summer, these troughs were primarily associated with cyclones that originated in central Canada and moved eastward and southeastward. The trailing cold fronts of these systems swept southeastward and mainly influenced areas in southeastern Canada, New England, and upstate New York. Map type JJA4 shows a variation of this general pattern with the trough located further offshore and the subtropical ridge building again over the eastern U.S (Figure 4.2d). The fact that many of the toughs seemed to weaken as they moved offshore may have accounted for the lower frequency (5%) of this map type.

Coastal cyclones, JJA5, were the least common summertime pattern occurring on only 5 % of the days in summers 2005 and 2006 (Figure 4.2e, Table 4.2). They typically developed as migrating upper–level synoptic waves approached the coastline. However, in at least one case, on June 15, 2006, the cyclone had incorporated remnants of a tropical storm (Alberto) that had moved across the eastern Florida Panhandle two days prior [http://www.nhc.noaa.gov/pdf/TCR-AL012006_Alberto.pdf]. As with east coast

cyclones in other seasons the JJA5 systems produced moderately strong WCBs flowing offshore and descending DA airstreams to the west over the continent.

Seasonal Composites of O_3 and CO Distributions

For DJF the 681 hPa O_3 seasonal composite exhibited very little spatial variation with O_3 levels in most areas being near 45 ppbv (Figure 4.3a), likely a result of low photochemical production owing to the winter being at the minimum in the annual solar radiation cycle. However, the 681 hPa CO composite suggested continental pollutant export to the lower free troposphere in a band of 100 - 110 ppbv mixing ratios extending from 30° N to 50° N along the east coast and further out to the central North Atlantic (Figure 4.3b). At 316 hPa there was a steep south to north O_3 gradient with levels increasing from <50 ppbv over Florida to >150 ppbv in Canada (Figure 4.3c). This strong gradient reflects the decreasing tropopause heights and increasing stratospheric influence toward the north. The 316 hPa CO composite showed very little spatial variability with most levels between 80 and 90 ppbv (Figure 4.3d).

In contrast, the JJA seasonal 681 hPa O_3 composite exhibited notable spatial variability and depicted a tongue of O_3 levels >60 ppbv emanating from the east coast of the U.S. and extending eastward into the central Atlantic (Figure 4.4a). The O_3 levels decreased slightly to the south (55-60 ppbv) and more dramatically to the north with mixing ratios mostly below 50 ppbv north of 50° N. Corresponding to the greater levels of O_3 enhanced CO mixing ratios at both 681 (95-105 ppbv) and 316 hPa (CO >85 ppbv) were found to be over most of the U.S. along an axis oriented southwest to northeast and exiting North America east of Newfoundland (Figures 4.4b and 4.4d). The northward

shift of this export pathway compared to winter is correlated with a northward shift of the storm track around the dominant subtropical Bermuda High as discussed in the previous section. While weak WCBs are likely responsible for transporting boundary layer pollutants to the lower free troposphere, the enhanced levels of CO at 316 hPa may have been made possible by rapid vertical transport in convective systems [*Kiley and Fuelberg et al.*, 2003; *Li et al.*, 2006; *Kim et al.*, 2008]. These possibilities are discussed in more detail in later in this chapter. The 316 hPa O_3 composite for JJA exhibited a homogeneous distribution with levels near 80 ppbv over the midlatitudes followed by a sharp increasing trend north of 50° N (Figure 4.4c). The uniformity of the pattern and lack of high O_3 levels south of 50° N suggested a much decreased influence of stratospheric air as compared to winter.

To identify the possible source types of the higher O_3 and CO levels at the 681 hPa we applied the correlation of observed O_3 and CO which has been proven to be a useful diagnostic indicator of the photochemical processing of an air mass [*Parrish et al.*, 1993, 1998; *Mao et al.*, 2004]. In export Regions 1, 2, and 3 indicated as dashed boxes in Figure 4.4a, O_3 was positively correlated with CO at 681 hPa with slopes near of 0.15-0.23 mol mol^{-1} (Figure 4.5, Table 3) which is close to the range of 0.2 – 0.35 indicted by previous in situ ground-based measurements [*Parrish et al.*, 1993, 1998; *Chin et al.*, 1994; *Mao et al.*, 2004]. Aircraft measurements during the NARE93 and ICARTT 2004 summer campaigns indicated similar slopes, which took place in the lower free troposphere just east of the North American coastline [*Daum et al.*, 1996]. However care must be taken in comparing the O_3-CO slopes to earlier studies since changing emissions of NOx and CO in North America over time may have impacted O_3-CO slopes of

anthropogenic influence [*Parrish et al.,* 2006; *Kim et al.,* 2006].
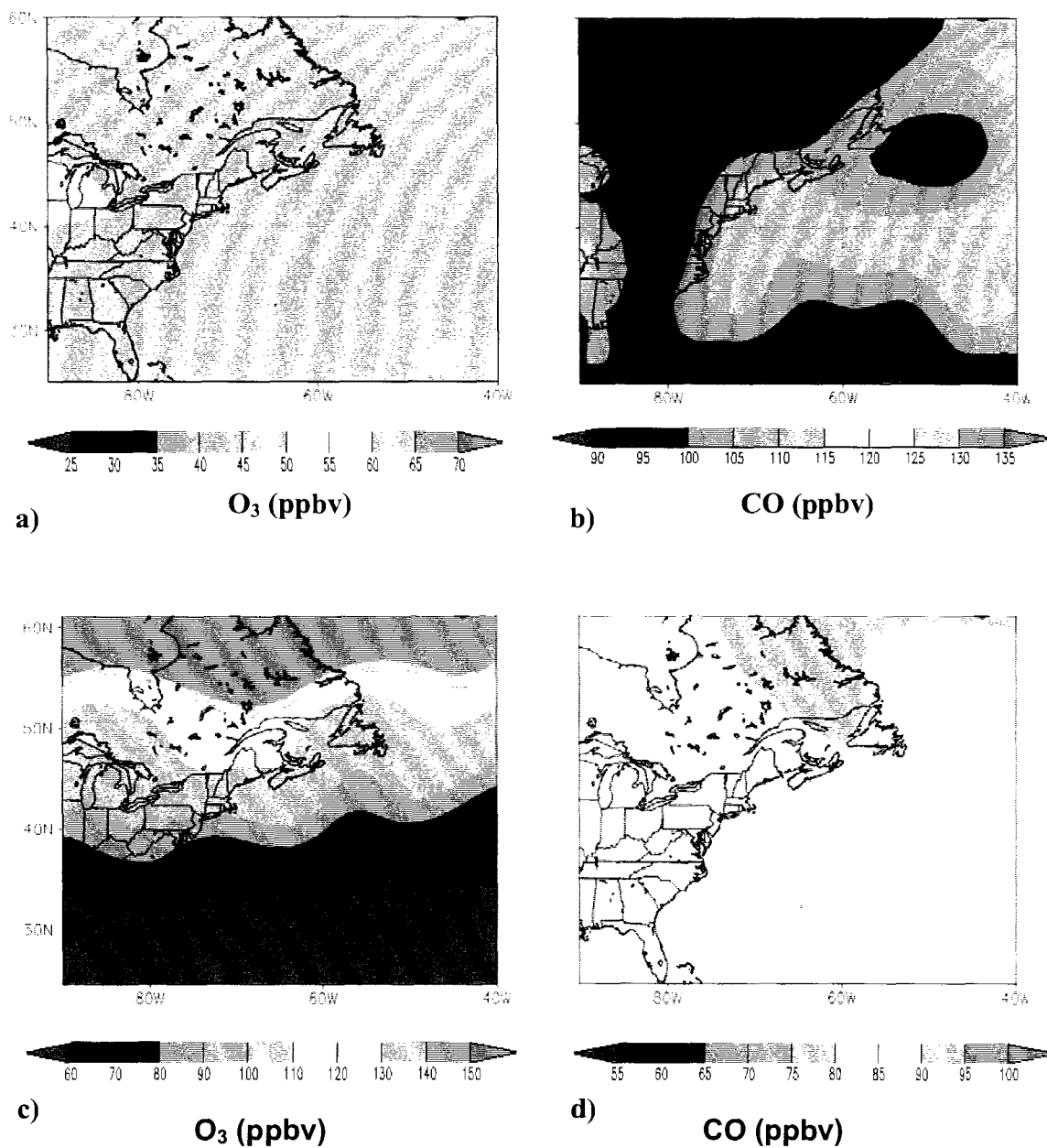
Figure 4.3. The DJF seasonal composites for a) 681 hPa O_3 (ppbv) b) 681 hPa CO (ppbv), c) 316 hPa O_3 (ppbv) and d) 316 hPa CO (ppbv).
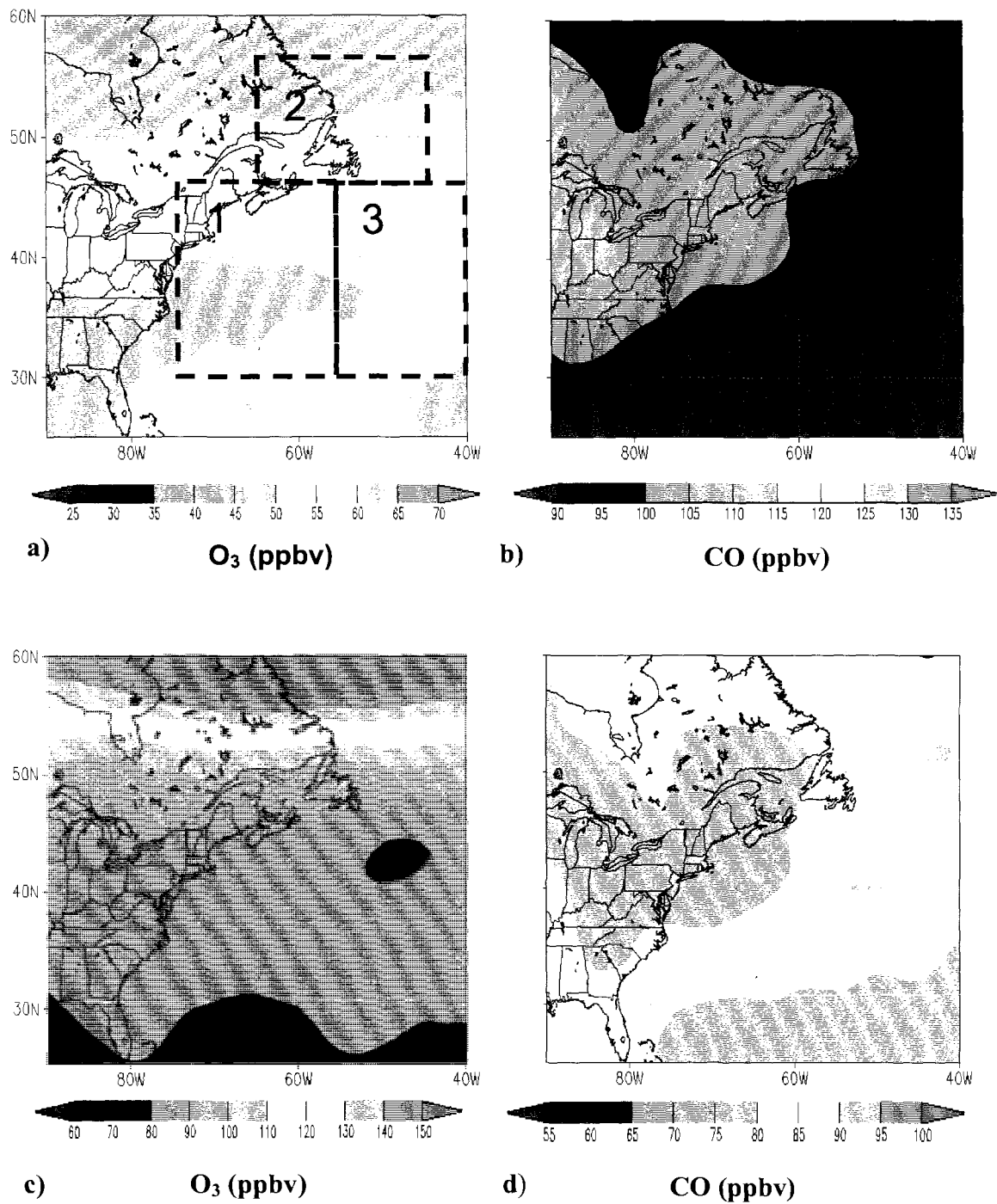
Figure 4.4. The JJA seasonal composites for a) 681 hPa O_3 (ppbv) b) 681 hPa CO (ppbv), c) 316 hPa O_3 (ppbv) and d) 316 hPa CO (ppbv). Regions 1, 2, and 3 are marked as dashed black lines on a.

105
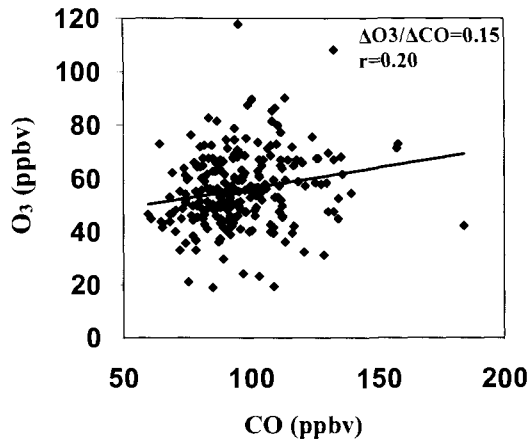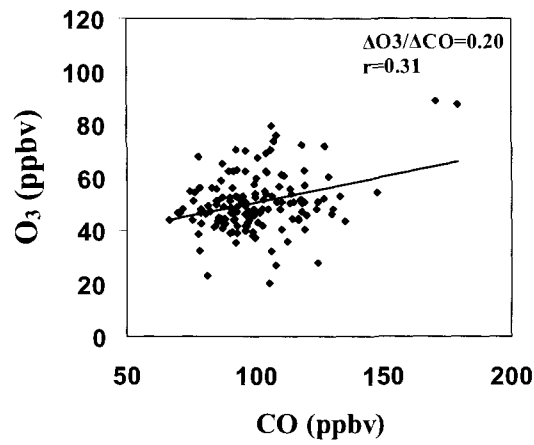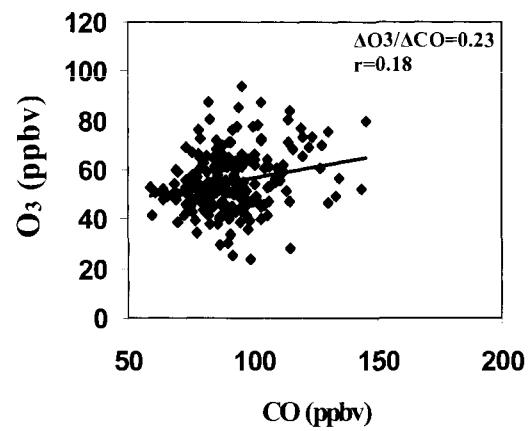
Figure 4.5. Scatter plots of 681 hPa O_3 versus CO for JJA a) Region 1, b) Region 2 and c) Region 3.

Table 4.3. JJA O_3-CO slope, correlation coefficient (r), and sample size N for circulation types in Region 1 30 – 45° N, 75-55° W, Region 2 45- 55° N, 65-45° W, and Region 3 30-45° N, 55-40° W.

		Region 1	Region 2	Region 3
All		0.15 (0.20)	0.20 (0.31)	0.18 (0.23)
		N=253	N=141	N=213
JJA1		0.17 (0.21)	0.33 (0.51)	-0.03 (0.0)
		N=91	N=34	N=82
JJA2		0.29 (0.32)	0.13 (0.28)	0.57 (0.66)
		N=46	N=23	N=38
JJA3		0.03 (0.04)	0.18 (0.48)	-0.06 (-0.13)
		N=29	N=18	N=16
JJA4		0.42 (0.46)	0.34 (0.31)	0.37 (0.46)
		N=9	N=12	N=10
JJA5		0.33 (0.48)	0.02 (0.06)	0.0 (-0.01)
		N=12	N=3	N=6

Circulation Influences on O_3 and CO Distributions in Winter

The composite distributions of O_3 and CO for DJF exhibited notable differences between individual map types. In general, the circulation types could be grouped into 2 main types, one representing and active midlatitude storm track comprised of map types DJF1, DJF3, and DJF4, which seemed to enhance continental export, and the other for a less active midlatitude storm track, DJF2 that seemed to be less conducive to export. The differences between these groups and individual map types are discussed in the following two sections.

DJF1, DJF3, and DJF4: Active Midlatitude Storm Track

A common feature of the 681 hPa CO composites for the map types DJF1, DJF3, and DJF4 was a channel of enhanced mixing ratios >110 ppbv between 30-45° N extending eastward into the central Atlantic Ocean (Figures 4.6a, 4.6c and 4.6d). This feature corresponded to the highest CO levels in the seasonal composites (Figure 4.3b). For DJF3 and DJF4 the highest CO levels were generally to the east of the cyclone positions implying that lofting of North American pollutants to the free troposphere by the WCB airstreams associated with the cyclones. This mechanism has been verified by aircraft studies of continental export [*Cooper et al.,* 2002a, 2001; *Parrish et al.,* 2000] and was also shown in Chapter III to be a cause of enhanced lower free tropospheric O_3 and CO measured by TES east of cyclones during springtime.

The cyclone in DJF1 is centered northeast of Newfoundland (Figure 4.1a), but some of the highest mixing ratios in the 681 hPa CO composite are located to the south and west of the center in a band streaming eastward from the coast line (Figure 4.6a).

This location is well displaced from the main branch of the WCB and instead is located near the DA which would restrict lofting of continental pollutants to the free troposphere. One possible explanation for this inconsistency was that pollutants lofted from the continent in the WCB were re-circulated to the rear of the storm in the secondary W2 branch as shown in Figure 4.1a, incorporated into the subsiding DA flow and subsequently transported offshore. Another possible explanation was localized convective lofting in the PCF over the continental locations as proposed by *Parish et al.* (2000). In the case of DJF1 the PCF was located over the ocean where shallow convection (1 - 2 km in depth) in wintertime may develop due to the instability caused by cold polar or arctic continental air flowing over the relatively warm offshore waters.

a)   b)   c)   d)
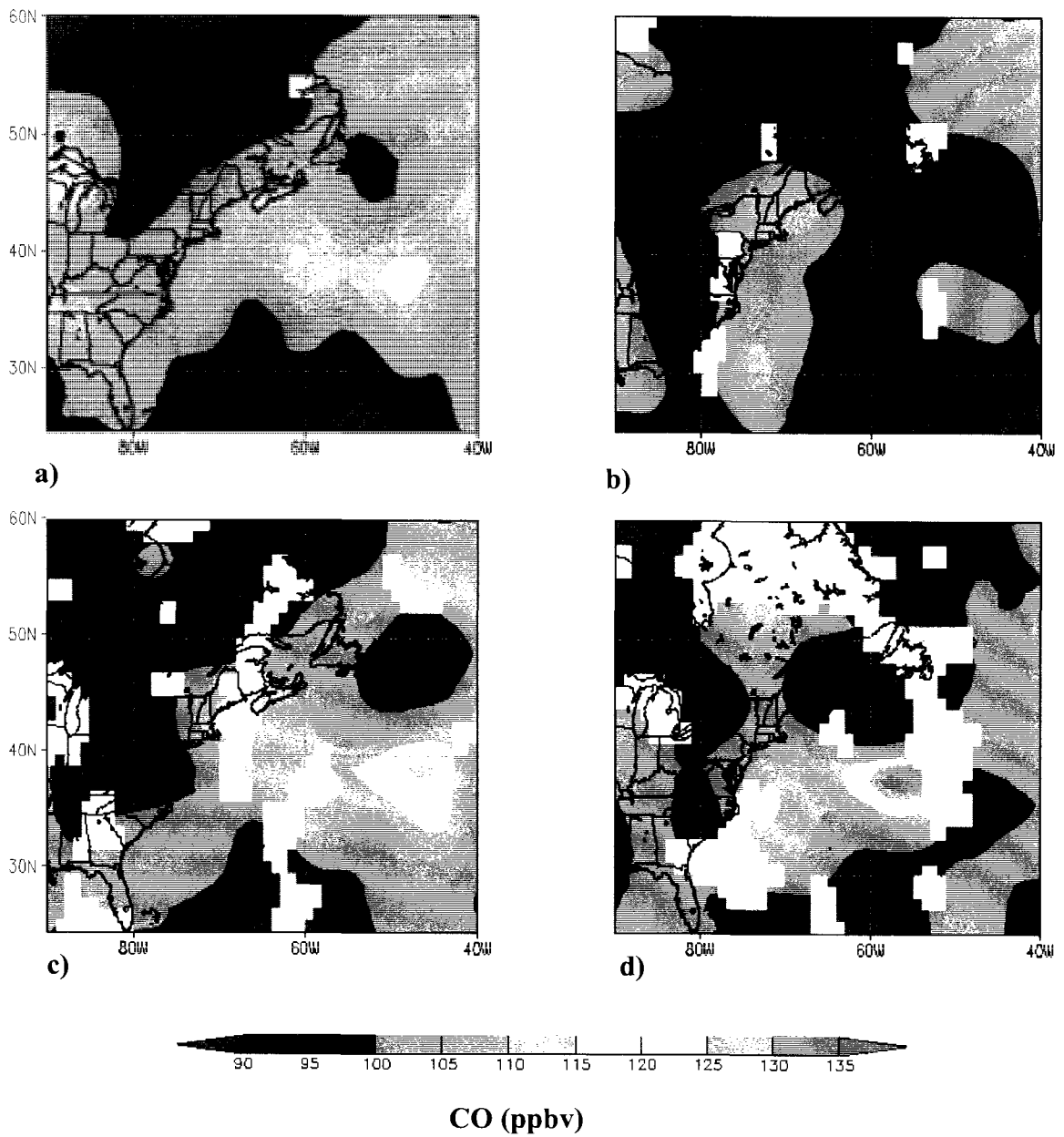
CO (ppbv)

Figure 4.6. The DJF 681 hPa CO (ppbv) composites for map types DJF1-DJF4 (a-d).

We examined eight DJF1 cases that had 681 hPa CO mixing ratios >110 ppbv in the offshore region of 35 – 45° N and west of 60° W using HYSPLIT ensemble back trajectories with EDAS meteorological data from the times and locations of the TES observations (figures not shown). One case on January 26, 2006 showed evidence of re-circulation of air to the W2 branch as a cyclone tracked over New England and into the Canadian Maritimes. A second case on January 2, 2006, had high CO mixing ratios located to the south near 35°N as a result of a WCB lofting from another approaching cyclone to the south and west of the main DJF1 cyclone. Back trajectories for the remaining 6 cases all indicated descending motions from the middle and upper troposphere typical of the DA. However, satellite images and loops for these cases indicated the presence of stratocumulus forming offshore indicative of shallow convection.

Two of the 6 DA cases that had very high offshore 681 hPa CO levels (> 150 ppbv) were January 10 and 27, 2006. On January 10, 2006 there were 4 CO retrievals during the 17 UTC overpass that ranged from 114 – 163 ppbv south of Nova Scotia to the western side of a cold front cloud band (Figure 4.7a). The points coincided with an area of offshore low clouds. The retrieved profiles showed that the CO was enhanced from the 908 hPa to the 681 hPa level before dropping off substantially (Figure 4.7b). The 1200 UTC sounding out of Grey, Maine clearly indicated a subsidence inversion beginning just above the 800 hPa and extending to approximately 700 hPa (Figure 4.7c) and this likely inhibited any large scale deep vertical transport over land. However, given that the offshore sea surface temperature (shown in red on Figure 4.7a) was 7° C compared to the land temperature of approximately -1° C positive sensible and latent heat

fluxes from the ocean to the air may have acted to destabilize rapidly the air flowing off the continent producing convection which may have been able to penetrate the inversion layer and loft some recently exported pollutants.

On January 27, 2006 three 681 hPa CO measurements during the 06 UTC descending overpass ranged from 146 – 153 ppbv coincident with a distinct line of shallow convection offshore extending from southern New Jersey to the Carolinas (Figure 8a). The vertical profile plot showed enhanced CO from the 908 hPa retrieval level up to the 422 hPa level before dropping off (Figure 4.8b). While some of the vertical depth of this high CO feature is a result of the smoothing affect of the retrieval process, a weaker inversion (Figure 4.8c) coupled with a greater air-ocean temperature contrast (Figure 4.8a) compared to the January 10, 2006 case may have enabled the shallow convection to penetrate somewhat higher into the atmosphere in some locations. Another interesting feature of this case was that the CO level decreased dramatically over land to the north (Figure 4.8a). For example the retrieved profile at 41° N and 71° W over Rhode Island does not show any evidence of the enhancement and closely follows the shape of the universal a priori (Figure 4.8b). This may be evidence that the subsidence inhibited any lofting of the pollutants to altitudes to which thermal infrared instruments such as TES are less sensitive to CO [*Emmons et al.*, 2007]. Finally to the south the profile at 25° N and 75° W also showed no CO enhancement and this was likely due to dispersion of the pollutant plume since surface winds near the Florida coast were backing to the east and while further to the northeast they remained westerly.

For both cases TES retrieved clouds with tops between 700-900 hPa, which seemed consistent with the IR images in Figures 4.7 and 4.8 depicting low clouds.

Caution must be used when interpreting TES trace gas retrievals in the presence of clouds since errors in the retrievals of cloud parameters by TES can cause errors in the retrievals of trace gases [*Kulawik et al.*, 2006, *Ederling et al.*, 2008]. However, simulations of TES retrievals have indicated that even in cloudy conditions TES has valuable skill in retrieving trace gases and that the presence of clouds will not cause systematic biases in the trace gas retrievals [*Kulawik, et al.*, 2006]. Furthermore, we did not find any bias in CO retrieval over clouds during our analysis and therefore conclude that the highly enhanced CO retrieved by TES for these two cases and others like it reflect a real trace gas feature caused by a specific set of meteorological and topographical conditions.

These cases indicate that PCF convection over the ocean enhanced by the air-ocean temperature contrast may be an important mechanism for transporting polluted boundary layer air into the free troposphere. Yet, lofting by shallow convection seems to be underrepresented in the trajectory analysis possibly due to the coarse grid spacing of the model domain (40 km for EDAS), which makes it unable to resolve shallow convective processes over the ocean. This further suggests that the contributions of continental pollutants to the O_3 levels in the lower free troposphere may be underestimated by chemical transport models that rely on these meteorological inputs.
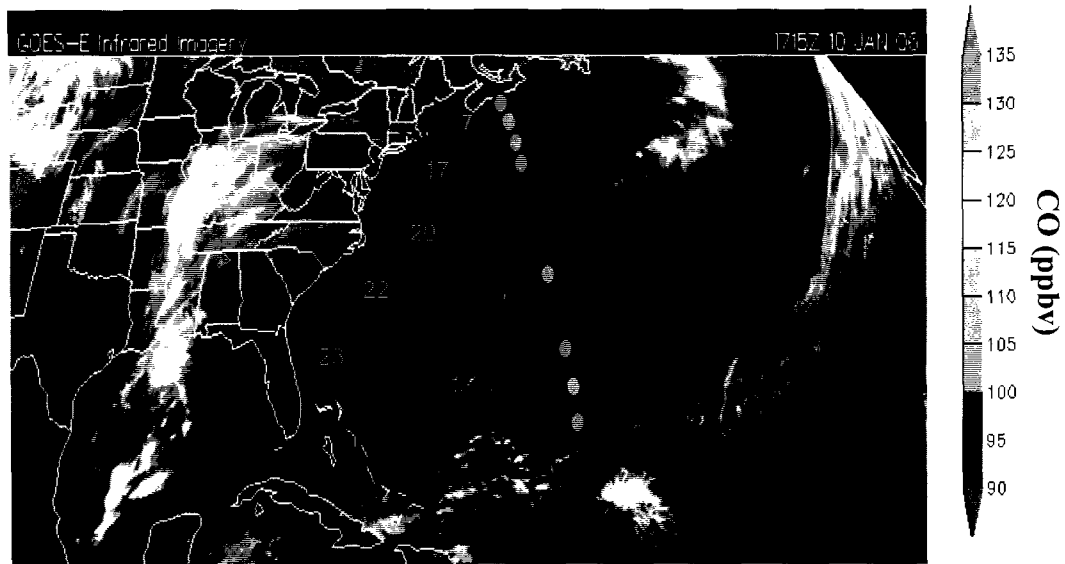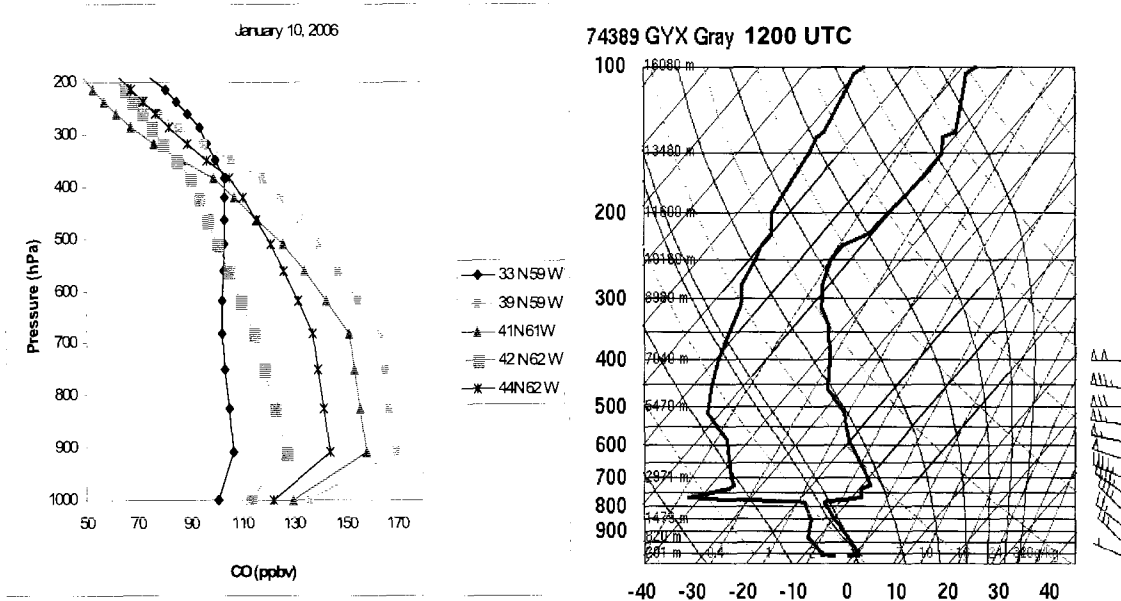
Figure 4.7. Surface level CO export case on January 10, 2006, a) GOES-East IR satellite image for 1715 UTC with TES 681 hPa CO (ppbv) plotted in colored dots b) TES CO retrieved profiles (ppbv) for 1700 UTC ascending orbit, and c) Skew-T sounding plot from Grey, ME for 1200 UTC. The blue arrows on a) show the orientation of surface streamlines and sea surface temperatures from buoy measurements are indicated with red numbers. Satellite images downloaded from Plymouth State University Weather Center [http: vortex.plymouth.edu] and sounding plots from the University of Wyoming [http://weather.uwyo.edu upper-air sounding.html].

114
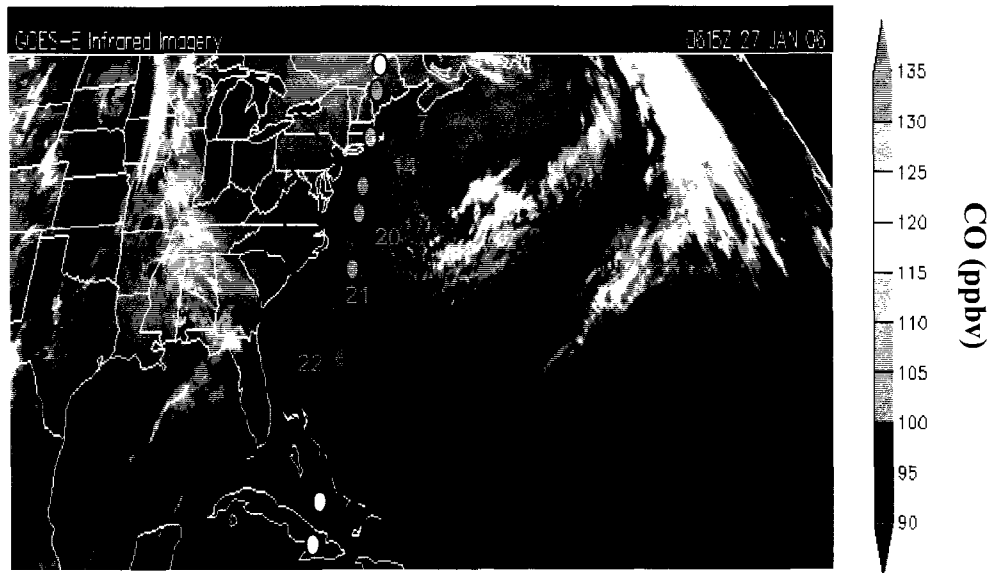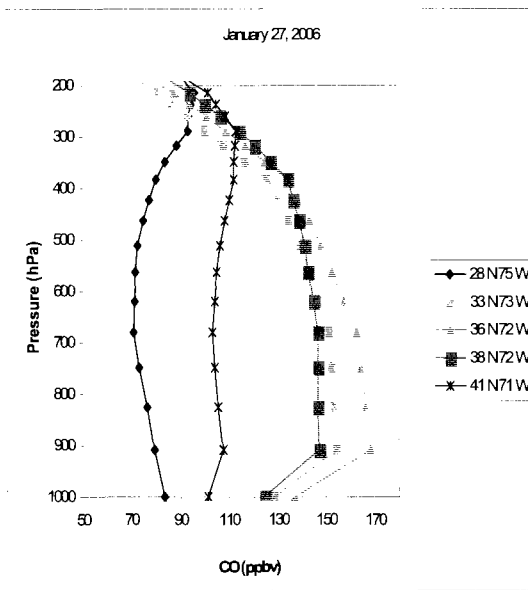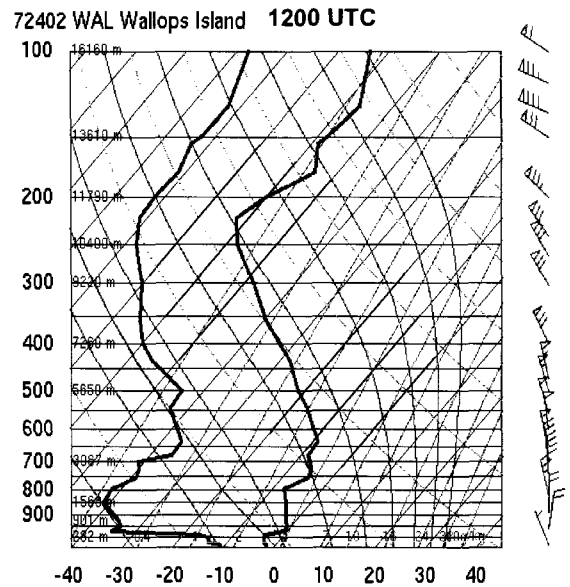
Figure 4.8. Surface level CO export case on January 27, 2006, a) GOES-East IR satellite image for 0615 UTC with TES 681 hPa CO (ppbv) plotted in colored dots b) TES CO retrieved profiles (ppbv) for 0600 UTC ascending orbit, and c) Skew-T sounding plot from Grey, ME for 1200 UTC. The blue arrows on a) show the orientation of surface streamlines and sea surface temperatures from buoy measurements are indicated with red numbers. Satellite images downloaded from Plymouth State University Weather Center [http: vortex.plymouth.edu] and sounding plots from the University of Wyoming [http: weather.uwyo.edu upper-air.sounding.html].

In contrast to the CO composites that had many enhanced features, the composite 681 hPa O_3 levels remained low (< 50 ppbv) likely due to the slower photochemical production of the winter season (Figures 4.9a, 4.9c, and 4.9d). The exceptions were the areas of O_3 levels > 55 ppbv in the DJF4 composite near the North Carolina Coast and slightly less enhanced levels extending well offshore to 55° W (Figure 4.9d). In this general region (denoted Region 1 in Figure 4.9d) O_3 and CO were positively correlated (r=0.56) with a slope of 0.40 (Figure 4.10). This slope value, which is the highest of all the DJF map types (Table 4.4), is more typical of summertime values suggesting a greater influence of photochemical production (*Parrish et al.,* 1993, 1998; *Chin et al.,* 1994; *Daum et al.,* 1996; *Mao et al.,* 2004; *Zhang et al.,* 2006). It probably resulted from the cyclones of further southern origin which may have entrained air masses that had been exposed to stronger solar radiation at lower latitudes. For example, ensemble HYSPLIT back trajectories using EDAS data indicated that 4 of 5 DJF4 cases that featured O_3>55 ppbv in Region 1, had ensemble members that passed through the boundary layers of the Gulf of Mexico, southeastern U.S., or the southern Ohio Valley. One illustrative case occurred on December 30, 2005 and with 681 hPa TES retrievals of O_3 > 60 ppbv and CO > 120 ppbv in a WCB airstream of a cyclone that intensified over the Carolinas (Figure 4.11). This case shows that contribution to the lower free tropospheric O_3 budget from continental export is possible even in winter months. Due to the lower frequency of DJF4 and the strict requirement of having both O_3 and CO retrievals pass all quality checks and the rigorous cloud screening, this slope calculation was based on <20 points and thus a longer term study is needed to confirm our hypothesis.
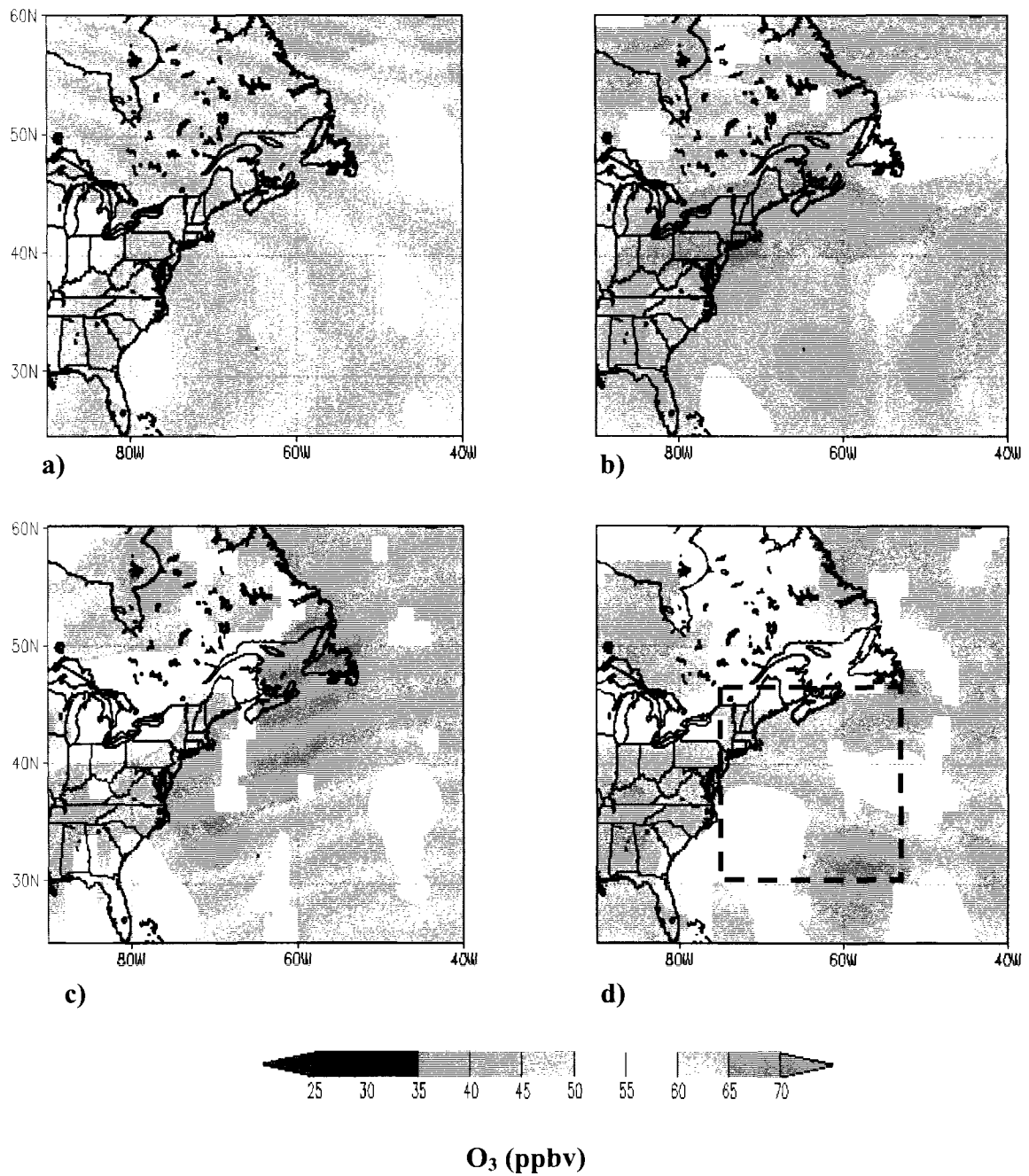
Figure 4.9. The DJF 681 hPa O_3 (ppbv) composites for the map types DJF1-DJF4 (a-d). The borders of Region 1 corresponding to scatter plots are marked as a dashed line on d.
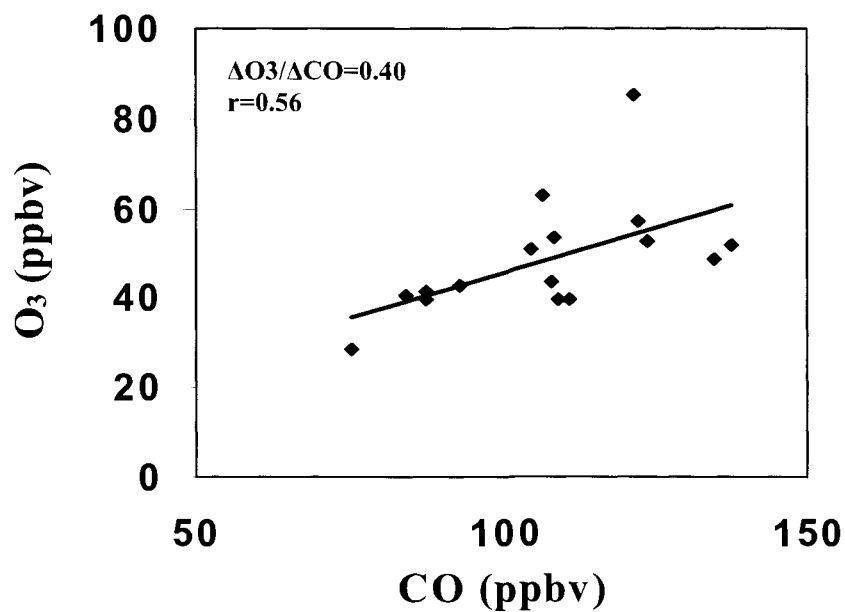
Figure 4.10. Scatter plot of 681 hPa O_3 versus CO in Region 1 for DJF4.

Table 4.4. DJF O_3-CO slope, correlation coefficient (r), and sample size N for circulation types in Region 1 30 – 45° N, 75-55° W.

All	0.09 (0.18), N=188
DJF1	0.03 (0.09), N=52
DJF2	0.11 (0.20), N=53
DJF3	0.13 (0.23), N=15
DJF4	0.40 (0.56), N=16
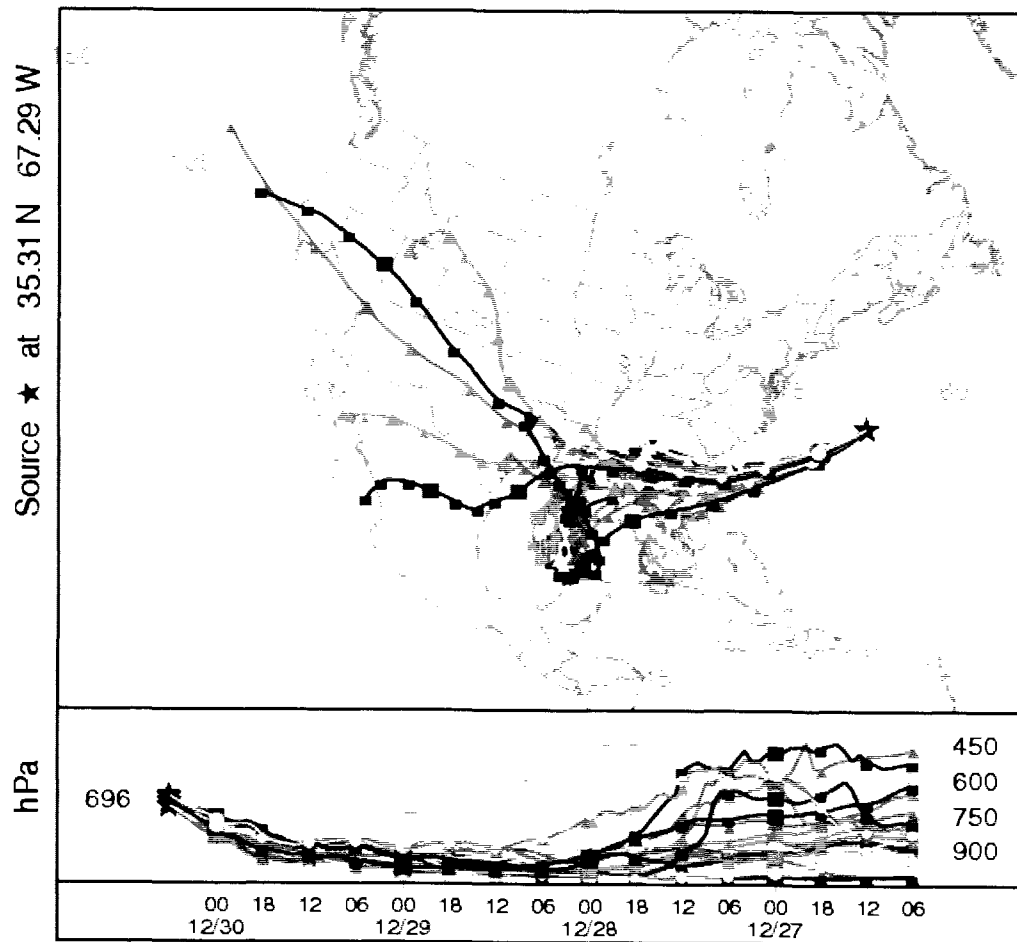
Figure 4.11. HYSPLIT ensemble 4-day back trajectories from 06 UTC, December 30, 2005 based on EDAS 40 meteorological data.

119

The 316 hPa O_3 composites for both DJF4 and DJF3 (frequently preceding DJF4) indicated penetrations of enhanced O_3 (> 80 ppbv) deep into the southeastern U.S. (Figures 4.12c, 4.12d), that were found to be associated with PV maximums at 400 hPa (4.13c and 4.13d) suggesting stratospheric intrusion into the upper troposphere in this region. It is possible that these stratospheric intrusions may have contributed to the high O_3 levels at 681 hPa for DJF4. However, we found only one case, January 7, 2006, that had enhanced O_3 and an ensemble of back trajectories from 681 hPa featuring exclusively descending motions. Other cases showed evidence of mostly ascent to 681 hPa or a mixture of ascending and descending trajectories which is consistent with the positive O_3 and CO correlation statistics and slopes for this region.

The 316 hPa CO composites for map types DJF1, DJF3, and DJF4 also showed a high degree of spatial variability. One of the striking features was the high levels of CO over the northeastern U.S. and southeastern Canada for DJF4 (and to a lesser extent DJF1) which in some locations exceeded 95 ppbv (Figure 4.14). These features were generally behind the surface cyclone positions making it difficult to identify anthropogenic contributions from North America in particular since pollutants from that source region would generally be lofted ahead of the cyclone in the WCB. Five-day HYSPLIT ensemble back trajectories using EDAS data originating from the area of 40 – 55 °N and 85 – 65 °W suggested that, out of the 6 DJF4 cases, one (December 30, 2005, as discussed earlier in this section) passed close to the North American boundary layer over the Gulf of Mexico states at the lowest altitude of ~2 km. The trajectories for the other 5 cases had generally remained in the upper troposphere and lower stratosphere with Asian origin and all had passed through the arctic at one point along the path. It is

120

possible that the enhanced CO levels are the result of pollutants that have accumulated in the lower stratosphere as shown by *Cooper et al.* [2002b].   In addition, aircraft and ground-based observations have shown that anthropogenic pollutants primarily from Eurasia can build up and persist in the arctic troposphere and extend to high altitudes forming the Arctic haze [*Wolfsy*, 1992; *Law and Stohl,* 2007].

DJF2: Less Active Midlatitude Storm Track

In contrast to the other wintertime map types the 681 hPa CO composites for DJF2 exhibited less evidence of pollutant export to the lower free troposphere. In general CO levels exceeding 105 ppbv were confined to the immediate U.S. coastal areas while offshore midlatitude regions mostly showed levels below 100 ppbv (Figure 4.6b).   For DJF2 the lower tropospheric circulation pattern was dominated by a large offshore anticyclone with near zonal to west-southwest flow over eastern U.S. and the adjacent oceans.   The anticyclone produced a generally weak subsidence over the region restricting synoptic-scale vertical transport from the boundary layer of the continent. The subsidence may have been occasionally disrupted by the passage of troughs extending from cyclones tracking further north in Canada. However, given the lower CO levels off the U.S. coast pollutant transport to the lower free troposphere from these systems was generally less than that produced by the cyclones in map types DJF1, DJF3, and DJF4.

One of the only significant features of the DJF2 composites was an area of enhanced 316 hPa CO levels (> 100 ppbv) offshore east of 55° W between 35° N and 40° N (Figure 4.9b).   Of nine cases that had 316 hPa CO > 95 ppbv in this region, only two showed evidence of export from the North American continent based on five-day GDAS back trajectories (not shown). In the December 9, 2005 case a sharp trough on the

extreme western side of the main anticyclone caused rapid uplift over the Gulf Coast states, and in the December 17, 2005 case rising motion occurred over the southeastern U.S. on the previous day in the WCB of a DJF3 cyclone These two cases were atypical of the DJF2 scenario as in both cases the anticyclone was not dominant and did not extend far inland allowing for export from the U.S. via other synoptic systems.
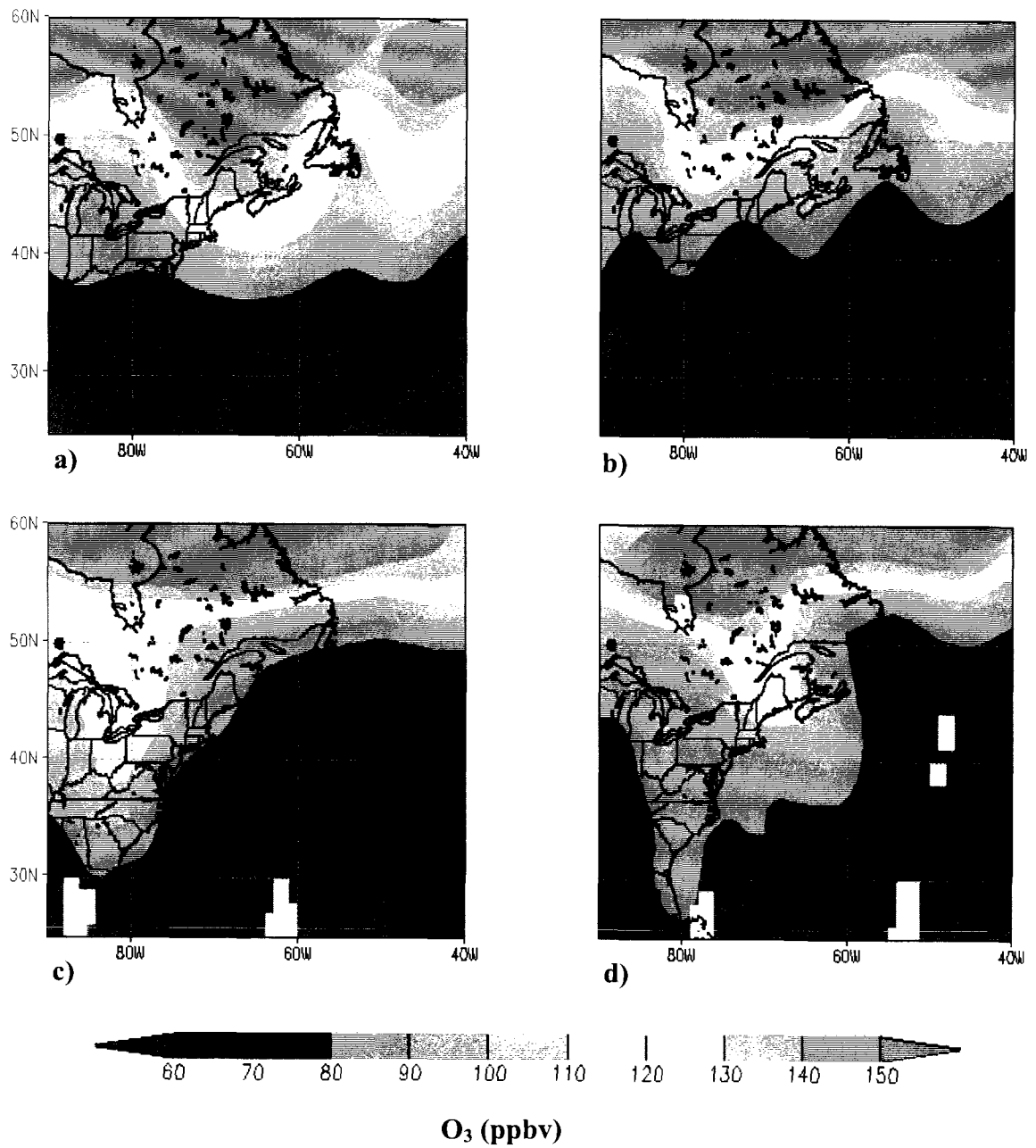
Figure 4.12. The DJF 316 hPa O_3 (ppbv) composites for map types DFJ1 – DFJ4 (a-d).

123
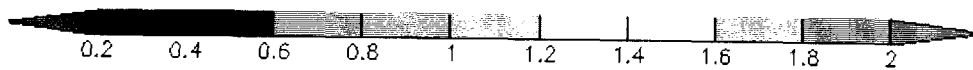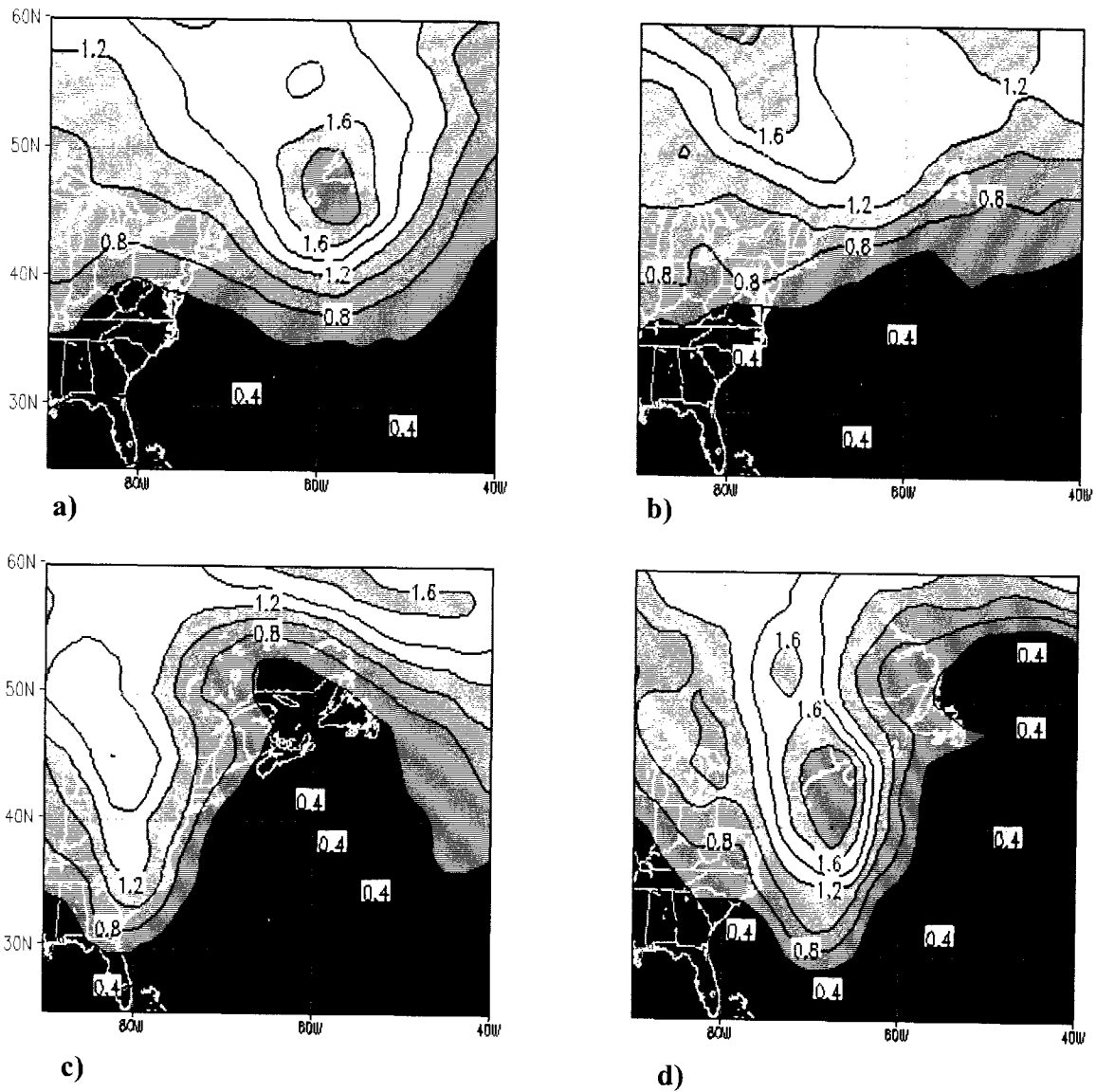
Figure 4.13. NNRA potential vorticity ($10^6 * Km^2s^{-1}kg^{-1}$) composites interpolated to 400 hPa for DJF1- DJF4 (a-d).

124
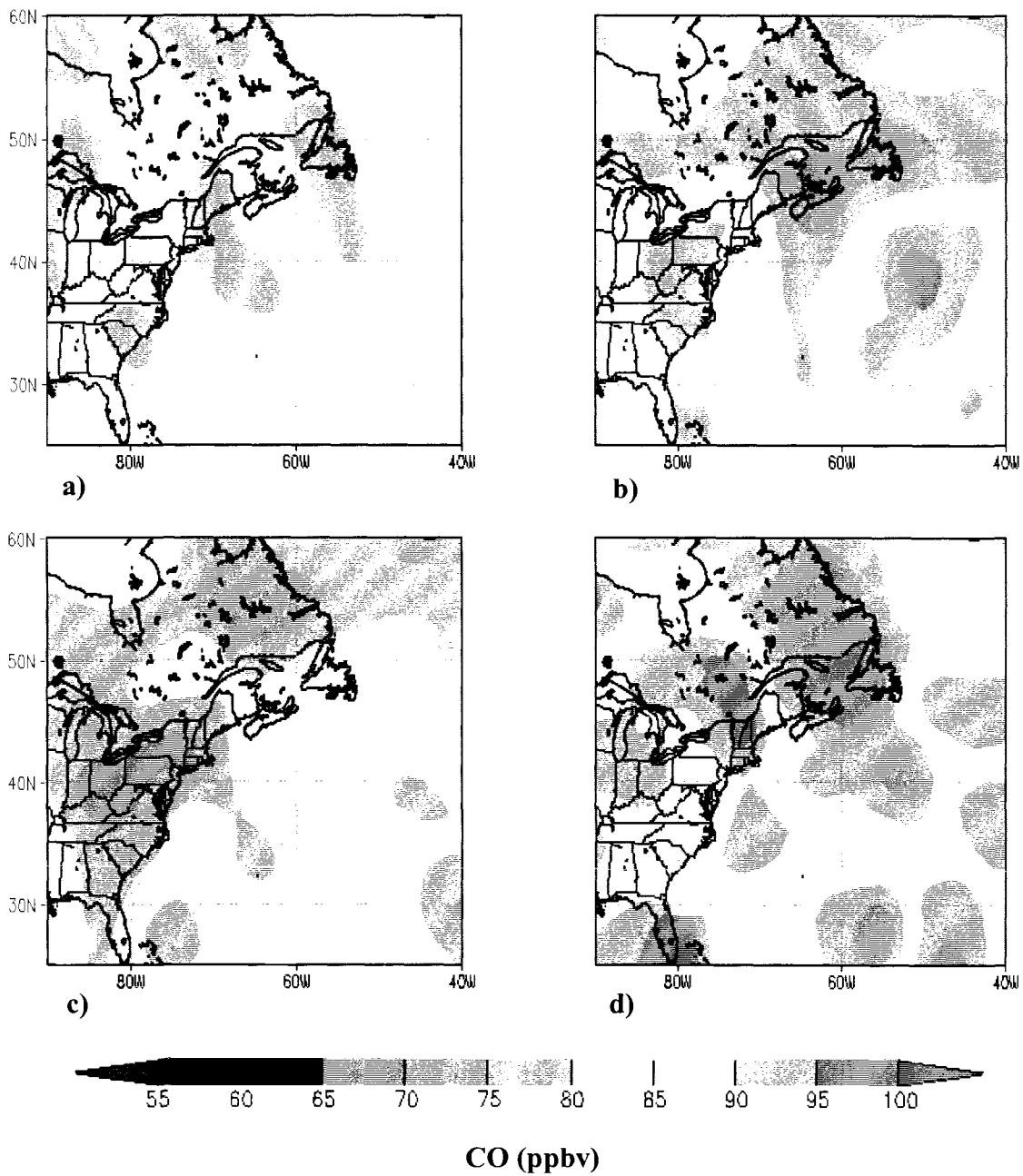
Figure 4.14. The DJF 316 hPa CO (ppbv) composites for map types DJF1 – DJF4 (a-d).

125

Circulation Influences on O_3 and CO Distributions in Summer

The five original map types for summer could be grouped into three more general flow patterns. The first pattern was a dominant subtropical anticyclone or Bermuda High and is represented by map types JJA1 and JJA3. The second was a cyclonic trough to the east of the northeastern U.S. and Canadian Maritimes coastlines, shown in map types JJA2 and JJA4. The third was a closed cyclone along the east coast represented by map type JJA5. The influence of these flow patterns on the pollutant distributions will be contrasted in the following 3 sub-sections.

JJA1 and JJA3: Subtropical Anticyclone

As discussed in previously the dominant Bermuda High produced a general southwest to northeast flow in the lower troposphere. As a consequence the pollutant transport from the continent to the free troposphere followed a northeasterly path around the western and northern edges of the anticyclone before exiting the continent east of the Canadian Maritimes. This pathway is indicated by the areas of enhanced CO in the 681 hPa composites that dropped steeply to below 95 ppbv over the ocean south of 50° N but remain high for quite some distance offshore north of 50° N (Figures 4.15a and 4.15c). A similar drop off in 681 hPa O_3 south of 50° N also occurred with levels decreasing from near 70 ppbv along the coast to 55 – 60 ppbv further offshore (Figures 4.16a and 4.16c). Furthermore, for both JJA1 and JJA3 O_3-CO slopes of 0.33 and 0.34 mol mol^{-1} in Region 2 were significantly greater than those in Region 1 (0.17 and 0.03 mol mol^{-1}) and Region 3 (-0.03 and -0.06 mol mol^{-1}) (Table 4.3). The influence of continental outflow appears to extend farther north facilitated by the circulation in these two map types.
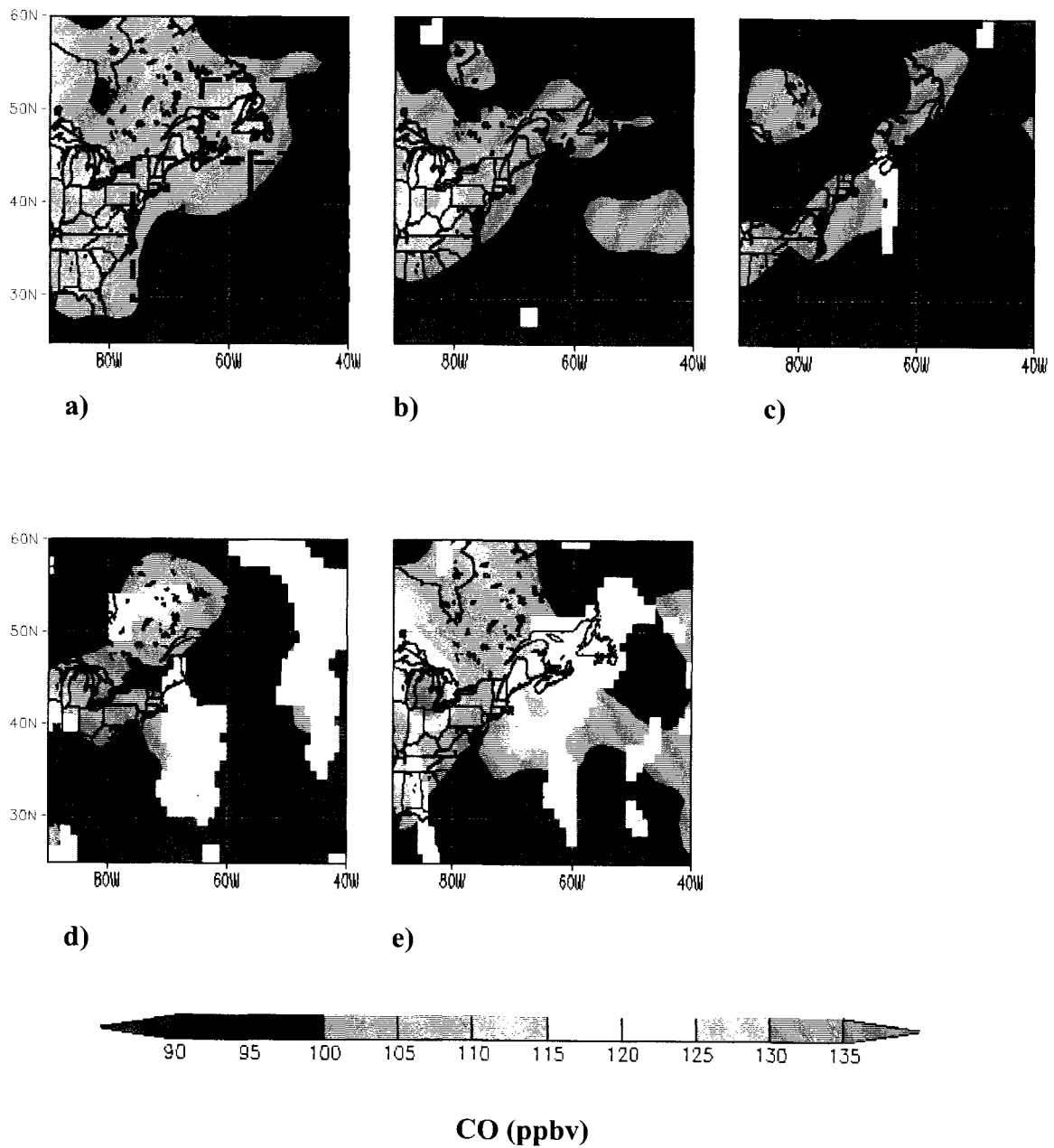
Figure 4.15. The JJA 681 hPa CO (ppbv) composites for map types JJA1 – JJA5 (a-e).
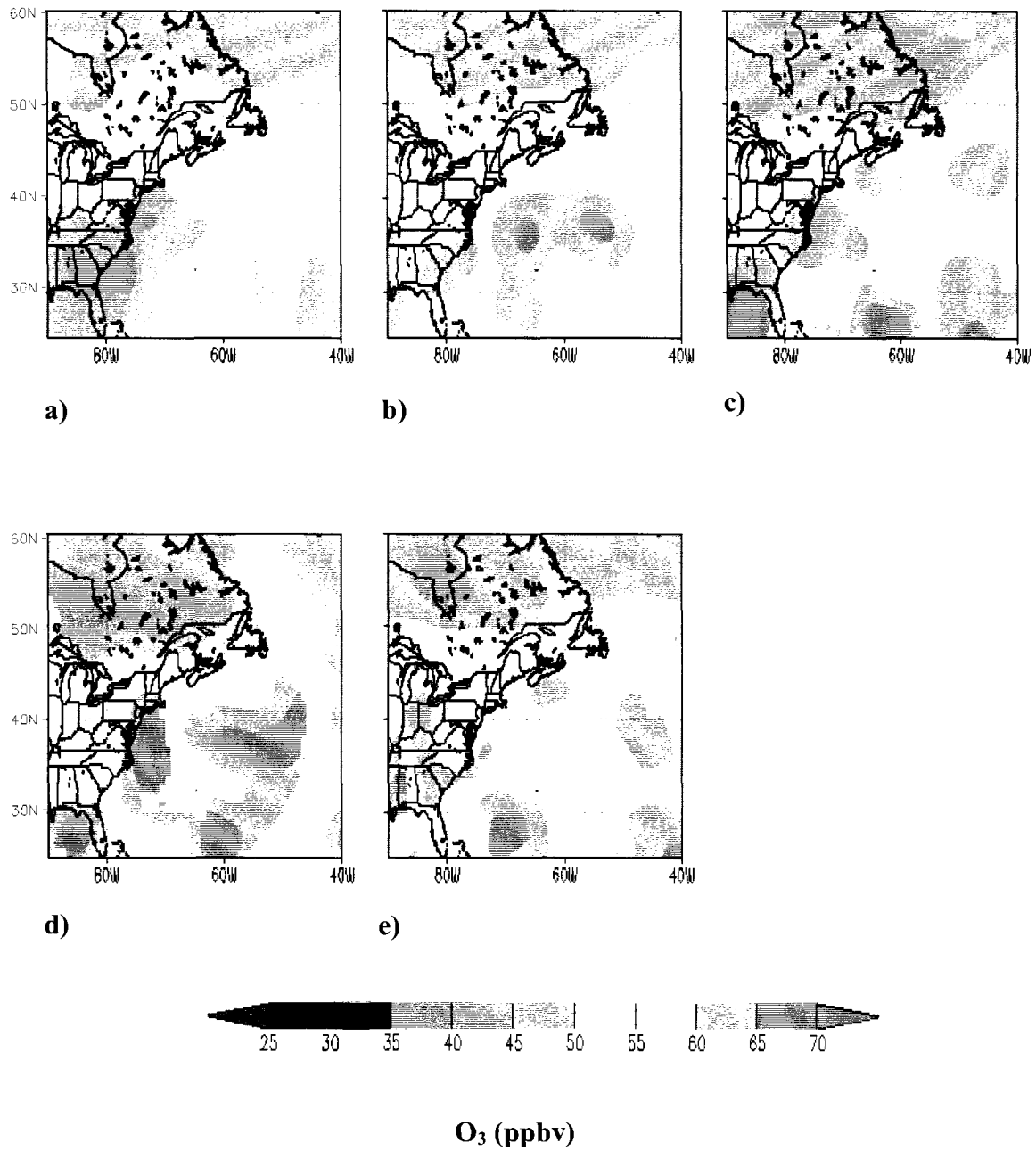
Figure 4.16. The JJA 681 hPa O3 (ppbv) composites for map types
JJA1 – JJA5 (a-e).

It should be noted that direct export to the free troposphere south of 50°N was still possible by mesoscale features such as sea breeze circulations that loft pollutants from the surface and may be transported over the ocean above the marine boundary layer [*Li et al.*, 2002]. This transport mechanism possibly contributed to the enhanced O_3 and CO and positive O_3-CO slopes in the western portion of Region 1. However, under this scenario it may take up to 10 days for an air parcel to cross the Atlantic Ocean [*Owen et al.*, 2006], and subsequently the considerable photochemical aging of the air mass in transit resulted in the reduced O_3-CO slopes as observed in Region 3.

This export pattern of JJA1 and JJA3 appeared to be consistent throughout the troposphere as the 316 CO composites showed a high degree of spatial correlation with the 681 hPa composites (not shown). While lofting of boundary layer pollutants near the center of the anticyclone was restricted due to general subsidence, satellite images (not shown) indicated that convection near the western edge of the anticyclone, some of which was concentrated over considerable areas in the U.S. Central Plains and Midwest, was common and likely lofted pollutants to high altitudes in the troposphere.

JJA2 and JJA4: Cyclonic Trough

In contrast to JJA1 and JJA3 the cyclonic trough patterns of JJA2 and JJA4 enabled continental export south of 50° N to flow well offshore. The 681 hPa O_3 and CO composites showed enhanced levels (O_3 > 60 ppbv, CO > 100 ppbv) south of 50° N extending to the eastern edge of the study domain at 40° W. In addition, the O_3-CO slopes for JJA2 were 0.29 mol mol^{-1} in Region 1 and 0.57 mol mol^{-1} in Region 3 indicating that O_3 production continued in exported plumes well offshore (Table 4.3). The O_3–CO slopes for JJA4 were also high at approximately 0.40 mol mol^{-1} in both

regions; however, these slopes are suspect given that they were based on 10 or fewer data points in each region.

There were 2 main export pathways associated with these cyclonic troughs. One was associated with the WCB which was located to the east side of the troughs. In this scenario cyclones developed over the U.S. or along the U.S. coast and eventually moved northeastward to Labrador lofting continental pollutants to the free troposphere in their WCBs and transporting them offshore as was shown to be common in springtime in Chapter III. An analysis of the maps preceding those classified as JJA2 or JJA4 revealed that this sequence occurred only about one third of the time.

The second pathway was associated with cyclones that originated in central Canada and moved eastward and southeastward with a cold frontal trough penetrating into the eastern U.S.. The cold fronts of these systems swept southeastward and possibly produced some WCB lofting of pollutants from populated areas of eastern North America, particularly in southeastern Canada, New England, and upstate New York.

One example of this transport pattern occurred over a three-day period of 1 – 3 August 2006 when the circulation was classified as either JJA2 or JJA4 as a succession of troughs passed off the east coast. Satellite loops for this case indicated that large areas of convection lofted air to the free troposphere where it was transported northeastward into Canada before being incorporated into the northwesterly flow behind the cyclonic troughs and transported to the central Atlantic Ocean. The infrared (IR) image of 0015 UTC August 2, 2006 shows this area of convection extending from the Central Plains across the upper Midwest into Canada to the west of a large anticyclone centered over the southeastern U.S. (Figure 4.17). Because of the succession of troughs during this period

the enhanced O_3 and CO levels in some cases may have been associated with the northwesterly descending motion from distant sources on the back side of a trough that had previously passed as shown by the back trajectories in Figure 4.18. However, contributions from sources along the east coast cannot be entirely dismissed since trajectories relying on meteorological data with a resolution of 1° x 1° may not have accurately resolved the smaller-scale convection in this area that was evident in the satellite images.
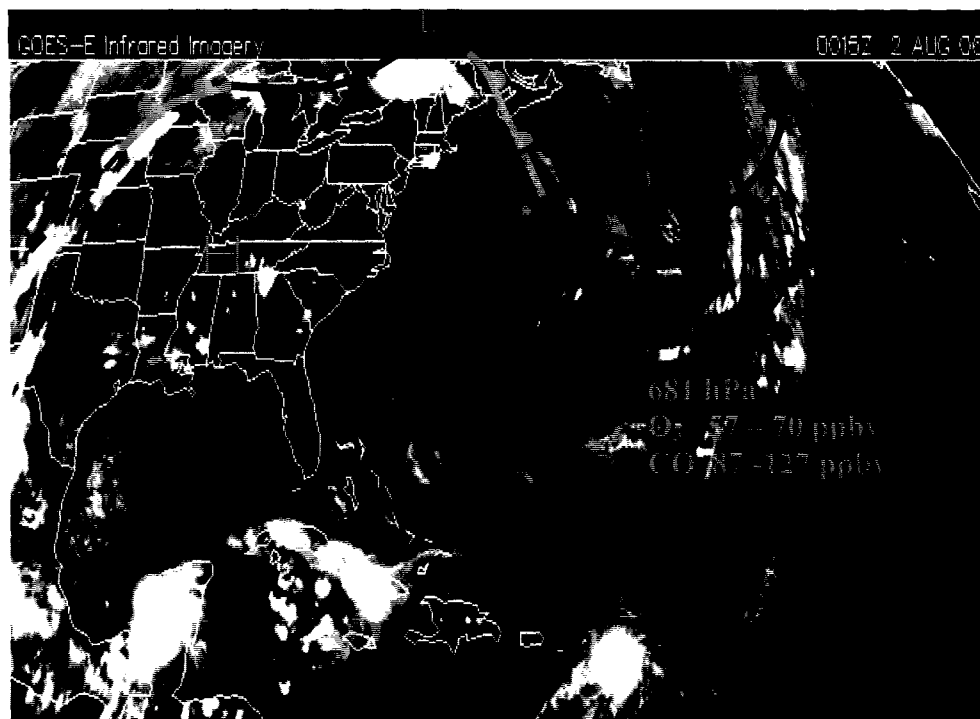
Figure 4.17. GOES IR image for 0015 UTC August 2, 2006 with frontal positions estimated from 2130 UTC August 1, 2006 NCEP Atlantic surface analysis [http://nomads.ncdc.noaa.gov.ncep-charts/hires/20060801/stlsfc18z.2006080121.gif]
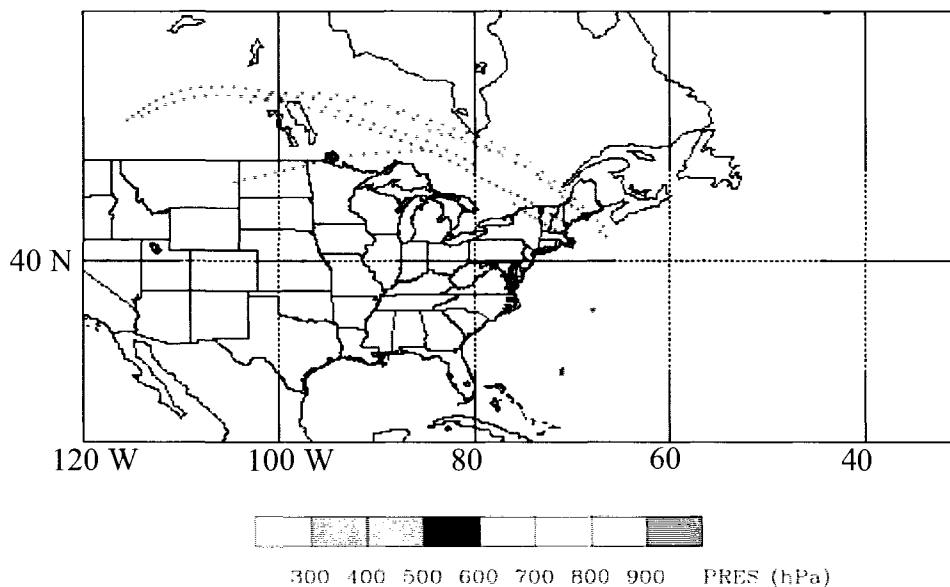
Figure 4.18. Three-day HYSPLIT back trajectories with GDAS meteorological data from times and locations of 681 hPa TES observations in western North Atlantic Ocean during August 1-3, 2006.

JJA5: Closed East Coast Cyclone

The 681 hPa O_3 and CO distributions for the coastal cyclonic type JJA5 were influenced by a number of transport factors. There was an area of enhanced 681 hPa CO (>100 ppbv) extending well out into the Atlantic Ocean along 40° N related to the WCB outflow as the cyclones moved up the east coast or tracked northeastward from the central U.S. (Figure 4.15e). The 681 hPa O_3 levels in this region were also enhanced to >55 ppbv but decreased to < 50 ppbv near the cyclone center (Figure 4.16e). Another interesting feature of the 681 hPa CO composites was the highly enhanced levels (110 - 130 ppbv) extending from New England out into the Gulf of Maine and the Gulf of St. Lawrence. The enhanced CO measurements in this region occurred on three different days and possibly had contributions from different sources.

The first occurrence was on July 23, 2005 due to a cyclone tracking from northern plain states of the U.S. to the Gulf of Maine. This system produced WCB lofting over the Midwest states resulting in 681 hPa CO > 120 ppbv (and 316 hPa CO as high as 140 ppbv) over the Gulf of St. Lawrence. The second occurrence was on June 11, 2006 when an intense east coast cyclone tracked northward from the coast of the southeastern U.S. This system circulated and lofted air originally from the boundary layer over Florida and the Gulf of Mexico all the way around its center to western New England and also transported air from the upper troposphere over northern Canada off the coast south of New England. In both these locations TES retrieved 681 hPa CO ranging over 104 – 110 ppbv. The third occurrence was on June 15, 2006 when a very intense cyclone developed from the remnants of tropical storm Alberto combined with a migrating upper level trough over the southeastern U.S. The corresponding 681 hPa CO in eastern New England and offshore ranged over 112-143 ppbv. The back trajectories indicated sources including WCB lofting over the mid-Atlantic and New England states by the cyclone, entrainment of air from the west coast associated with the migrating upper-level trough, and downward transport from the middle and upper troposphere of northern Canada.

Interestingly, the highest CO measurements for both the second and third cases came from the northern Canadian route. Five and six-day back trajectories indicated that the air had been transported in the middle and upper troposphere over the boreal forest regions of Alaska and eastern Siberia before turning southward in central Canada and descending to the lower troposphere in the DA of the cyclone (Figure 4.19). Since the boreal forest fire season generally starts in late May and continues through the summer and fire pollutants can be transported upward as high as the lower stratosphere by Pyro-

convective updrafts it is possible that fire outflow may have contributed to the higher CO levels as has been documented in previous studies [*Wotawa and Trainer*, 2001; *Fromm et al.*, 2005; *Cammas et al.*, 2008]. While further study is needed to verify this scenario, our results suggest that well-developed cyclones that produce strong northerly DA flow through Canada may provide a mechanism for transporting pollutants from boreal fires regions to the east coast of the U.S. and southern Canada.
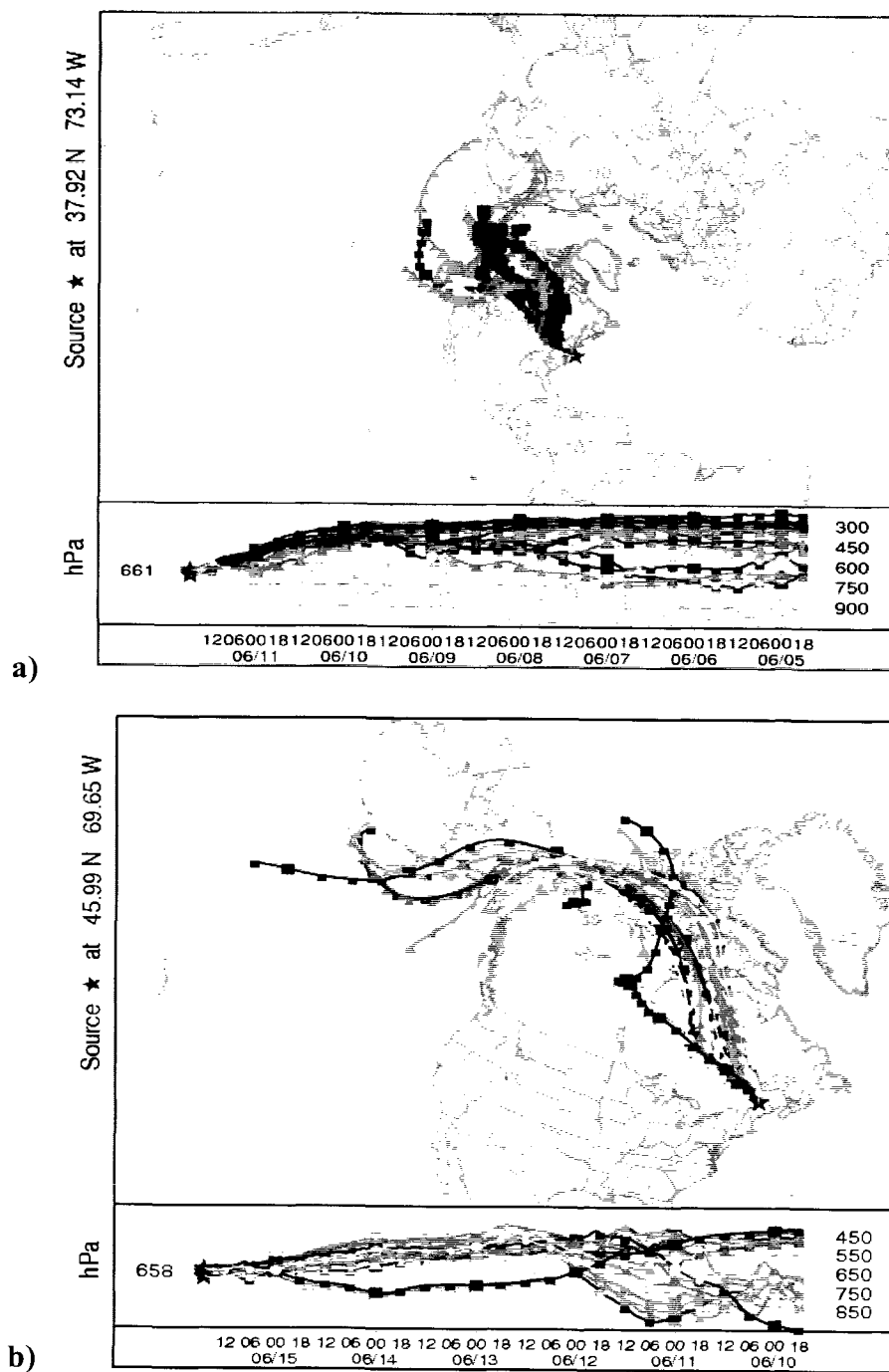
Figure 4.19. HYSPLIT ensemble back trajectories using GDAS data from enhanced 681 hPa CO measurement locations classified as map type JJA5; a) six-day back trajectories starting at 1800 UTC June 11, 2006 from 37.9 N and 73.14 and b) five-day back trajectories starting at 1700 UTC June 15, 2006 from 46.0 N and 69.6 W.

135

Conclusion

The TES free tropospheric O_3 and CO composites clearly showed enhancements in pollutant levels downwind from North America in both DJF and JJA and the seasonal differences in these distributions. In DJF the evidence for pollutant export was primarily in the CO measurements as the lack of solar radiation limited O_3 production in exported pollutants. In JJA both CO and O_3 showed enhanced levels downwind of North America. In addition, the TES seasonal composites indicated a northward shift of the axis of greatest export from winter to summer corresponding to the northward shift of the storm track. While the a priori used in the retrieval process may add temporal and spatial structure to the retrieved distributions the observations in our study were reprocessed with a universal a priori to remove this artificial artifact. Therefore the clear differences in the seasonal composites were due to real differences in the trace gas distributions bought about by the seasonal changes in solar radiation and circulation patterns.

In DJF the lower tropospheric CO enhancements over the western North Atlantic Ocean were due in large part to lofting of pollutants from the boundary layer of North America by the WCB of passing cyclones. There seemed to be little evidence of pollutant export in the O_3 fields due to slow photochemical production. The exception was for cyclones developing in southern latitudes that could incorporate air exposed to sunnier, warmer and more humid conditions favoring O_3 production. Enhancements to upper tropospheric O_3 during DJF were mainly due to stratospheric intrusions associated with cyclones. Enhancements to upper tropospheric CO did not appear to be tied to regional circulation patterns as defined by a map type on a particular day, but the result of long-range transport over the many days. Many of the back trajectories associated with

136

high 316 hPa CO measurements passed through the arctic suggesting the build-up of high pollutant levels that in that region.

A potentially important finding was that lower free troposphere CO levels over the ocean immediately downwind of the coast could be enhanced to greater than 150 ppbv behind a cold front.   While the tropospheric flow in this region tends to be dominated by descending motions associated with the DA, shallow smaller-scale convection behind the cold front may also occur to loft pollutants from the boundary layer to the free troposphere. Behind a cold front that has just passed offshore shallow convection is facilitated by rapid destabilization of polar or arctic air as it flows over much warmer ocean surface. This process, typically not resolved in the back trajectory analysis due to the coarse resolution of the meteorological inputs, was associated with some of the most enhanced 681 hPa CO levels in the composites and may indicate a significant contribution to pollutant levels in the free troposphere over the western North Atlantic Ocean.

During JJA the general circulation over eastern North America and the western North Atlantic Ocean was dominated by the subtropical Bermuda High anticyclone. This pattern caused the main band of export, most evident in 681 hPa CO composites, to flow anticyclonically around the high pressure system through New England and off the coast of the Canadian Maritime. However, weak cyclones moving northeastward across the U.S. and those tracking across Canada with cold frontal troughs penetrating south of the U.S. Canadian border enhanced O_3 and CO levels in the Atlantic Ocean south of the main seasonal export band through WCB lofting and incorporation of convectively lofted pollutants into the northwesterly flow behind preceding systems.   Intense cyclonic

systems were the least common circulation pattern in JJA, but also showed evidence of WCB export of both O_3 and CO. In addition these systems produced strong northerly flow on their western sides as they move northward along the east coast which facilitated long-range transport of air from northern latitudes that was possibly contaminated with pollutants related to boreal fire outflow.

The analysis of TES measurements in DJF and JJA showed clear evidence of the influence of seasonal circulation patterns on pollutant levels over the western North Atlantic Ocean and provided evidence of previously studied mechanisms of continental export such as WCB outflow. In addition the TES measurements suggested other mechanisms such as oceanic convective lofting in winter could be an important factor. These observations should therefore prove to be invaluable in future observational and modeling efforts geared toward a more complete understanding of all the contributing factors involved in regulating pollutant levels in the continental export region.

CHAPTER V

SUMMARY

One of the main objectives of this work, addressed in Chapter II, was to develop relationships between the synoptic circulation patterns and surface O_3 over the northeastern US during the summertime when pollution episodes are most common. The synoptic analysis for 2000-2004 identified five common surface circulation patterns, referred to as map types, which accounted for nearly two-thirds of the days. The highest daily maximum O_3 levels over the entire Northeast were associated with the most common pattern (Map Type I) which featured the Bermuda High. Elevated O_3 levels also existed on the western side of high pressure systems and to the east of advancing cold fronts or retreating anticyclones. In general these systems provided warm southwesterly flow favorable for O_3 production from precursors built-up under the stagnant conditions of the anticyclones over the polluted northeastern U.S. In contrast low daily maximum O_3 levels were associated with migrating anticyclones centered over the Upper Great Lakes and Southern Canada, and coastal anticyclone / Midwest cyclone or trough combinations. The migrating anticyclones, typically following cold fronts, transported cooler less polluted air from Canada to the northeastern states and the cyclones created cloud cover unfavorable for O_3 production.

There was statistically significant interannual variability in the O_3 levels as the domain-averaged mean daily maximum O_3 level rose to a peak of 64 ppbv in 2002, and

declined to its lowest value of 52 ppbv in 2004. Only <10 % of the interannual variability could be explained by the map type frequency, as documented in previous studies. In this dissertation work, I developed an improved O_3 trend reconstruction technique by incorporating a ΔO_3 term based on the circulation intensity index for each map type. This reproduced 46% the observed O_3 interannual variability, with the rest likely due to circulations not adequately addressed by our classification procedure and environmental factors such as recent reductions in power plant emissions of NO_x over the Eastern U.S. and the impact of temperature on biogenic precursor emissions.

A second objective of this work was to examine continental export from North America using data from the new TES sensor on Aura. This objective was addressed in Chapter 3, which focused on springtime continental outflow featuring a combination of peak O_3 levels and strong synoptic variability, and Chapter IV which focused on the contrasting synoptic controls over continental export in winter and summer seasons.

The synoptic classification technique developed in Chapter II was further applied to identify 6 predominant map types in spring for which composites of tropospheric O_3 and CO distributions were created from TES observations in 2005 and 2006. The highest O_3 and CO levels in the lower free troposphere, based on the observations at 681 hPa, over the western North Atlantic Ocean were associated with map types featuring cyclones near the east coast of the U.S. A hypothesis supported by case studies using ensemble back trajectories was that these enhanced levels were due to lofting of anthropogenic pollutants from the continental boundary layer via the warm conveyor belt (WCB) of cyclones. Another important finding emerging from these case studies was that boundary layer pollutants were exported to the lower free troposphere via a secondary WCB branch

(W2) circling around the back of the cyclone center, in addition to those transported by the main WCB branch to the east of the cold front. This result suggested an additional mechanism for O_3 enhancement in a region which had been considered to be influenced mainly by stratospheric intrusions facilitated by the dry airstream (DA) and is typically clearer than the main WCB branch where clouds may obscure many of the TES measurements. The TES O_3 composites did also reveal evidence of stratospheric intrusions associated with the DA mostly north of 45° N. However, a complicating issue was that in these regions the averaging kernel tended to shift to higher altitudes and thus observed increases in the 681 hPa O_3 levels were partly due to the fact that the TES retrieval was weighted more toward the upper troposphere where O_3 levels were extremely enhanced.

Composites of TES O_3 and CO retrievals showed the main export band extending from 30° N to 45° N with a seasonal O_3-CO slope of 0.13 mol mol^{-1} at 681 hPa ranging up to 0.20 mol mol^{-1} for the most favorable circulation patterns. These slopes were generally consistent with those derived from *in situ* measurements at surface sites and from aircraft in the lower free troposphere downwind of urban and industrial areas of North America [*Parrish et al.,* 1993, 1998; *Daum et al.,* 1996; *Zhang et al.,* 2006]. The O_3-CO slopes tended to increase further offshore as photochemical production continued to enhance O_3 along with mixing down of high O_3 air from the upper troposphere in the DAs of cyclones further east.

As in springtime, the TES measurements of O_3 and CO clearly showed enhancements in pollutant levels downwind from North America in both winter and summer. In winter the pollutant export was primarily noted in the CO measurements as

141

the lack of solar radiation limited O_3 production in exported pollutants. In summer both CO and O_3 showed evidence of continental export, although its influence was confined to the near-coastal region. Furthermore TES observations indicated a northward shift of the main axis of export from winter to summer corresponding to the northward shift of the storm track.

In winter the lower tropospheric CO enhancements east of North America were due in large part to WCB lofting of pollutants from the continental boundary layer by passing cyclones. In addition, a potentially important finding was that such enhancements could also be found over the near-coastal region due to lofting of continental pollutants by shallow convection induced by the rapid destabilization of cold arctic or polar air passing over relatively warm ocean water. A map type composite for cyclones that had tracked from southern latitudes showed slightly enhanced O_3 levels that were due to the incorporation of air exposed to sunnier, warmer and more humid conditions that favored O_3 production. Ozone enhancements were also noted in the upper troposphere associated with cyclonic map types due in large part to incursions of stratospheric air.

In summer the general circulation over eastern North America and the western North Atlantic Ocean was dominated by the subtropical Bermuda High anticyclone. This pattern caused the main band of export to flow anticyclonically around the high pressure system over New England and off the coast of the Canadian Maritimes. However, weak cyclones moving across the U.S. and Canada with cold fronts extending into the U.S. enhanced O_3 and CO levels in the Atlantic Ocean south of the mean export band through WCB lofting and incorporation of lofted pollutants from inland convective systems.

Intense cyclonic systems were the least common circulation pattern in summer, but their occurrence produced notable WCB export, and the strong northerly flow on their western flanks facilitated long-range transport of air from northern latitudes possibly contaminated with pollutants from boreal fires.

My studies show that overall the TES retrievals captured a high degree of variability with circulation patterns that was consistent with previous studies in spite of satellite retrieval problems such as the obscuring effects of clouds, the low vertical resolution (i.e. broad averaging kernel peaks), and lack of boundary layer sensitivity. Furthermore the fact that TES observations revealed distinct dominant circulation patterns and photochemical production potential for each season clearly shows that this data may be valuable for interseasonal and longer term climate studies.

This dissertation warrants future research on several topics. The technique we developed in Chapter II to associate the interannual variability of summertime surface O_3 in the northeastern U.S. with circulation based on map types could be useful for assessing the impact of future circulation changes on regional air quality. Future research should focus on applying the technique to longer time periods and refining its input parameters. My studies in Chapters III and IV using the TES observations showed a clear response to synoptic circulation patterns, and a future investigation extended over more years may uncover links between the interannual variability of continental export and circulation. The hypotheses of transport mechanisms related to continental export in Chapters III and IV were somewhat limited by the use of the TES retrievals only, two chemical compounds (i.e. O_3 and CO), and trajectories based on coarse-grid meteorological inputs. These hypotheses could be strengthened with the use of other atmospheric composition

data, particularly those of hydrocarbon precursors, and higher resolution meteorological and chemical transport models. Overall it is my hope that this work can be used as a solid starting point for a great number of future interdisciplinary studies focusing on climate and air quality issues.

LIST OF REFERENCES

Angevine, W. M., Senff, C., J., White, A. B., et al. (2004), Coastal boundary layer influence on pollutant transport in New England, *J. Appl. Meteorol.*, *43*, 1425-1437.

Appenzeller, C., Davies, H. C. and W. A. Norton, (1996), Fragmentation of stratospheric intrusions, *J. Geophys. Res.*, 101, 1435-1456.

Auvray, M., and I., Bey, (2005), Long-range transport to Europe: Seasonal variations and implications for the European ozone budget, *J. Geophys. Res.*, *110*, D11303, doi:10.1029/2004JD005503.

Auvray, M., Bey, I., Llull, E., Schultz, M. G., and S., Rast, (2007), A model investigation of tropospheric ozone chemical tendencies in long-range transported pollution plumes, *J. Geophys. Res.*, *112*, D05304, doi:10.1029/2006JD007137.

Banic, C. M., Leaitch, W. R., Isaac, G. A., Couture, M. D., Kleinman, L. I., Springston, S. R., and J. I. MacPherson, (1996), Transport of ozone and sulfur to the North Atlantic atmosphere during the North Atlantic Regional Experiment., *J. Geophys. Res.*, *101*, 29,091 – 29,104.

Beer, R. (2006), TES on the Aura Mission, Scientific objectives, measurements and analysis overview, *IEEE Trans. Geosci. Remote Sens.*, *44(5)*, 1102 -1105.

Beer, R., Glavich, T. A., and D.M. Rider, (2001), Tropospheric Emission Spectrometer for the Earth Observing System's Aura satellite, *Appl. Opt. 40*, 2356– 2367.

Bell, G.D., and L.F. Bosart, (1989), A 15-year climatology of Northern hemisphere closed cyclone and anticyclone centers. *Mon. Wea. Rev.*, 117, 2142-2163.

Berkowitz, C. M., Daum, P. H., Spicer, C. W., and K. M. Busness, (1996), Synoptic patterns associated with the flux of excess ozone to the western North Atlantic, *J. Geophys. Res.*, *101*, 28,923-28,933.

145

Bowman, K. W., Rodgers, C. D. Kulawik, S. S., et al., (2006), Tropospheric Emission Spectrometer Retrieval method and error analysis, *IEEE Trans. Geosci. Remote Sens.,* *44(5),* 1297-1307.

Bowman K. W., Worden, J., Steck, T.,Worden, H. M., Clough, S., and C. D. Rodgers, (2002), Capturing time and vertical variability of tropospheric ozone, A study using TES nadir retrievals, *J. Geophys. Res., 107,* NO. D23, 4723, doi:10.1029/2002JD002150.

Brasseur, G. P., Hauglustaine, D. A., Walters, S., et al., (1998), MOZART: A global chemical transport model for ozone and related chemical tracers: 1. Model description, *J. Geophys. Res., 103,* 28,265-28,289.

Cammas, J.P., Brioude, J., Chaboureau, J.P., et al., (2008), Injection in the lower stratosphere of biomass fire emissions followed by long-range transport, a MOZAIC case study, *Atmos. Chem. Phys. Discuss., 8,* 20925-20964.

Carlson, T. N. (1998), *Midlatitude Weather Systems,* Am. Meteorol. Soc., Boston, 507 pp.

Chin, M., Jacob, D. J., Munger, J. W., Parrish, D. D., and B. G. Doddridge, (1994), Relationship of ozone and carbon monoxide over North America, *J. Geophys. Res., 99,* 14,565-14,573.

Comrie A.C. (1992a), An enhanced synoptic climatology of ozone using a sequencing technique, *Physical Geography, 14,* 295-316.

Comrie, A.C. (1992b), A procedure for removing the synoptic climate signal from environmental data, *International Journal of Climate, 12,* 177-183.

Comrie, A.C. (1994), A synoptic climatology of rural ozone pollution at three forest sites in Pennsylvania, *Atmospheric Environment, 28,* 1601-1614.

Comrie A.C. and B. Yarnal, (1992), Relationships between synoptic-scale atmospheric circulation and ozone concentrations in metropolitan Pittsburgh, Pennsylvania, *Atmospheric Environment, 26B,* 301-312.

146

Cooper, O. R., et al., (2002a), Trace gas composition of midlatitude cyclones over the western North Atlantic Ocean: A conceptual model, *J. Geophys. Res., 107,* doi1011029/2001JD000902.

Cooper et al., (2002b), Trace gas composition of mid-latitude cyclones over the western North Atlantic Ocean: A seasonal comparison of O3 and CO, *J. Geophys. Res., 107,* D7, 10.1029/2001JD000902.

Cooper, O. R., Cooper, O. R., J.L. Moody, D.D. Parrish, M. Trainer, T.B. Ryerson, J.S. Holloway, G. Hubler, F.C. Fehsenfeld, S.J. Oltmans, and M.J. Evans, (2001), Trace gas signatures of the airstreams within North Atlantic cyclones: Case studies from the North Atlantic Regional Experiment (NARE '97) aircraft intensive, *J. of Geophys. Res., 106,* 5437-5456.

Cooper, O. R., Stohl, A., Eckhardt, S., et al., (2005), A springtime comparison of tropospheric ozone and transport pathways on the east and west coasts of the United States, *J. Geophys. Res., 110,* D05S90, doi:10.1029/2004JD005183.

Crawford, J., Olson, J., Davis, D., Chen, G., et al., (2003), Clouds and trace gas distributions during TRACE-P, *J. Geophys. Res., 108,* NO. D21 8818, doi:10.1029/2002JD003177, 2003.

Creilson, J. K., Fishman, J., and A. E. Wozniak, (2003), Intercontinental transport of tropospheric ozone: A study of its seasonal variability across the North Atlantic utilizing tropospheric ozone residuals and its relationship to the North Atlantic Oscillation, *Atmos. Chem. Phys., 3,* 2053-2066.

Daum, P. H., Kleinman, L.I., Newman, L., et al., (1996), Chemical and physical properties of plumes of anthropogenic pollutants transported over the North Atlantic during the North Atlantic Regional Experiment, *J. Geophys. Res., 101,* 29,029-29,042.

Derber, J. C., Parrish, D. F., and S. J. Lord, (1991), The new global operational analysis system at the National Meteorological Center, *Weather and Forecasting, 6,* 538-547.

Draxler, R. R. and G. D. Rolph, (2003), HYSPLIT (HYbrid Single-Particle Lagrangian Integrated Trajectory) Model access via NOAA ARL READY, NOAA Air Resources Laboratory, Silver Spring, MD, http://www.arl.noaa.gov/ready/hysplit4.html .

Eckhardt, S., Stohl, A., James, P., Forster, C., and N. Spichtinger, (2004), A 15-year climatology of warm conveyor belts, *J. Climate, 17,* 218 -236.

147

Ederling, A., Kulawik, S.S., Worden, J., Bowman, K., and G. Osterman, (2008), Implementation of cloud retrievals for TES atmospheric retrievals: 2. Characterization of cloud top pressure and effective optical depth retrievals, *J. Geophys, Res.*, *113*, D16S37, doi:10.1029/2007JD008858.

Environmental Protection Agency, (2005), *Evaluating Ozone Control Programs in Eastern United States: Focus on the NO_x Budget Trading Program*, EPA454-K-05-001, available at: http://www.epa.gov/airtrends/2005/ozonenbp.pdf, 35 pp.

Edwards, D.,P., Emmons, L.k., Hauglustaine, D.A., Chus, D.A., et al., (2004), Observations of carbon monoxide and aerosols from the Terra satellite: Northern Hemisphere variability, *J. Geophys. Res.*, *109, D24202, doi:10.1029/2004JD004727.*

Fehsenfeld, F. C., Ancellet, G., Bates, T. S., Goldstein, A. H., Hardesty, R. M., Honrath, R., et al., (2004), International Consortium for Atmospheric Research on Transport and Transformation (ICARTT): North America to Europe – Overview of the 2004 summer field study, *J. Geophys. Res.*, *111*, D23S01, doi:10.1029/2006JD007829.

Fishman, J., Watson, C. E., Larsen, J. C., and J. A. Logan, (1990), Distribution of tropospheric ozone determined from satellite data, *J. Geophys. Res.*, *95,* 3599-3617.

Fishman, J., Creilson, J. K., Wozniak, A. E., and P. J. Crutzen, (2005), Interannual variability of stratospheric and tropospheric ozone determined from satellite measurements, *J. Geophys. Res.*, *110,* D20306,doi:10.1029/2005JD005868.

Fromm, M., Belavicqua, R., Servranckx, R., Rosen, J., Thayer, J. P., Herman, J., and Larko, D. (2005), Pyro-cumulonimbus injection of smoke to the stratosphere: observations and impact of a super blowup in northwestern Canada on 3–4 August 1998, *J. Geophys. Res.*, *110,* D08205, doi:10.1029/2004JD005350, 20927.

Frost, G.J., et al., (2006), Effects of changing power plant NOx emissions on ozone in the eastern United States: Proof of Concept, *J. Geophys. Res.*, *111,* D12306, doi:10.1029/2005JD006345.

Gaza, R.S., (1998), Mesoscale meteorology and high ozone in the northeastern United States. *Journal of Applied Meteorology, 37,* 961-977.

148

Heidorn, K.C., and D. Yap, (1986), A synoptic climatology for surface ozone concentrations in southern Ontario, 1976-1981, *Atmospheric Environment, 20*, 695-703.

Hogrefe, C., et al., (2004), Simulating regional-scale ozone climatology over the eastern United States: model evaluation results, *Atmospheric Environment, 38*, 2627-2638.

Honrath, R. E., Owen, R. C., Val Martin, M., et al., (2004), Regional and hemispheric impacts of anthropogenic and biomass burning emissions on summertime CO and O3 in the North Atlantic lower free troposphere, *J. Geophys. Res., 109*, D24310, doi:10.1029/2004JD005147.

Huntrieser, H., et al. (2005), Intercontinental air pollution transport from North America to Europe: Experimental evidence from airborne measurements and surface observations, *J. Geophys. Res., 110*, D01305, doi:10.1029/2004JD005045.

IPCC (Intergovernmental Panel on Climate Change), (2001), Climate change 2001: the scientific basis. Contribution of Working Group I to the Third Assessment Report of the Intergovernmental Panel on Climate Change. Cambridge University Press, Cambridge, UK, 881 pp (ISBN 0521 807670).

Jacob D. J., J. A. Logan, J. A., Gardner, G. M., Yevich, R. M., Spivakovsky, C. M., and S. C. Wofsy, (1993), Factors regulating ozone over the United States and its export to the global atmosphere., *J. Geophys. Res., 98*, 14,817- 14,826.

Kasibhatla, P., Levy II, H., Klonecki, A., and W. L. Chameidas, (1996), Three-dimensional view of large-scale tropospheric distribution over the North Atlantic Ocean During Summer. *J. Geophys. Res., 101*, 29,305-29,316.

Key, J. R., and A. C. K. Chan, (1999), Multidecadal global and regional trends in 1000 mb and 500 mb cyclone frequencies, *Geophys. Res. Let., 26*, 2053-2056, 1999.

Kiley, C. M., and H .E. Fuelberg, (2006), An examination of summertime cyclone transport during Intercontinental Chemical Transport Experiment (INTEX-A), *J. Geophys. Res., 111*, D25S06, doi:10.1029/2006JD007115.

Kim, S.W, et al., (2006), Satellite-observed US power plant NOx emission reductions and their impact on air quality, *Geophys. Res. Let., 33*, L22812, doi:10.1029/2006GL027749.

Kim, S. Y., Talbot, R., Mao, H., et al., (2008), Continental outflow from the US to the upper troposphere over the North Atlantic during the NASA INTEX-NA Airborne Campaign, *Atmos. Chem. Phys. 8,* 1989-2005.

Kirchhofer, W., (1973), Classification of European 500 mb patterns. *Arbeitsbericht der Schweizerischen Meteorologischen Zentralanstatlt 43,* 205-207, Geneva.

Kulawik, S. S., Worden, J., Eldering, A., et al., (2006), Implementation of cloud retrievals for Tropospheric Emission Spectrometer (TES) atmospheric retrievals: 1. Description and characterization of errors on trace gas retrievals, *J. Geophys. Res., 111,* D24204, doi:10.1029/2005JD006733.

Lamaraque, J. F., Langford, A. O. and M. H. Proffitt, (1996), Cross-tropopause mixing of ozone through gravity wave breaking: Observation and modeling, *J. Geophys. Res., 101,* 22,969-22,976.

Law, K.S., and A. Stohl, (2007), Arctic air pollution: Origins and impacts, *Science, 315,* 1537-1540.

Li, Q., et al., (2002), Transatlantic transport of pollution and its effects on surface ozone in Europe and North America, *J. Geophys. Res., 107,* doi:10.1029/2001JD001422.

Li, Q., Jacob, D. J., Rokjin, P., et al., (2005), North American pollution outflow and the trapping of convectively lifted pollution by upper-level anticyclone, *J. Geophys. Res., 110,* D10301, doi:10.1029/2004JD005039.

Luo, M., Beer, R., Jacob, D. J., et al., (2002), Simulated observation of tropospheric ozone and CO with Tropospheric Emission Spectrometer (TES) satellite instrument, *J. Geophys. Res., 107,* NO. D15, doi:10.1029/2001JD000804.

Lorenz, E.N., (1956), *Empirical Orthogonal Functions and Statistical Weather Prediction,* Scientific Report No. 1, Contract AF19 (604)-1566, Meteorology Department, Massachusetts Institute of Technology, Cambridge, MA.

Lund, I.A., (1963), Map-pattern classification by statistical methods. *Journal of Applied Meteorology, 2,* 56-65.

150

Mao, H. and R. Talbot, (2004), Role of meteorological processes in two New England ozone episodes during summer 2001, *J. Geophys. Res., 109*, doi:1029/2004JD004850.

Mao, H., R. Talbot, R., Troop, D., Johnson, R., Businger, S., and A. M. Thompson, (2006), Smart balloon observations over the North Atlantic: O3 data analysis and modeling, *J. Geophys. Res., 111*, D23S56, doi:10.1029/2005JD006507.

Merrill, J. T., Moody, J. L., Oltmans, S. J., and H. Levy II, (1996), Meteorological analysis of tropospheric ozone profiles at Bermuda, *J. Geophys. Res., 101*, 29,201-29,211.

Moody, J. L., Davenport, J. C., Merrill, J. T., et al., (1996), Meteorological mechanisms for transporting O_3 over the western North Atlantic Ocean: A case study for August 24-29, 1993, *J. Geophys. Res., 101*, 29,213-29,277.

Moody, J.L., et al., (1998), Harvard Forest regional-scale air mass composition by Patterns is Atmospheric Transport History (PATH), *J. Geophys. Res., 103*, 13,181-13,194.

Monks, P. S., (2000), A review of the observations and origins of the spring ozone maximum, *Atmospheric Environment, 34*, 3545-3561.

Nassar R., Logan J. A., Worden, H. M. et al., (2008), Validation of Tropospheric Emission Spectrometer (TES) nadir ozone profiles using ozonesonde measurements, *J. Geophys. Res., 113*, D15S17, doi:10.1029/2007JD008819.

Oltmans, S. J., Levy II, H., Harris, J. M., et al.:, (1996), Summer and spring ozone profiles over the North Atlantic from ozonesonde measurements, *J. Geophys. Res., 101*, 29,179-29,200.

Osterman, G., Bowman, K., Cady-Pereira, K., et al., (2007a), Tropospheric Emission Spectrometer (TES), validation report, JPL D#102, version 2.0, http://eosweb.larc.nasa.gov/PRODOCS/tes/validation/TESValidationReport_v2_0.pdf.

Osterman G., Bowman K. W., Eldering, A., Fisher, B., et al., (2007b), TES Level 2 (L2) Data User's Guide, Version 3.0, Jet Propulsion Laboratory, Pasadena, CA, http://tes.jpl.nasa.gov/uploadedfiles/TES L2 Data Users Guide-1.pdf.

Owen, R. C., Cooper, O. R., Stohl, A., and R. E. Honrath, (2006), An analysis of the mechanisms of North American pollutant transport to the central North Atlantic lower free troposphere, *J. Geophys. Res., 111*, D23S58,doi:10.1029/2006JD007062.

Parrish, D. D., Holloway, J. S., Trainer, M., et al., (1993), Export of North American ozone pollution to the North Atlantic Ocean, *Science, 259*, 1436-1439.

Parrish, D. D., Trainer, M., Holloway, J. S., et al., (1998), Relationships between ozone and carbon monoxide at surface sites in the North Atlantic region, *J. Geophys. Res., 103*, 13,357-13,376.

Parrish, D. D., Holloway, J. S., Jakoubek, R., et al., (2000), Mixing of anthropogenic pollution with stratospheric ozone: A case study from the North Atlantic wintertime troposphere, J. Geophys. Res., 105, 24,363–24,374.

Parrish, D.D. (2006), Critical Evaluation of US on-road vehicle emission inventories, *Atmospheric Environment, 40*, 2288-2300.

Polvani, L. M., and J. G. Esler, (2007), Transport and mixing of chemical air masses in idealized baroclinic life cycles, *J. Geophys., Res. 112*, D23102, doi:10.1029/2007JD008555.

Richman, M.B., (1981), Obliquely rotated principal components – an improved meteorological map typing technique? *Journal of Applied Meteorology, 20*, 1145-1159.

Rodgers, C. D. (2000), *Inverse Methods for Atmospheric Sounding: Theory and Practice,* World Sci., Hackensack, N.J.

Rodrigues, S., Torres, C., Guerra, J.-C. and E. Cuevas, (2004), Transport pathways of ozone to marine and free-troposphere sites in Tenerife, Canary Islands, *Atmospheric Environment, 38*, 4733-4747.

Schictel, B.A and R.B. Husar (2001), Eastern North American transport climatology during high- and low-ozone days, Atmospheric *Environment, 35*, 1029-1038.

152

Schoeberl, M. R. (2006), Overview of the EOS Aura mission, *IEEE Trans. on Geosci. and Rem. Sens.*, *44*, NO. 5., 1066-1074.

Seaman, N., and S. Michelson (2000), Mesoscale meteorological structure of a high-ozone episode during the 1995 NARSTO-Northeast study, *Journal of Applied Meteorology*, *39*, 384-398.

Seinfeld, J. H., (1989), Urban air pollution: state of the science. *Science*, *243*, 745-752.

Serreze, M.C., (1995), Climatological aspects of cyclone development and decay in the Arctic, *Atmospheric-Ocean*, *33*, 1-23.

Serreze, M.C., et al., (1997), Icelandic Low Cyclone Activity: Climatological Features, Linkages with the NAO, and Relationships with Recent Changes in the Northern Hemisphere Circulation, *J. Climate, 10*, 453-464.

Shapiro, M. A., Hampel, T., and A. J. Krueger, (1987), The arctic tropopause fold, *Mon. Wea. Rev., 115*, 444-454.

Shim, C., Li., Q., Luo, M., et al., (2007), Characterizing mega-city pollution with TES O_3 and CO measurements, *Atmos. Chem. Phys. Discuss., 7*, 15189-15212.

Singh, H. B., Brune, W. H., Crawford, J. H., Jacob, D. J., and P. B. Russell, (2006), Overview of the summer 2004 International Chemical Transport Experiment- North America (INTEX-A), *J. Geophys. Res., 111*, D23S02, doi:10.1029/2006JD007905.

Staehelin, J., Thudium, J., Buehler, R., Volz-Thomas, A., Graber, W., (1994), Trends in Surrface Ozone Concentrations at Arosa (Switzerland). Atmopsheric Environment 28 (1), 75-87.

Stohl, A. M., and T. Trickl, (1999), A textbook example of long-range transport: Simultaneos observation of ozone maxima of stratospheric North American origin in the free troposphere over Europe, *J. Geophys. Res., 104*, 30,445-30,462.

Stohl, A., Huntrieser, H., Richter, A., et al., (2003a), Rapid intercontinental air pollution transport associated with a meteorological bomb, *Atmos. Chem. Phys., 3*, 2101-2141.

Stohl, A., Forster, C., Eckhardt, S., et al., (2003b), A backward modeling study of intercontinental transport using aircraft measurements, *J. Geophys. Res., 108,* D12, 4370, doi:10.1029/2002JD002862.

Tangborn, A., Stajner, I., Buchwitz, M., Khlystova, I., et al., (2009), Assimilation of SCIAMACHY total column CO observations: Global and regional analysis of data impact, *J. Geophys. Res., 114,* D07307, doi:10.1029/2008JD010781,2009.

Taubman B. F. et al., (2006), Aircraft vertical profiles of trace gas and aerosol pollution over the mid-Atlantic United States: Statistics and meteorological cluster analysis, *J. Geophys. Res., 111,* D10S07, doi:10.1029/2005JD006196.

Trickl, T., Cooper, O. R., Holger, E., et al., (2003), Intercontinental transport and its influence on the ozone concentrations over Europe: Three case studies, *J. Geophys. Res., 108,* D12, 8530, doi:10.1029/2002JD002735.

Vingarzan V. (2004), A review of surface ozone background levels and trends, *Atmospheric. Environment, 38,* 3431-3442.

Vukovich, F.M., (1995), Regional-scale boundary layer ozone variations in the eastern United States and their association with meteorological variations, *Atmospheric Environment, 29 (17),* 2259-2273.

Vukovich, F.M. and J. Sherwell, (2003), An examination of the relationship between certain meteorological parameters and surface ozone variations in the Baltimore-Washington corridor, *Atmospheric Environment, 37,* 971-981.

Warner, J., Comer, M.M., Barnet, C.D., Mcmillan, W.W., et al., (2007), A comparison of satellite tropospheric carbon monoxide measurements from AIRS and MOPITT during INTEX-A, *J. Geophys. Res., 112,* D12S17, doi:10.1029/2006JD00792, 2007.

Wolfsy, S.C., Sachse, G.W., Gregory, G.L., Blake, D.R., Bradshaw, J.D., et al., (1992), Atmospheric chemistry in the Arctic and Sub-arctic: Influence of natural fires, industrial emissions, and stratospheric inputs, *J. Geophys., Res., 97,* 16721-16746.

Wotawa, G. and Trainer, M. (2000), The influence of Canadian forest fires on pollutant concentrations in the United States, *Science, 288,* 324–328.

Worden, H. M., Logan, J. A., Worden, J. R., et al., (2007), Comparisons of Tropospheric Emission Spectrometer (TES) ozone profiles to ozonesondes: Methods and initial results, *J. Geophys. Res., 112,* D03309, doi:10.1029/2006JD007258.

Worden, J., Kulawik, S. S., Shephard, M. W., et al., (2004), Predicted errors of Tropospheric Emission Spectrometer nadir retrievals from spectral window selection, *J. Geophys. Res., 109,* D09308, doi:10.1029/2004JD004522.

Worden, J., Liu, X., Bowman, K., et al., (2007), Improved tropospheric ozone profile retrievals using OMI and TES radiances, *Geophys. Res. Let., 34,* L01809, doi:10.1029/2006GL027806.

Yarnal, B., (1993), *Synoptic Climatology in Environmental Analysis: A Prime,* Bellhaven Press, London, UK, 195 pp.

Yarnal, B., A.C. Comrie, B. Frakes, and D.P. Brown, (2001), Developments and prospects in synoptic climatology, *International Journal of Climatology, 21,* 1923-1950.

Zhang, L., Jacob, D. J., Bowman, K., W., et al., (2006), Ozone-CO correlations determined by the TES satellite instrument in continental outflow regions, and prospects in synoptic climatology, *Geophys. Res. Let., 33.,* L18804, doi:10.1029/2006GL026399.

Zishka, K. M., and P. J. Smith, (1980), The climatology of cyclones and anticyclones over North America and surrounding ocean environs for January and July, 1950-77, *Mon. Wea. Rev., 108,* 387-401.